Wintertime nitrate isotope dynamics in the Atlantic sector of the Southern Ocean

Sandi Smart

Dissertation presented for the degree of Master of Science

in the Department of Oceanography

University of Cape Town

February 2014

Supervisors:
Prof. Daniel Sigman
Dr. Sarah Fawcett
Dr. Sandy Thomalla
Prof. Chris Reason

Plagiarism Declaration

I know the meaning of plagiarism and declare that all of the work in the dissertation, save for that which is properly acknowledged, is my own.

……

Sandi Smart

……

Date

ABSTRACT

We provide the first data on wintertime patterns of the nitrogen (N) and oxygen (O) isotopes of seawater nitrate for the region south of Africa. Water column profile and underway surface samples collected in July 2012 span a range of latitudes from the subtropics to 57.8°S, just beyond the Antarctic winter sea-ice edge (56.7°S). The data are used in the context of simple models of nitrate consumption (including the Rayleigh model) to estimate the isotope effect (the degree of isotope discrimination) associated with the assimilation of nitrate by phytoplankton.

We focus on the Antarctic region (south of 50.3°S), where application of the Rayleigh model to depth profile N isotope data yields considerably lower isotope effect estimates (1.6-3.3‰) than commonly observed in the summertime Antarctic (~5‰). O isotope data from the same winter Antarctic depth profiles, on the other hand, yield isotope effect estimates (4.2-5.8‰) that are more similar to those suggested by summertime data. The decoupling of the N and O isotopes of nitrate, which would appear similar if purely recording the effects of nitrate assimilation, is interpreted as the result of active nitrification (i.e., *in situ* regeneration of organic matter to nitrate) within the Antarctic winter mixed layer. The prevalence of nitrification in the surface ocean is a central unknown in the effort to relate nitrate assimilation to organic matter export in the Antarctic.

The second key unknown concerns the question of which water mass should be regarded as the ultimate nitrate source to the summertime Antarctic surface, as this affects estimates of modern summertime phytoplankton production as well as the understanding of the N isotope dynamics that underlies efforts to reconstruct the relationship between climate and biological nitrate consumption in the Antarctic over ice age cycles. The winter data reported here suggest that the remnant winter mixed layer observed in summertime depth profiles, rather than the underlying deep waters, best represents the source, and consequently provide support for a higher summertime isotope effect (by ~1.2‰) than initially estimated for the Antarctic based on a deeper nitrate source.

Acknowledgements

First of all, I would like to thank Danny Sigman for granting me the opportunity to work with him and his group at Princeton University in this exciting field of research. The stimulating and challenging discussions afforded by the collaboration were essential to the development of the ideas presented in this thesis, and pushed me to strive beyond what I could have achieved on my own.

My sincere thanks must go to Sandy Thomalla for her hands-on assistance at sea and her guidance throughout the course of my Master's degree. It is thanks to her prompting and the vision of Pedro Monteiro that this collaborative project became a reality.

I am extremely thankful for the mentorship, technical assistance and moral support offered by Sarah Fawcett – my South African support-base in Princeton.

I would like to extend my appreciation to Chris Reason for always making the time to assist and advise me, even at the busiest of times.

Furthermore, I would like to acknowledge Patrick Rafter, François Fripiat and Raïssa Philibert for helpful discussions in their respective areas of expertise.

Special thanks to Alexa Weigand and Sergey Oleynik, technical staff at the Sigman Lab, for providing an efficient and enjoyable working environment.

I would like to thank my fellow students aboard the R/V *S.A. Agulhas II* for their assistance in sampling, as well as the captain and crew for a safe wintertime voyage across the stormy Southern Ocean in July 2012.

Support for this study was provided by the National Research Foundation (NRF), the Applied Centre for Climate and Earth Systems Science (ACCESS) and the University of Cape Town (UCT), without which this study would not have been possible.

Last, but not least, I thank my family – Mike, Jenny, and Dale Smart – as well as Alain Plattner for their unfailing support and encouragement, keeping me grounded through the ups and downs of the past two years.

Contents

1. Introduction

One of the key uncertainties facing our current understanding of the Earth's climate system is the role played by biology in the Southern Ocean. By consuming nutrients more or less completely in the surface ocean, marine phytoplankton have the power to either enhance or hinder the drawdown of carbon dioxide (an important greenhouse gas) from the atmosphere, and thus regulate global climate (Sarmiento & Toggweiler, 1984; Knox & McElroy, 1984; Sigman & Boyle, 2000). Nitrate (NO_3^-), an essential macro-nutrient for growth, exists in excess across the surface of the modern-day Southern Ocean (Pollard et al., 2002). Quantifying the biological consumption of nitrate in the Southern Ocean today and through past climate cycles is, therefore, a primary objective of ongoing biogeochemical research (Sigman & Boyle, 2000; DiFiore et al., 2009).

Natural variations in the nitrogen isotope ratios ($^{15}N/^{14}N$) of nitrate have been identified as a means to trace various processes in the marine nitrogen cycle, including the uptake of nitrate by phytoplankton (Altabet & Francois, 1994b; Sigman et al., 1999a; Trull et al., 2008; Sigman et al., 2009b). Thanks to advancements in the measurement procedure (Casciotti et al., 2002), the oxygen isotope ratios ($^{18}O/^{16}O$) of nitrate now offer an additional constraint on these processes (Sigman et al., 2005; Sigman et al., 2009a; DiFiore et al., 2009). Summertime studies of nitrate isotope dynamics in the Southern Ocean are often limited by uncertainties regarding the initial nitrate source; i.e., the isotopic composition and concentration of nitrate supplied to phytoplankton at the beginning of the productive summer season. In the absence of winter data, previous studies have been forced to rely on assumptions regarding this initial source (Sigman et al., 1999a; Karsh et al., 2003; DiFiore et al., 2010).

In this study, we provide a wintertime perspective on nitrate isotope dynamics in the Southern Ocean, with the goal of providing clarity on such concerns that have complicated previous studies. The maiden scientific voyage of the R/V *S.A. Agulhas II* in July 2012 offered a rare glimpse into the winter conditions of the Southern Ocean south of Africa, and an opportunity to produce the first nitrate isotope data from the region. Specifically, the key questions that we aim to address with these data are as follows:

(a) What do the wintertime patterns of nitrate N and O isotopes look like in the Southern Ocean south of Africa?

(b) What biogeochemical and physical processes do the N and O isotopes of nitrate, together, indicate in the wintertime Southern Ocean (and in particular, the Antarctic Zone)?

Although we address these questions within the context of the present-day Atlantic sector, the findings are more broadly applicable, with important implications in the realms of paleo- and modern oceanography alike. To set the scene for our investigation, we begin with an overview of the physical and biogeochemical characteristics of the Southern Ocean.

2. Literature Review

2.1 The Southern Ocean setting

2.1.1 Physical controls and biological modification

The distinguishing characteristic of the Southern Ocean is its striking banded structure, reflected in the meridional gradients of most physical and biogeochemical fields (e.g., temperature, salinity, nutrients) (Deacon, 1933; Belkin & Gordon, 1996; Pollard et al., 2002), and ultimately the distribution of marine plants and animals (Deacon, 1982). For decades, researchers have sought to determine the physical controls behind the observed circumpolar patterns. The main driving force appears to be the overlying wind field, in particular, the mid-latitude westerly wind belt that propels the Antarctic Circumpolar Current (ACC) (Deacon, 1982) (Figure 2.1).

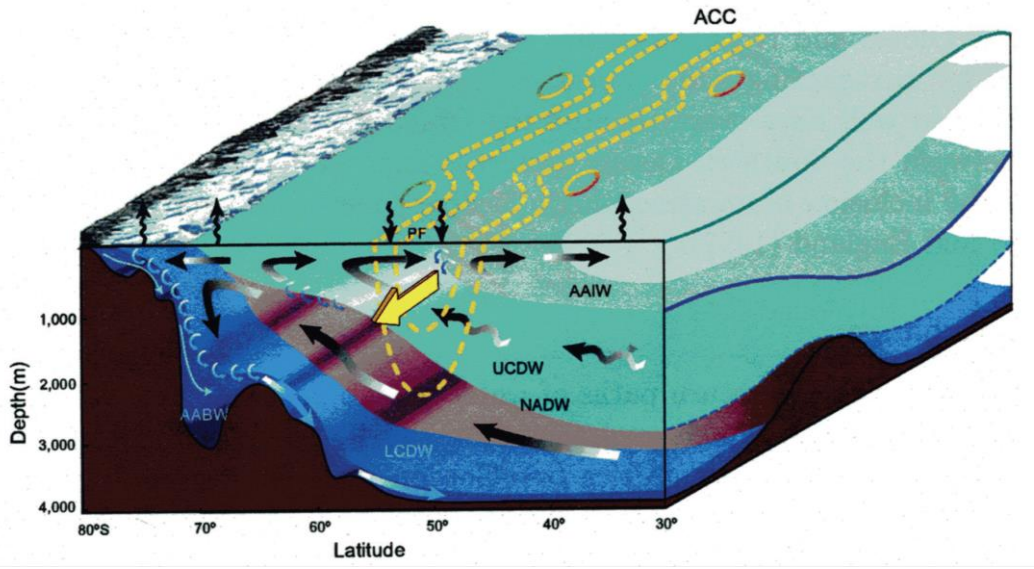

Figure 2.1 Schematic representation of the Antarctic Circumpolar Current (ACC) system; with the yellow dashed lines demarcating its core flow, the yellow arrow indicating the main direction of flow (from west to east) and the yellow and red or green surface circles representing eddies. Major water masses are labelled and their meridional flows are indicated by thick black arrows along density surfaces. Thin curly arrows indicate water conversion from one density to another (diapycnal mixing). Thin wavy black arrows at surface represent atmosphere-ocean-ice surface buoyancy fluxes. [source: Cunningham, 2005; adapted from Olbers et al., 2004]

In order for the ACC to maintain geostrophic balance, the isopycnals (density contours) must slope upwards to the south across the current (Pollard et al., 2002). The outcropping of these

isopycnals at the surface tends to occur in clusters, giving rise to the sharp property gradients and concentrated flow (known as jets) that characterise the Southern Ocean fronts (Deacon, 1937; Whitworth & Nowlin, 1987; Belkin & Gordon, 1996; Pollard et al., 2002). Since isopycnals are associated with particular water masses, their outcropping acts to expose different water masses to, or remove them from, the surface at frontal boundaries (Pollard et al., 2002). The properties of deep water masses (including the concentrations of major nutrients, like nitrate) can thus be imprinted upon the surface layer by advection and mixing along upward sloping density surfaces (isopycnal mixing). Together with diapycnal mixing (mixing between different density surfaces), these physical processes draw nutrients from deeper, denser waters closer to the surface the further south one goes, and is largely responsible for the poleward increase in nitrate concentration ($[NO_3^-]$) at a given depth across the Southern Ocean (Pollard et al., 2002) (Figure 2.2).

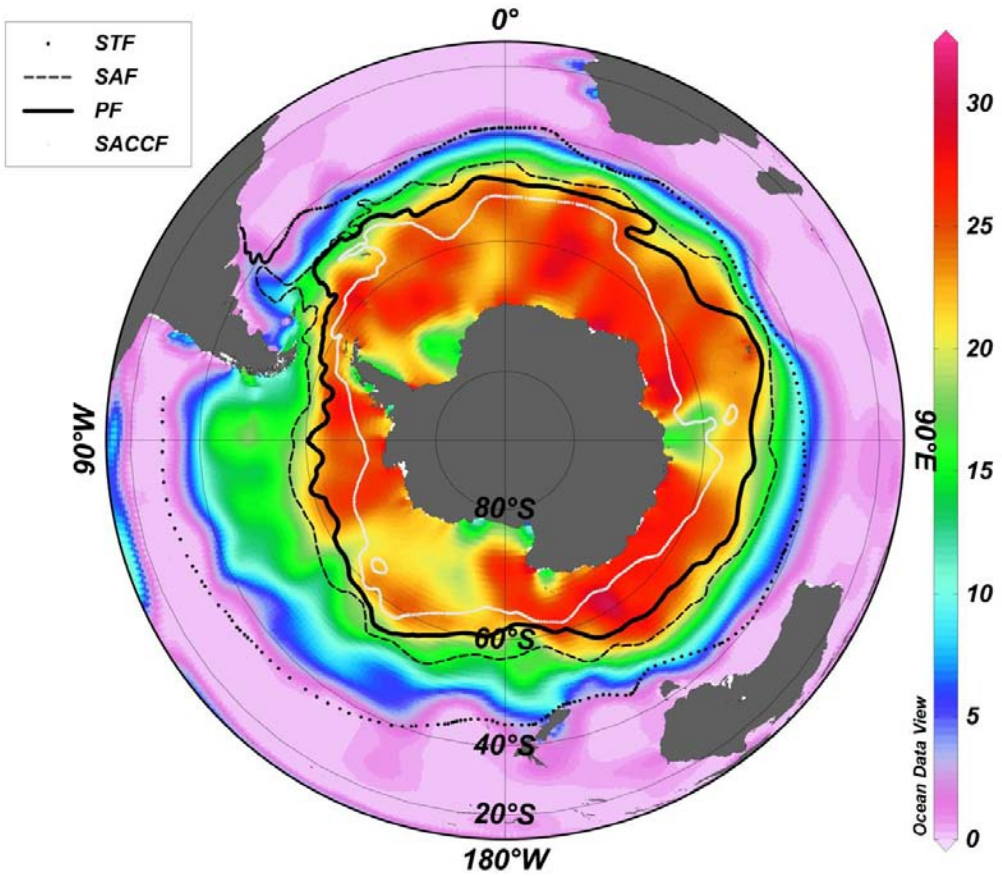

Figure 2.2 Polar orthographic view of the Southern Ocean displaying the January (summer) surface nitrate concentrations (in µmol l^{-1}) from the *World Ocean Atlas* 2009 (WOA09; http://www.nodc.noaa.gov/OC5/WOA09/pr_woa09.html). The positions of the major Southern Ocean fronts are overlaid (Orsi et al., 1995) and the legend is given top-left; from north to south, they are the Subtropical Front (STF; black dots), the Subantarctic front (SAF; thin dashed black line), the Polar Front (PF; thick solid black line) and the Southern Antarctic Circumpolar Current Front (SACCF; light grey dots).

Because of the distinctive gradients associated with the fronts, they are commonly employed as a means to categorize the Southern Ocean into different zones with like properties. The northernmost domain of the Southern Ocean is termed the Subantarctic Zone (SAZ), bounded by the Subtropical Front (STF; black dots in Figure 2.2) to the north and the Subantarctic Front (SAF; thin dashed black line in Figure 2.2) to the south. The band between the SAF and the Polar Front (PF; thick solid black line in Figure 2.2), further south, is known as the Polar Frontal Zone (PFZ). South of the PF lies the Antarctic Zone (AZ), which is further sub-divided by the Southern Antarctic Circumpolar Current Front (SACCF; light grey dots in Figure 2.2) into a northern and a southern domain: the Open Antarctic Zone (OAZ; which is "ice-free" year round) and the Polar Antarctic Zone (PAZ; which experiences seasonal ice cover), respectively (Whitworth, 1980; Orsi et al., 1995; DiFiore et al., 2010).

The bulk of the Southern Ocean interior is occupied by Circumpolar Deep Water (CDW), which can be sub-divided into an upper (UCDW) and a lower (LCDW) layer (Whitworth & Nowlin, 1987) (Figure 2.1). UCDW is distinguished from LCDW by its higher [NO_3^-] and lower dissolved oxygen content, stemming from its source waters in the Indian and Pacific basins (Callahan, 1972; Orsi et al., 1995; Park et al., 1993). LCDW, under the influence of North Atlantic Deep Water (NADW) incorporation, has higher salinities, lower [NO_3^-] and higher oxygen content than UCDW (Whitworth & Nowlin, 1987).

UCDW supplies the base of the winter mixed layer in the OAZ (between the SACCF and the PF) at around 200 m, which, in summer, is capped by a shallower (50-100 m thick), fresher, warmer mixed layer. Compared to the summer mixed layer above and UCDW below it, the remains of the winter mixed layer appear as a relative temperature minimum (T_{min}) (Whitworth & Nowlin, 1987; Sigman et al., 2000). In the PAZ (south of the SACCF), the winter mixed layer, which appears as a relative temperature maximum in summer (T_{max}), is fed by LCDW or a modified form thereof (Whitworth & Nowlin, 1987; DiFiore et al., 2010). In fact, it is the absence of UCDW in this zone that marks the southern boundary of the ACC (Orsi et al., 1995; Pollard et al., 2002).

In addition to the strong zonal flow of the ACC, the westerly winds induce an Ekman transport northwards in the surface layer (Deacon, 1982; Nowlin & Klinck, 1986; Pollard et al., 2002) (Figure 2.1). Heading north from the AZ across the PFZ and SAZ surface, temperature and salinity increase, while nitrate and oxygen levels decrease. These trends largely reflect the erosion of AZ surface water properties under the growing influence of sub-

tropical waters, which are warm, saline, nutrient depleted and oxygen poor relative to Southern Ocean waters (Whitworth & Nowlin, 1987). The fresher, oxygen-rich waters of the AZ surface plunge rapidly northwards, producing the characteristic salinity minimum of Antarctic Intermediate Water (AAIW; Figure 2.1) in the SAZ (Whitworth & Nowlin, 1987; Belkin & Gordon, 1996).

The existence of circumpolar features like the T_{min} and AAIW points to another major physical control on the zonal nature of the Southern Ocean (in addition to the overlying wind-field); namely, the latitudinal regime shift from temperature-dominated stratification (permitting a sub-surface salinity minimum to exist in the SAZ) to salinity-dominated stratification (allowing a shallow sub-surface temperature minimum in the AZ). The PFZ falls in the transition zone, and can thus be identified by the absence of both AAIW and a T_{min} (Pollard et al., 2002).

Importantly, the biogeochemical patterns set by physics can be modified significantly by biology (Pollard et al., 2002; Altabet & Francois, 1994b). Indeed, biological processes (such as the regeneration of nutrients) play an important role in setting the biogeochemical property distributions within deep waters to begin with. However, once conveyed to the surface via physical processes like mixing, these properties can be substantially altered by processes like nutrient uptake by phytoplankton, particularly under bloom conditions (Pollard et al., 2002). The physically-driven south-to-north decline in major-nutrient concentrations across the Southern Ocean surface (as illustrated by Figure 2.2) is thus compounded by the equatorward increase in biological nutrient utilization (Pollard et al., 2002; Altabet & Francois, 1994b).

2.1.2 The link between nitrate and climate

Observations show, however, that nitrate (an important macro-nutrient required by all phytoplankton), is never fully consumed across the surface of the Southern Ocean; not even during the productive summer season (Pollard et al., 2002) (Figure 2.2). The excess of nitrate suggests that some other factor currently limits growth in the Southern Ocean, such as insufficient iron (an essential trace nutrient) or unfavourable light conditions (Martin, 1990; Chisholm & Morel, 1991; Boyd et al., 1999; Karsh et al., 2003). The high-nutrient, low-chlorophyll (HNLC) state of the present-day Southern Ocean represents a ‘leak’ in the global ocean’s ‘biological pump’ – the ability of marine phytoplankton to sequester carbon-dioxide

(CO_2) by fixing carbon and exporting it to the deep ocean via sinking organic matter (Broecker, 1982; Sigman & Boyle, 2000).

The nitrate-rich deep waters that are upwelled and mixed into the Antarctic surface layer are also laden with dissolved CO_2. Thus, by consuming nitrate more completely in the surface (and simultaneously preventing, or largely compensating for, the escape of CO_2 to the atmosphere), biology in the Southern Ocean has the potential to significantly lower the atmospheric concentrations of this important greenhouse gas (Sigman & Boyle, 2000). This concept, a more efficient biological pump at high latitudes, is the premise for a leading hypothesis to explain the ~80-100 ppm lowering of atmospheric CO_2 (and amplified global cooling effect) during glacial periods (Knox & McElroy, 1984; Sarmiento & Toggweiler, 1984; Sigman & Boyle, 2000). Consequently, quantifying biological nitrate utilization in the modern ocean and reconstructing its past variations is central to our understanding of the internal feedbacks that regulate the Earth's climate system (Sigman & Boyle, 2000).

Direct measurements of nitrate uptake rates in the modern ocean (obtained from on-board 'bottle' incubations) provide only a snapshot of a spatially and temporally complex system, and can be biased by the measurement procedure itself (Sigman et al., 2005; DiFiore et al., 2006). While dissolved [NO_3^-] fields provide a broader (and more robust) perspective, they too are limited, as biological uptake and physical effects like mixing can be difficult to distinguish (Francois et al., 1992; Sigman et al., 2005; DiFiore et al., 2006). Nitrogen (N) isotopes offer a unique tool with which to trace the transfers between and transformations of the various N reservoirs, including the assimilation of nitrate into the particulate nitrogen (PN) pool (Trull et al., 2008; Sigman et al., 2009b). We proceed with an overview of N isotope systematics and the potential application of these principles to the ocean.

2.2 N isotopes: fractionation theory and two simple models

In nature, N exists in two stable forms: ^{14}N (the more abundant variety, comprising 99.63%) and ^{15}N (making up the remaining 0.37%) (Sigman et al., 2009b). The value of these isotopes (atoms of the same element with differing mass numbers) as tracers of ecosystem processes in both terrestrial and aquatic environments has long been recognized (Mariotti et al., 1981; Karsh et al., 2003; Trull et al., 2008). Their usefulness arises from the tendency for the lighter isotope (i.e., ^{14}N, containing 7 protons and 7 neutrons) to undergo

transformation or transfer more readily than its heavier counterpart (i.e. ^{15}N, containing 7 protons and 8 neutrons).

The partitioning that results from a unidirectional physical, chemical or biological process is known as kinetic isotope fractionation (Mariotti et al., 1981). One such process is the biological uptake and assimilation of nitrate by phytoplankton. Within a finite nitrate pool, preferential incorporation of ^{14}N causes the remaining nitrate pool (and thus also the organic particles (i.e., PN) subsequently produced from it) to become progressively enriched in ^{15}N (Wada & Hattori, 1978; Waser et al., 1998; Pennock et al., 1996). The degree of isotopic fractionation or discrimination against the heavier molecules (i.e., ^{15}N-bearing nitrate) is termed the "isotope effect" (ε) of nitrate assimilation (in units of in per mil, ‰), and is defined as:

$$\varepsilon\ (‰) = \left({}^{k^{14}}/_{k^{15}} - 1 \right) \times 1000$$

where k^{14} and k^{15} are the reaction rate coefficients of the light and heavy forms of nitrate, respectively (Francois et al., 1997; DiFiore et al., 2006).

The redistribution of N isotopes causes subtle, but detectable, changes in the $^{15}N/^{14}N$ ratios of both the reactant (dissolved nitrate pool) and the product (PN pool) (Sigman et al., 2009b). By convention, N isotopic composition is expressed in delta notation (with units of per mil, ‰), relative to atmospheric N_2 (Mariotti et al., 1981):

$$\delta^{15}N\ (‰) = \frac{(^{15}N/^{14}N)_{sample} - (^{15}N/^{14}N)_{atm\ N_2}}{(^{15}N/^{14}N)_{atm\ N_2}} \times 1000$$

2.2.1 The Rayleigh model

In the case of a closed system, where nitrate consumption proceeds with a constant isotope effect and without any removal or replenishment of the reactant or product pools, isotope systematics are described by the Rayleigh model (Mariotti et al., 1981) (black curves in Figure 2.3). Under these conditions, the $\delta^{15}N$ of the remaining nitrate pool ($\delta^{15}N_{reactant}$) is defined by the following equation:

$$\delta^{15}N_{\ reactant} = \delta^{15}N_{\ initial} - \varepsilon\{\ln(f)\}$$

where $\delta^{15}N_{initial}$ refers to the starting $\delta^{15}N$ value of the nitrate being consumed, ε denotes the isotope effect of nitrate assimilation and *f* is the fraction of nitrate remaining (calculated as

$[NO_3^-]/[NO_3^-]_{initial}$). At any one point during the reaction, the $\delta^{15}N$ of the PN instantaneously generated from the nitrate pool is approximated by:

$$\delta^{15}N_{\text{ instantaneous}} = \delta^{15}N_{\text{ reactant}} - \varepsilon$$

As a result, the $\delta^{15}N$ of the instantaneous product increases in tandem with the reactant nitrate $\delta^{15}N$, at an offset determined by the isotope effect (Mariotti et al., 1981) (black vertical arrow in Figure 2.3). The $\delta^{15}N$ of the total accumulating PN pool ($\delta^{15}N_{integrated}$) increases more gradually according to:

$$\delta^{15}N_{\text{ integrated}} = \delta^{15}N_{\text{ initial}} + \varepsilon\{\frac{f}{1-f}\}\ln(f)$$

As required by isotope mass balance, once all of the nitrate has been consumed (i.e., $f = 0$), the $\delta^{15}N$ of the total accumulated PN pool converges on the $\delta^{15}N$ of the initial nitrate supplied to the system (i.e., $\delta^{15}N_{integrated} = \delta^{15}N_{initial}$) (Figure 2.3), since all the N isotopes (heavy and light) are ultimately transferred to the product PN.

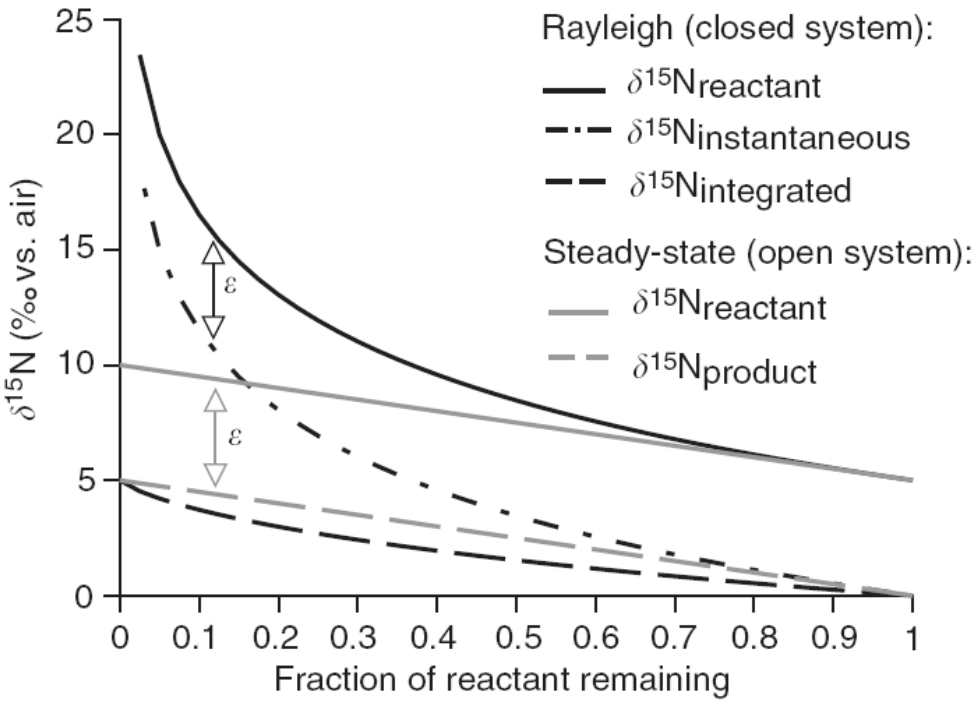

Figure 2.3 Two models of N isotope systematics, illustrating the changes in $\delta^{15}N$ (‰ vs. air) of the reactant (solid lines) and product (dashed lines) N pools as the reactant is consumed. The Rayleigh model (black lines) applies to a closed system, while the steady-state model (grey lines) applies to an open system. In both models, an initial reactant $\delta^{15}N$ of 5‰ and an isotope effect (ε) of 5‰ are used. A legend is provided in the top right-hand corner and model equations are given in text. [source: Sigman et al., 2009b]

2.2.2 The steady-state model

The end-member alternative to the closed-system Rayleigh model is the open-system steady-state model. In this system, nitrate is continually re-supplied to balance the N losses to consumption and export (i.e., to retain steady-state) (Sigman et al., 1999a; Hayes, 2002). The isotopic variation of the ambient nitrate ($\delta^{15}N_{reactant}$) and the resultant PN pools ($\delta^{15}N_{product}$) are governed by the following equations:

$$\delta^{15}N_{\ reactant} = \delta^{15}N_{\ initial} + \varepsilon(1 - f)$$

$$\delta^{15}N_{\ product} = \delta^{15}N_{\ initial} - \varepsilon f$$

and illustrated by the grey lines in Figure 2.3. The similarity between Rayleigh and steady-state predictions of $\delta^{15}N_{reactant}$ (black and grey solid lines in Figure 2.3, respectively) at low levels of consumption (essentially indistinguishable for $f > 0.7$) is an important observation for Southern Ocean studies, since nitrate drawdown is generally low (Sigman et al., 1999a).

Although neither the Rayleigh model nor the steady-state model is a perfect fit for the real ocean, if used appropriately (i.e., within the right hydrodynamic regime), these models can provide a useful framework for the interpretation of N isotope data from a variety of oceanic settings (Sigman et al., 1999a; Karsh et al., 2003; Sigman et al., 2003; DiFiore et al., 2006).

2.3 N isotopes as a paleo-proxy

Crucial to the application of N isotopes in modern- and paleo-studies is an understanding of how such theoretical relationships translate, firstly, to the open ocean and, secondly, to the sedimentary archive (Altabet & Francois, 1994b).

2.3.1 The basic principle

Early investigations in the modern ocean have demonstrated an inverse relationship between [NO_3^-] and the $\delta^{15}N$ of PN, both spatially (e.g., with depth or distance) and temporally (e.g., during the course of spring bloom), within near-surface waters (e.g., Wada & Hattori, 1976; Altabet & McCarthy, 1985; Altabet et al., 1991). The potential of N isotopes as a paleo-nutrient proxy was recognized by Francois et al. (1992) and Altabet & Francois (1994a) who found the northward decrease in [NO_3^-] across the major circumpolar fronts of the Southern

Ocean to be mirrored by an increase in the $\delta^{15}N$ of both surface suspended PN and the underlying core-top sediments. They interpreted these spatial anticorrelations as reflecting the equatorward increase in nitrate utilization, the implication being that down-core $\delta^{15}N$ variations might record the same information (i.e., changes in surface nutrient status) through geological time.

What makes this proxy potentially so powerful is that PN $\delta^{15}N$ is inherently a function of the *fractional* nitrate utilization (as prescribed by *f* in the Rayleigh and steady-state equations; see section 2.2) rather than the absolute $[NO_3^-]$ (in which changes in biological uptake can be obscured by changes in physical mixing and circulation patterns). Thus, in principle, sedimentary $\delta^{15}N$ signals should specifically record changes in the efficiency of the biological pump (Francois et al., 1992; Altabet & Francois, 1994b), the key parameter in the 'high-latitude hypothesis' for glacial-interglacial atmospheric CO_2 variations (Knox & McElroy, 1984; Sarmiento & Toggweiler, 1984).

On this basis, the 3-4‰ elevation observed in the $\delta^{15}N$ of both bulk and diatom-bound (and thus physically protected) N from glacial-age AZ sediments has been interpreted as enhanced nutrient utilization relative to today's AZ (Francois et al., 1997; Sigman et al., 1999b). Observations from the modern AZ suggest the $\delta^{15}N$ of sinking PN to be best approximated by the integrated product of the Rayleigh model (black dashed line in Figure 2.3), a system where nutrients are supplied vertically (e.g., by wintertime mixing or upwelling) and consumed locally with minimal resupply (e.g., during summer stratification). It is possible, however, that the glacial AZ was a regime dominated by lateral nitrate supply and progressive northward utilization, making the instantaneous product (black dot-dashed line in Figure 2.3) a more appropriate model for the $\delta^{15}N$ of PN sinking from its surface waters (Sigman et al., 1999b).

Using these two equations as end-member scenarios, and assuming no glacial-interglacial change in source nitrate $\delta^{15}N$ ($\delta^{15}N_{initial} \sim 5‰$, the average for modern CDW; Sigman et al., 1999b; Sigman et al., 2000) or nitrate assimilation isotope effect ($\varepsilon \sim 5‰$, the average from diatom culture- and field-based estimates; Waser et al., 1998; Sigman et al., 1999a) in the AZ, a 4‰ rise in sinking-PN $\delta^{15}N$ would require 60-100% nitrate utilization in the glacial AZ (compared to today's 25%). According to the "Cyclops" ocean geochemistry model (Kier, 1988; Sigman et al., 1998), even the lower limit of this estimation (50-65% utilization in the

glacial AZ) would be sufficient to induce the ~80 ppm lowering of atmospheric CO_2 observed during glacial times (Sigman et al., 1999b).

2.3.2 Three potential complications

As demonstrated, however, the quantitative link between the $\delta^{15}N$ of PN sinking to the seafloor and the extent of nitrate drawdown in the Southern Ocean surface relies on several major assumptions, particularly that (1) the source nitrate $\delta^{15}N$ and (2) the isotope effect of nitrate assimilation have remained constant through past climate cycles, and that (3) the nitrate assimilation signal is not significantly altered or lost due to N cycling processes (Francois et al., 1997; Sigman et al., 1999b; DiFiore et al., 2009). We now address each of these in turn.

The first assumption is that the $\delta^{15}N$ of nitrate supplied to the AZ surface has not changed appreciably on glacial-interglacial timescales. In the modern ocean, measuring the $\delta^{15}N$ of potential nitrate sources is relatively straightforward. Determining the relative contributions of these different source waters and establishing how this might have been different during glacial periods, however, poses more of a challenge (Sigman et al., 1999a; Sigman et al., 1999b; DiFiore et al., 2006). Knowledge of the hydrodynamic regime is also necessary to ensure that the most appropriate model (e.g., Rayleigh integrated vs. instantaneous product) is applied in the interpretation of the data (Sigman et al., 1999b; Altabet & Francois, 1994b).

Fortunately, the nitrate $\delta^{15}N$ of CDW, the ultimate supply to the AZ surface, is linked to that of the global deep ocean, which is relatively homogenous (Sigman et al., 1999a; Sigman et al., 2000) and appears not to have varied significantly through past glacial-interglacial cycles (Francois et al., 1992; Francois et al., 1997). This observation stems from the sedimentary archive underlying the oligotrophic, sub-tropical gyres. Here, nitrate supplied from the thermocline or intermediate-depth ocean is fully consumed at surface (i.e., $f = 0$), such that the integrated $\delta^{15}N$ of the sinking flux predominantly records changes in the source nitrate $\delta^{15}N$ (Altabet, 1988; Francois et al., 1992). Based on these records, an increase in nitrate $\delta^{15}N$ of the global deep ocean, and thus CDW feeding the AZ surface, seems unlikely to account for more than 1‰ of the observed ~4‰ glacial $\delta^{15}N$ elevation (Sigman et al., 1999b; Francois et al., 1997).

The second major assumption is that the isotope effect of nitrate uptake is well defined in the modern ocean, and that its amplitude has remained constant through time. Phytoplankton

culture studies indicate a large potential variation in the nitrate assimilation isotope effect, with estimates ranging between 0‰ and 20‰ (Wada & Hattori, 1978; Montoya & McCarthy, 1995; Pennock et al., 1996; Waser et al., 1998; Granger et al., 2004). Thus, in principle, the ~4‰ $\delta^{15}N$ rise in glacial AZ sediments could instead reflect a ~4‰ lowering of the isotope effect during glacial times (Sigman et al., 1999a; Sigman et al., 1999b; Karsh et al., 2003) (i.e., less discrimination against the heavy isotope causing the product PN to have a higher $\delta^{15}N$ at the same degree of consumption). If this were the case, it would have major repercussions for the biological-pump-centred interpretation of glacial-interglacial CO_2 variations.

Laboratory measurements indicate that the fractionation associated with nitrate assimilation occurs not at the uptake step (where nitrate is actively transported across the cell membrane), but rather inside the cell at the reduction step (where nitrate is converted to nitrite by the nitrate reductase enzyme) (Wada & Hattori, 1978). Thus the degree to which fractionation is expressed in the environment (i.e., the measured isotope effect) depends on the rate at which the partially-consumed, ^{15}N-enriched intracellular nitrate pool is effluxed to the surroundings, relative to the influx rate (Needoba & Harrison, 2004).

Tests on several marine diatom species suggest light to be the key controlling factor on the efflux:influx ratio and, thus, the isotope effect. Cultures grown under continuous, saturating light generally yield low isotope effects (2-6‰), presumably because most of the nitrate taken up is assimilated to sustain high growth rates; thus, efflux from the cell is low relative to influx (Waser et al., 1998; Needoba et al., 2003; Needoba & Harrison, 2004). Low-light conditions, on the other hand, tend to induce high isotope effects; commonly close to double the high-light value (Needoba & Harrison, 2004). The observed response is thought to be an evolutionary adaptation to deep water column mixing; whereby cells continue to take up more nitrate than they can assimilate under the present light-limiting conditions, in the event that conditions suddenly improve (i.e., if phytoplankton are abruptly and briefly mixed into the well-lit euphotic zone). In the interim, proportionally more of the imported nitrate is effluxed than under favourable light conditions, resulting in greater expressed fractionation (Needoba et al., 2004).

While low temperature and low iron conditions (under continuous, saturating light) affect growth rate and cell volume, their influence on the isotope effect is found to be minor;

perhaps a result of adjusting nitrate influx to suit the low assimilation rates, such that the efflux:influx ratio remains low (Needoba et al., 2004).

Although laboratory studies have proven valuable in elucidating the mechanism behind the isotope effect and identifying potential controls, this information alone is not sufficient to predict the isotope effect and its variation in the dynamic and complex environment of the Southern Ocean. For instance, changes in community structure (e.g., cell-size or species dominance) in response to sea-ice (Sigman et al., 1999a) or iron availability (Karsh et al., 2003) might alter the overall expression of the isotope effect in the environment. Such effects would go undetected in batch culture experiments. It follows that accurate estimates of the isotope effect from the open ocean are required (Altabet & Francois, 1994b; Sigman et al., 1999a; DiFiore et al., 2009). In section 2.4 (to follow), we review the approaches, outcomes and limitations of past field-studies in their attempts to derive the isotope effect of nitrate assimilation from nitrate N isotope distributions in the modern Southern Ocean.

The third major assumption in the interpretation of glacial-interglacial variations in sedimentary $\delta^{15}N$ is that the original assimilation signal is not masked by other processes like N cycling within the surface ocean. Organic PN that is remineralized to ammonium in the euphotic zone can be directly assimilated back into the PN pool, a process that lowers the $\delta^{15}N$ of near-surface suspended PN (since ammonium offers a lower-$\delta^{15}N$ pool for assimilation than the alternative nitrate source) (Altabet, 1988; Rau et al., 1991; Altabet & Francois, 1994b). This 'ammonium recycling', in itself, does not pose a threat to paleo-interpretations, since it is the sinking (not suspended) PN $\delta^{15}N$ that determines sedimentary $\delta^{15}N$ (Altabet & Francois, 1994b). If, however, some of the ammonium is oxidized (i.e., "nitrified") to nitrate within the euphotic zone, this could potentially alter the $\delta^{15}N$ of nitrate and thus also the sinking PN produced from it, leading to incorrect estimates of past nitrate utilization from sedimentary $\delta^{15}N$ (DiFiore et al., 2009). In section 2.5, we introduce a recently developed approach that might address this concern; namely, using the N and O isotope ratios of nitrate together to distinguish between assimilation and non-assimilation signals within nitrate $\delta^{15}N$.

2.4 Nitrate N isotope patterns and processes in the Southern Ocean: estimating the isotope effect

Nitrate isotope patterns in the open ocean are a composite of both the physical circulation and biological processes (including, but not exclusive to, nitrate uptake). Several studies have attempted to estimate the isotope effect of nitrate assimilation for the different zones of the Southern Ocean in the Pacific and Indian sectors (e.g., Sigman et al., 1999a; Altabet & Francois, 2001; Karsh et al., 2003; DiFiore et al., 2006). This, however, requires disentangling the effects of hydrography and biology. Taking each zone in turn (from the AZ to the SAZ), we now review the approaches and key findings of these previous studies; providing context for the wintertime Atlantic sector data presented in this study. Comparison between the different sectors might allow for some assessment of the circumpolar continuity of nitrate isotope dynamics in the Southern Ocean.

The AZ as a whole (consisting of the PAZ and the OAZ) has been regarded as a near-ideal case for the application of the Rayleigh model in the open ocean, with wind-driven upwelling and deep winter mixing supplying the surface with nitrate, and stratification (due to warming and ice-melt) essentially isolating the surface layer during summer, fostering growth and nutrient uptake (Sigman et al., 1999a). If nitrate drawdown in the AZ follows closed-system dynamics, then upper-ocean nitrate samples should fall along a straight line in "Rayleigh space" (with nitrate $\delta^{15}N$ plotted against the natural log of the concentration), where the slope of the line approximates the isotope effect (Mariotti et al., 1981; Sigman et al., 1999a).

Conforming to expectations, profile data from the Pacific and Indian PAZ falls roughly along a straight line in $\delta^{15}N$ vs. $\ln([NO_3^-])$ space (grey symbols in Figure 2.4). Best-fit slopes connecting the PAZ summer mixed layer with LCDW at depth indicate an isotope effect of ~5‰ (Sigman et al., 1999a; DiFiore et al., 2009) (slope of the solid grey line in Figure 2.4, and red symbols in Figure 2.5). OAZ profiles, on the other hand, exhibit a distinct deviation from the expected Rayleigh trend. In $\delta^{15}N$ vs. $\ln([NO_3^-])$ space, data from the T_{min} layer (the remnant of the winter mixed layer situated directly below the summer mixed layer; see bottom-left panel in Figure 2.5) fall well below the linear trendline connecting the OAZ summer mixed layer with UCDW at depth (Sigman et al., 1999a) (compare black symbols with dashed line in Figure 2.4).

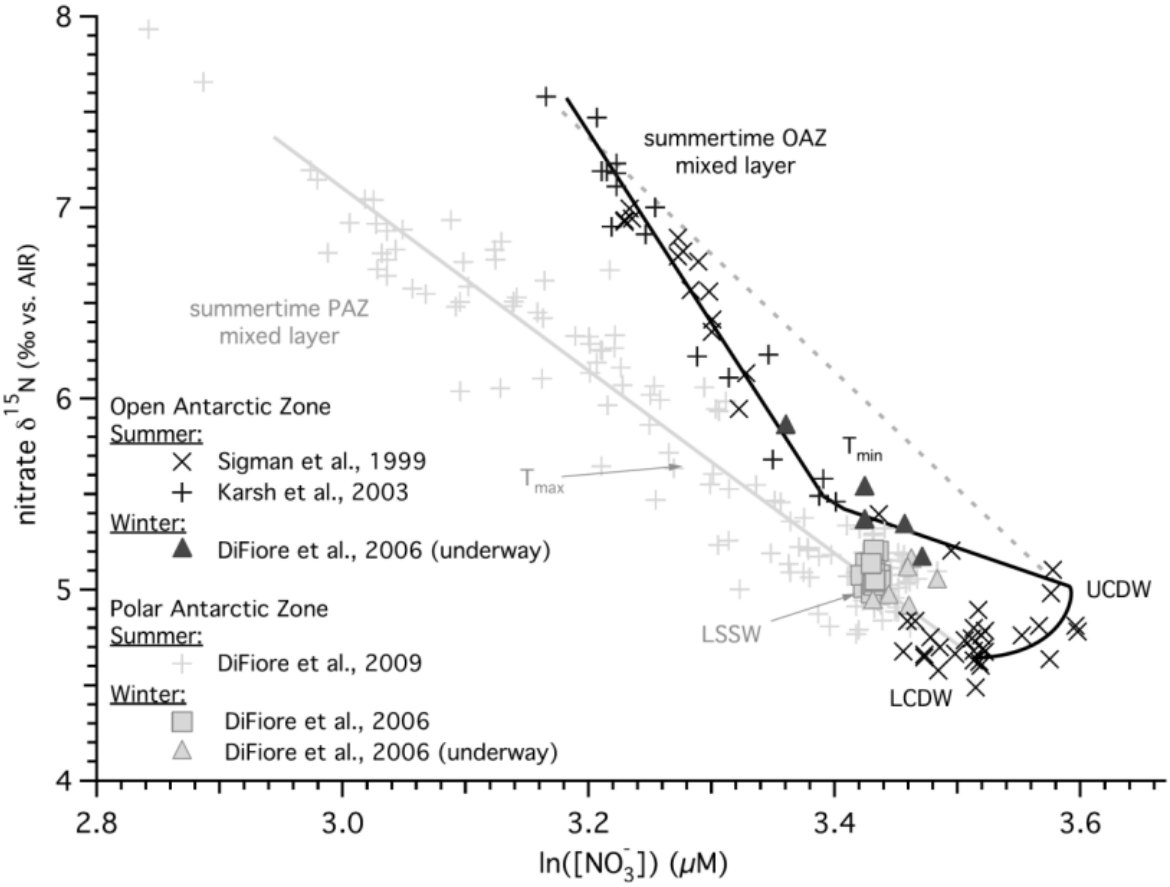

Figure 2.4 Compilation of winter and summer AZ data from the region south of Australia plotted in nitrate $\delta^{15}N$ vs. $\ln([NO_3^-])$ space (OAZ in black, PAZ in grey). Solid symbols represent winter measurements, while summer measurements are denoted by crosses and x's. The solid grey and black lines indicate the depth progression through the data in the PAZ and OAZ, respectively, along which key water masses are labelled (see text for definitions of acronyms). The dashed grey line indicates the expected trajectory for OAZ profiles under conditions of pure Rayleigh assimilation of UCDW nitrate. Original data sources indicated bottom left. [source: DiFiore et al., 2010]

Several explanations for this deviation have been offered. A sudden resupply event, for instance, would cause the data to fall on a mixing line between the "new" water parcel (i.e., unaltered UCDW introduced from below) and the one that has already undergone partial nitrate extraction and associated isotopic elevation (i.e., the OAZ mixed layer) (as demonstrated by the long-dashed curves in Figure 2.6). The curvature of a mixing line in $\delta^{15}N$ vs. $\ln([NO_3^-])$ space is due to the tendency for the nitrate $\delta^{15}N$ of the resulting mixture to be weighted towards the $\delta^{15}N$ of the end-member with the higher $[NO_3^-]$, in accordance with isotope mass balance (DiFiore et al., 2006; Sigman et al., 2000). Under low nutrient utilization conditions such as those of the AZ, however, the $[NO_3^-]$ and nitrate $\delta^{15}N$ of the two water parcels would not be sufficiently different to account for the full extent of the observed deviation (Sigman et al., 1999a; DiFiore et al., 2010) (as illustrated by Figure 2.6a).

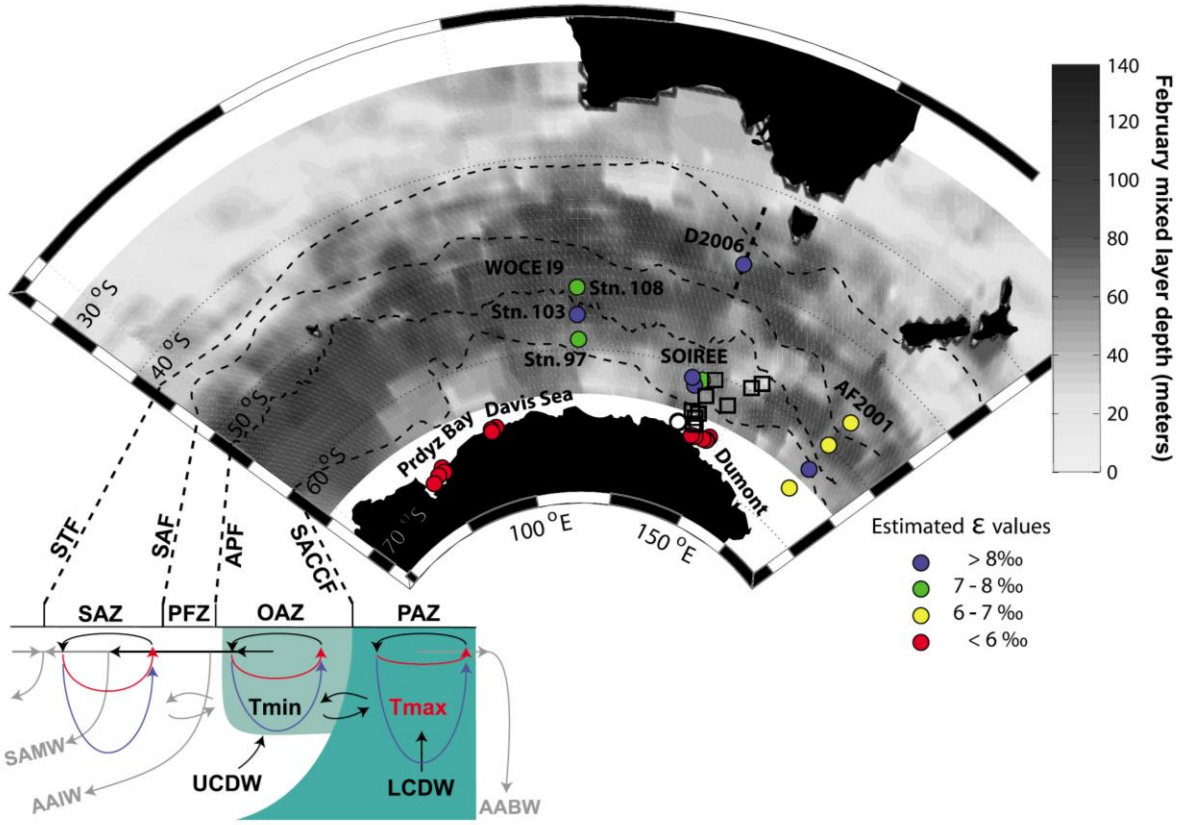

Figure 2.5 Geographical overview of existing summertime estimates for the isotope effect of nitrate assimilation (with the ε value in ‰ indicated by the colour of filled circles; legend bottom-right) from the region south of Australia. Open black squares and circles represent underway and profile wintertime sampling locations, respectively. Original data sources are Sigman et al., 1999a (WOCEI9); Altabet & Francois, 2001 (AF2001); Karsh et al., 2003 (SOIREE); DiFiore et al., 2006 (D2006); and DiFiore et al., 2009 (Prydz Bay, Davis Sea and Dumont). Symbols are plotted against the mixed-layer depth climatology for February (Dong et al., 2008), with the major Southern Ocean fronts indicated by black dashed lines (Orsi et al., 1995). A cartoon depth-section of the Southern Ocean (bottom-left) illustrates the relevant water masses (acronyms given in text) and circulation features in the region (including wind-driven upwelling of UCDW and LCDW into the AZ and the exchange between the OAZ T_{min} and PAZ T_{max}). Blue and red loops indicate winter and summer mixed-layer depths respectively. [source: DiFiore et al., 2010]

Another possibility is the regeneration of PN sinking out of the OAZ summer mixed layer above, which is low in $\delta^{15}N$ due to the modest degree of nitrate assimilation there. This would also force the T_{min} data in the observed direction by introducing lower-$\delta^{15}N$ nitrate into the subsurface (Sigman et al., 1999a). Additional isotope constraints from the Pacific and Indian OAZ, however, suggest that this explanation too is lacking (DiFiore et al., 2009).

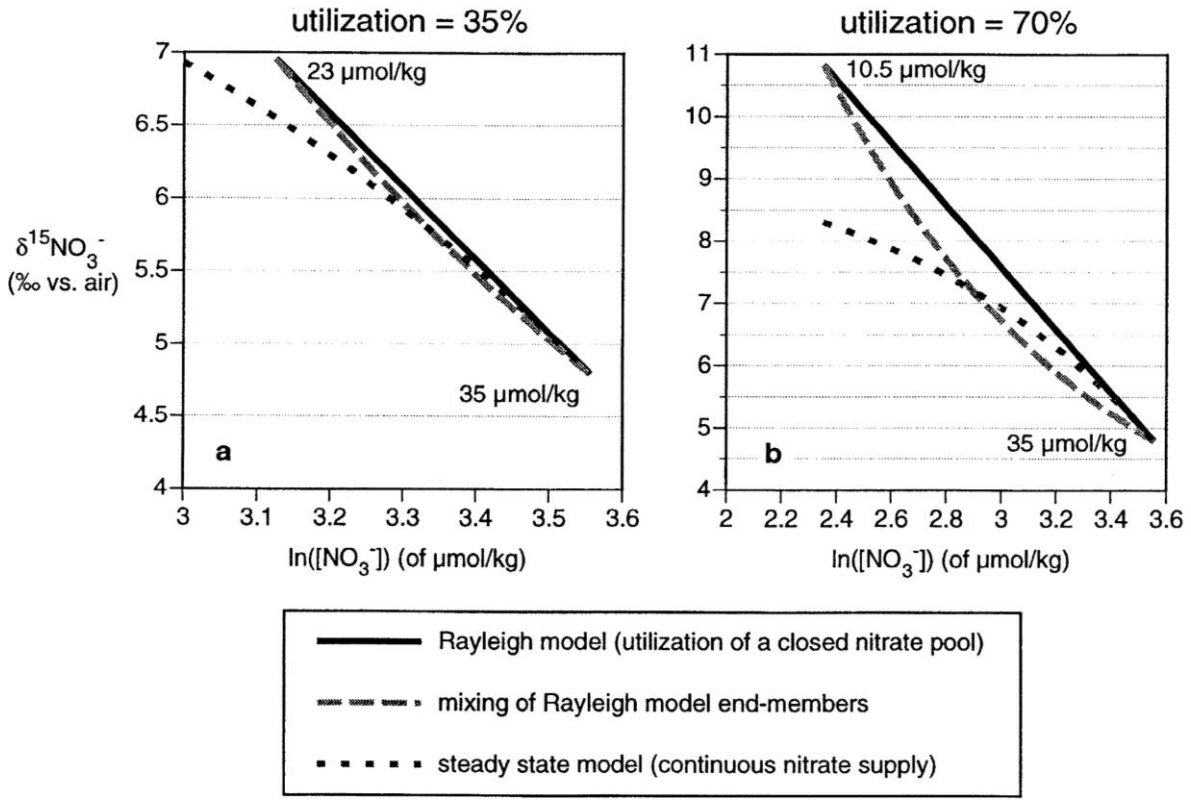

Figure 2.6 The expected pathway in $\delta^{15}N$ vs. $\ln([NO_3^-])$ space followed by a nitrate pool undergoing consumption from an initial $\delta^{15}N$ of 4.8‰ and $[NO_3^-]$ of 35 µmol kg^{-1} to (a) 23 µmol kg^{-1} (i.e., 35% utilization), and (b) 10.5 µmol kg^{-1} (i.e., 70% utilization). The black solid line simulates Rayleigh conditions (i.e., consumption within a closed system) while the dotted line simulates steady-state conditions (i.e., consumption in an open system). The dashed line illustrates the deviation that would result from the mixing together of the initial and final nitrate pools of the Rayleigh model; the greater the $[NO_3^-]$ difference between the mixing end-members, the greater the deviation of the mixing line from the predicted Rayleigh utilization trend (hence the greater curvature of the mixing line in (b) than in (a)). [source: Sigman et al., 1999a]

A recent study by DiFiore et al. (2010) proposes that the T_{min} anomaly of the OAZ is best explained by lateral exchange with the T_{max} of the PAZ. The nitrate properties of the T_{max} layer evolve from those of its LCDW source (~4.8‰ at 33µM) (Sigman et al., 2000). The nitrate $\delta^{15}N$ signature carried by LCDW, and much of the abyssal ocean, in fact, stems ultimately from the completeness of nitrate utilization across most of the global surface ocean; firstly because the $\delta^{15}N$ of accumulated PN raining out of the surface will converge on that of the nitrate source (thus any remineralization will have a negligible effect on the $\delta^{15}N$ of subsurface nitrate), and secondly because, regardless of how elevated its $\delta^{15}N$, the contribution of nitrate-deficient surface waters to the $\delta^{15}N$ of newly formed deep waters (e.g., NADW, which later gives rise to LCDW) can only be minor (Sigman et al., 2000).

The properties of the T_{min} layer, on the other hand, appear to be a product of both the adjacent T_{max} and the underlying UCDW, which typically has a higher $\delta^{15}N$ for its $[NO_3^-]$ (~5.3‰ at 35 μM in the OAZ) due to communication with low-latitude denitrification zones (where ^{14}N-bearing nitrate is preferentially removed under oxygen-deficient conditions) (Cline & Kaplan, 1975; Barford et al., 1999; Sigman et al., 2000). The unexpectedly low $\delta^{15}N$ of the T_{min} samples suggests that the lateral nitrate contribution from the PAZ dominates, supplying on the order of 60% during the summer and likely more during winter (DiFiore et al., 2010).

This raises the question of which water mass should be regarded as the ultimate source to the OAZ summertime surface. That is, which $\delta^{15}N$ and $[NO_3^-]$ values should be used as the starting point for nitrate utilization in Rayleigh space? Selecting UCDW as the source, yields low estimates for the isotope effect in the range of 4-6‰ (Sigman et al., 1999a) (slope of the dashed line in Figure 2.4), while choosing the summertime T_{min} as the source leads to higher estimates of 7-10‰ (Karsh et al., 2003) (slope of the solid black line between 'T_{min}' and 'summertime OAZ mixed layer' in Figure 2.4). To avoid the bias caused by continued T_{max}–T_{min} exchange during the summer, DiFiore et al. (2010) instead advocate the use of T_{min} wintertime values as the source (black triangles in Figure 2.4) and provide revised estimates for the OAZ south of Australia that are intermediate to these earlier estimates (symbols labelled 'WOCEI9' and 'SOIREE' in Figure 2.5).

This type of complication is avoided in the PAZ, where all potential nitrate sources to the summertime surface – LCDW, Low Salinity Shelf Water (LSSW; which too derives from LCDW) and, for the most part, T_{max} – fall along the same Raleigh nutrient utilization trend (solid grey line in Figure 2.4), such that the choice of initial values has minimal impact on the isotope effect estimates (DiFiore et al., 2009).

In the PFZ and the SAZ, it is less clear which model should be applied to interpret the isotope data, as they exhibit aspects of both open- and closed-system behaviour, in the form of equatorward nitrate transport within the mixed layer and intense seasonal stratification, respectively (Sigman et al., 1999a; Lourey et al., 2003). This uncertainty led Altabet & Francois (2001) to provide isotope effect estimates from both models. Summertime profile data down to 100 m (i.e., assuming a summertime T_{min} source) together with seasonal surface measurements from the PFZ south of New Zealand (symbols labelled 'AF2001' in Figure 2.5) yield estimates of 6-8‰ using the Rayleigh model and 7-10‰ using the steady-state model.

Fortunately, the choice of model for the PFZ appears not to have a major effect on the estimates, for two reasons: first because, under the relatively modest nutrient drawdown of the PFZ, open- and closed-system nitrate utilization pathways are almost indistinguishable (as illustrated by Figure 2.3); and second because both possible routes of resupply (whether by the T_{min} from below or AZ surface waters from the south) have similar nitrate $\delta^{15}N$-to-[NO_3^-] relationships and would fall on a common nitrate utilization trajectory (Altabet & Francois, 2001; Lourey et al., 2003). The latter is demonstrated by the general agreement between surface- and profile-based estimates of the isotope effect.

The SAZ poses a greater challenge in both respects: firstly because of the higher degree of nitrate drawdown here; and secondly because the SAZ thermocline and more polar surface waters – the two potential nitrate sources to the SAZ mixed layer – have such different $\delta^{15}N$-to-[NO_3^-] relationships (Sigman et al., 1999a; Lourey et al., 2003). Assuming Rayleigh conditions with a purely lateral supply of nitrate from south of the PF yields an assimilation isotope effect of ~4.5‰ from the summertime surface of the Pacific SAZ (illustrated schematically by the slope of the green arrow in Figure 2.7). This would apply to a nitrate parcel undergoing progressive consumption on its equatorward journey into and across the SAZ. Profile-based Rayleigh estimates assuming the SAZ thermocline as the sole source, on the other hand, yield much higher estimates in the region of 7-15‰ from the Pacific and Indian sectors (Sigman et al., 1999a) (as illustrated by the slopes of the grey dashed lines in Figure 2.7).

The unusually steep slopes (and thus high isotope effect estimates) obtained in the latter case stem from Subantarctic Mode Water (SAMW), the water mass that constitutes the SAZ thermocline (the red line in Figure 2.7). SAMW has a remarkably low nitrate-$\delta^{15}N$ for its [NO_3^-] relative to other Southern Ocean water masses; too low to be accounted for by *in situ* vertical mixing of SAZ surface waters with AAIW or UCDW below (Sigman et al., 2000). Instead, the isotopic character of SAMW appears to be the product of isopycnal mixing with the subtropical thermocline (indicated by 'STT' in Figure 2.7), which acts to lower the concentration of more polar-sourced nitrate (perhaps originating from the AZ winter surface; where the red line meets the black arrow in Figure 2.7) without increasing its $\delta^{15}N$ (Sigman et al., 1999a; Sigman et al., 2000). The characteristic $\delta^{15}N$-to-[NO_3^-] relationship of the subtropical thermocline, in turn, is set by its vertical communication with the nitrate-depleted surface waters, and potentially also the contribution of newly fixed N (with $\delta^{15}N \sim 0$‰)

which, when regenerated (i.e., remineralized to ammonium and then oxidised to nitrate), adds low-$\delta^{15}N$ nitrate to the thermocline (Sigman et al., 2000).

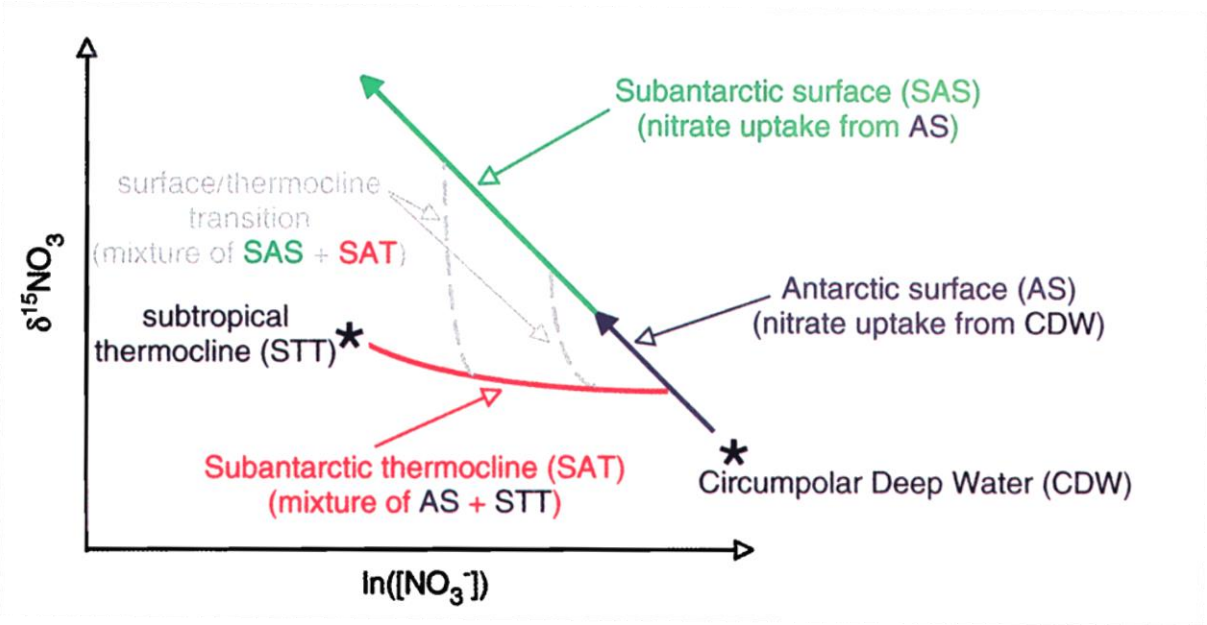

Figure 2.7 Schematic representation of AZ and SAZ nitrate data in $\delta^{15}N$ vs. $\ln([NO_3^-])$ space, illustrating the two possible routes of nitrate supply to the SAZ surface. The black arrow depicts the evolution of AZ nitrate during uptake under Rayleigh conditions, starting from CDW values (bottom right). The green arrow illustrates the trend that SAZ surface data would follow during nitrate uptake under Rayleigh conditions from an Antarctic source. The red line represents the Subantarctic thermocline as a mixture between Antarctic-sourced waters and the subtropical thermocline. The grey dashed lines illustrate the depth progression observed in SAZ profile data in the transition from the thermocline to the surface. [source: Sigman et al., 2000]

From the apparent disagreement between surface- and profile-based estimates of the isotope effect has arisen the need to quantify the relative contributions of the two major routes of supply to the SAZ surface (Sigman et al., 1999a; DiFiore et al., 2006). Apart from several physical indicators (in the form of temperature and salinity observations), existing nitrate isotope data provides strong evidence for cross-frontal transport of AZ or PFZ waters into the SAZ mixed layer and periods of limited vertical exchange during the summer. In particular, summertime SAZ profiles that exhibit a nitrate-$\delta^{15}N$ increase into the surface despite little change or even an increase in $[NO_3^-]$, precludes purely thermocline-sustained assimilation (Sigman et al., 1999a; DiFiore et al., 2006).

A model study undertaken by DiFiore et al. (2006), however, has demonstrated that the sheer magnitude of the observed winter-to-summer change in $\delta^{15}N$ of SAZ surface nitrate cannot be achieved with lateral nitrate supply alone. Wintertime measurements south of Australia have

revealed that the $\delta^{15}N$-to-$[NO_3^-]$ signature of SAMW is imposed upon the SAZ surface by deep winter mixing each year (with only a modest assimilation-driven nitrate-$\delta^{15}N$ elevation into the surface). In order to produce the observed increase in the surface nitrate $\delta^{15}N$ on such a short timescale (~4 months or less), an isotope effect higher than 4.5‰ (as estimated by Sigman et al., 1999a) is required. Alone, the change from a low $\delta^{15}N$-to-$[NO_3^-]$ thermocline source to a higher $\delta^{15}N$-to-$[NO_3^-]$ polar source is not sufficient, particularly since this transition takes some time (i.e., it is not feasible for the entire SAZ wintertime nitrate reservoir to be replaced with PFZ or AZ nitrate during the ~4 month growing season). Based upon these findings, DiFiore et al. (2006) propose the 'true' assimilation isotope effect of the SAZ to be around 8-9‰ (labelled 'D2006' in Figure 2.5). The case of the SAZ demonstrates the value of simple models like the Rayleigh model in the interpretation of nitrate isotope data, even when the oceanic setting clearly violates Rayleigh conditions (DiFiore et al., 2006).

Taking a step back and considering together all the field-based estimates from the region south of Australia, a latitudinal progression emerges (Figure 2.5). The isotope effect of nitrate assimilation appears to increase equatorwards across the Southern Ocean (DiFiore et al., 2010). The size of the isotope effect is well correlated with mixed-layer depth, which generally increases northwards from the PAZ (where local ice-melt encourages stratification) to the SAZ (where strong winds drive deep mixing) (DiFiore et al., 2009; DiFiore et al., 2010). This observation supports the findings of laboratory culture experiments that implicate light as the dominant control on the expressed isotope effect (Needoba & Harrison, 2004; Needoba et al., 2004).

A regional comparison between the isotope effect estimates from Pacific PAZ (with $\varepsilon \sim 4.2$‰) and Indian OAZ (with $\varepsilon \sim 5.5$‰) profiles reveals another potential contributor; namely, sea-ice (Sigman et al., 1999a). Apart from possible species-related differences, sea-ice can impose a physical control on the expression of the isotope effect. Nitrate that is taken up into sea-ice can be fully consumed there by sea-ice phytoplankton, such that the fractionation associated with its assimilation is not expressed in the oceanic environment Fripiat et al., *accepted*; Sigman et al., 1999a). In this way, near-surface $[NO_3^-]$ can be lowered without raising the ambient nitrate $\delta^{15}N$ (i.e., lowering the slopes in $\delta^{15}N$ vs. $\ln([NO_3^-])$ space), potentially leading to under-estimation of the organism-level isotope effect in marginal ice environments (Sigman et al., 1999a).

Despite good progress in quantifying the isotope effect in the Southern Ocean, several uncertainties remain. Such studies are often limited in their ability to diagnose the cause of a deviation from the expected Rayleigh utilization trend, as there is frequently more than one process that could produce a deviation in the observed direction in Rayleigh space. This complicates estimation of the isotope effect, and calls for an additional constraint on nitrate isotope dynamics. In the following section we consider the potential of the O isotopes of nitrate as that additional constraint.

2.5 The N and O isotopes of nitrate: a dual isotope approach

Thanks to recent method developments, it is now possible to measure the O isotope ratios of nitrate in seawater, in conjunction with the N isotope ratios (Casciotti et al., 2002). O isotope ratios are similarly expressed in delta notation with units of per mil (‰), and are referenced to Vienna Standard Mean Ocean Water (VSMOW):

$$\delta^{18}O\ (‰) = \frac{(^{18}O/^{16}O)_{sample} - (^{18}O/^{16}O)_{VSMOW}}{(^{18}O/^{16}O)_{VSMOW}} \times 1000$$

Because the N and O isotopes of nitrate are affected differently by some aspects of the N cycle, nitrate $\delta^{18}O$ has the potential to provide an additional constraint on the processes behind nitrate $\delta^{15}N$ signals observed in the ocean (Casciotti et al., 2002; Granger et al., 2004; Sigman et al., 2009a). Specifically, coupled $\delta^{15}N$ and $\delta^{18}O$ measurements of nitrate enable assimilation to be distinguished from non-assimilation processes, which, if unaccounted for, could bias estimates of the N isotope effect of nitrate assimilation from $\delta^{15}N$ data alone (DiFiore et al., 2009).

The assimilation of nitrate by phytoplankton produces roughly equal elevations in the $\delta^{15}N$ and $\delta^{18}O$ of the remaining nitrate pool, such that nitrate samples purely under the influence of assimilation will fall along a 1:1 line in $\delta^{18}O$ vs. $\delta^{15}N$ space (Figure 2.8). In other words, the ratio of the O and N isotope effects is close to one (i.e., $^{18}\varepsilon/^{15}\varepsilon \approx 1$) (Granger et al., 2004). The same kind of "1:1 relationship" is observed for the removal of nitrate by denitrification (Granger et al., 2008).

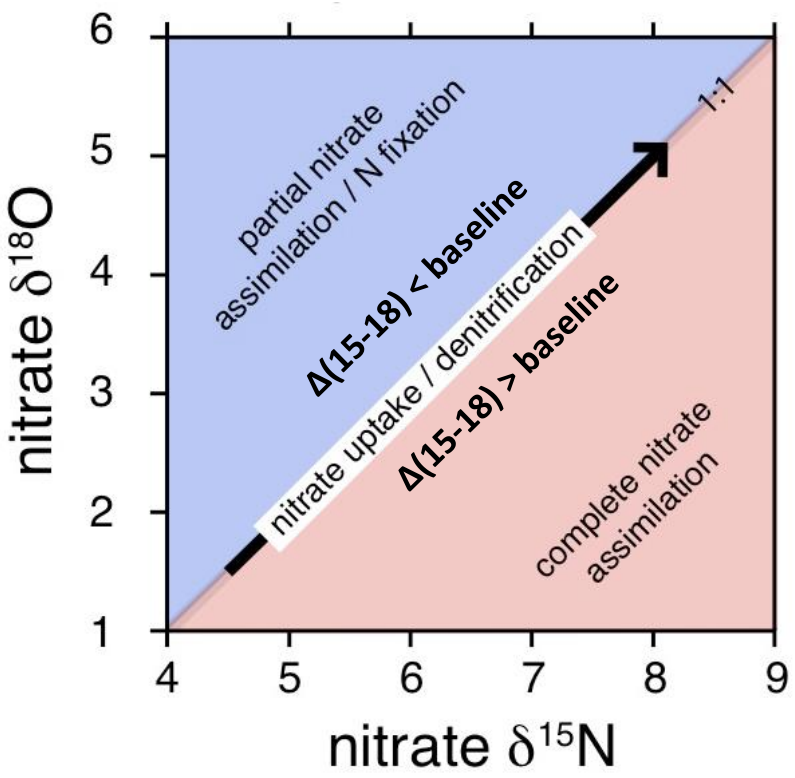

Figure 2.8 Schematic illustrating the decoupling effect of regeneration on the N and O isotopes of nitrate. The solid black arrow indicates the trajectory of a nitrate pool along a 1:1 line $\delta^{18}O$ vs. $\delta^{15}N$ space, as occurs during uptake by phytoplankton or denitrification. The pink shaded area below the 1:1 line represents the territory into which a nitrate pool will shift under the influence of complete nitrate assimilation followed by nitrification (i.e., yielding a nitrate Δ(15-18) greater than the baseline value). The blue shaded area above the 1:1 line represents the territory into which a nitrate pool will shift under the influence of either partial nitrate assimilation or N_2-fixation followed by nitrification (i.e., yielding a Δ(15-18) less than the baseline value). [source: modified from Rafter et al., 2013]

The regeneration of PN, however, specifically the nitrification steps (the oxidation of ammonium to nitrite, and subsequently nitrate), can decouple the N and O isotopes of nitrate, yielding a deviation from the 1:1 line in $\delta^{18}O$ vs. $\delta^{15}N$ space. The reason for the decoupling, is that the $\delta^{15}N$ of the nitrate introduced by nitrification depends on the $\delta^{15}N$ of the PN being regenerated, while its $\delta^{18}O$ is independent of the PN isotopic composition (since it contains, and thus contributes, no O atoms) (Sigman et al., 2005; Sigman et al., 2009a; Sigman et al., 2009c). Instead, the $\delta^{18}O$ of newly nitrified nitrate is set predominantly by the $\delta^{18}O$ of ambient water, since at least 5 out of 6 O atoms in the resulting nitrate derive from ambient H_2O (with the remaining 1 in 6 O atoms potentially deriving from ambient O_2) (Casciotti et al., 2002; Sigman et al., 2009a). This "$\delta^{18}O$ of nitrification" is estimated to be ~1.1‰ higher than the $\delta^{18}O$ of ambient water (i.e., $\delta^{18}O$ ~ 1.1‰ vs. VSMOW) (Sigman et al., 2009a).

The magnitude and the direction of the deviation caused by nitrification in $\delta^{18}O$ vs. $\delta^{15}N$ space depend on the context in which that nitrification takes place (Sigman et al., 2009a; Sigman et al., 2009c; Rafter et al., 2013). Below, we consider three cases, each coupled with nitrification: (1) complete nitrate consumption, (2) N_2-fixation and (3) partial nitrate consumption. For the purposes of this explanation, it is assumed in each case that PN is fully converted to nitrate, such that no fractionation associated with the regeneration process is expressed and, thus, the $\delta^{15}N$ of the newly nitrified nitrate is simply equal to the $\delta^{15}N$ of the PN being regenerated (Rafter et al., 2013).

In the low-latitude ocean (case 1), nitrate is fully (or almost fully) consumed at surface, such that the $\delta^{15}N$ of the PN sinking to, and being regenerated within, the subsurface is not substantially different from the $\delta^{15}N$ of the surrounding sub-surface nitrate (the initial source to the surface). The $\delta^{18}O$ of ambient sub-surface nitrate, on the other hand, is progressively lowered towards the nitrification value (~1.1‰) in the process (Sigman et al., 2009a). Under these conditions, nitrification causes a deviation below the 1:1 line in $\delta^{18}O$ vs. $\delta^{15}N$ space (into the pink shaded area in Figure 2.8), since the $\delta^{18}O$ of nitrate is lowered without a corresponding decrease in $\delta^{15}N$ (Sigman et al., 2009c).

An important exception exists in regions of active N_2-fixation (case 2; such as the sub-tropical gyres), where PN produced in the surface and available for regeneration in the thermocline, where it accumulates, is low in $\delta^{15}N$ (close to 0‰) (Sigman et al., 2000). In this setting, nitrification acts instead to lower the $\delta^{15}N$ of sub-surface nitrate more than it lowers its $\delta^{18}O$, yielding a deviation above the 1:1 line in $\delta^{18}O$ vs. $\delta^{15}N$ space (Sigman et al., 2005) (into the blue shaded area in Figure 2.8).

In the high-latitude ocean (case 3; e.g., the Southern Ocean), nitrate is only partially consumed within surface waters, such that the $\delta^{15}N$ of PN produced there is relatively low (i.e., compared to the original nitrate source) (Sigman et al., 1999a). When this PN undergoes regeneration to nitrate, both the $\delta^{15}N$ and $\delta^{18}O$ of the surrounding nitrate are lowered (with $\delta^{18}O$ lowered towards the nitrification value of ~1.1‰, and $\delta^{15}N$ lowered towards the $\delta^{15}N$ of the PN being regenerated) (Sigman et al., 2009a). The overall effect of nitrification in this environment, however, is to lower ambient nitrate $\delta^{15}N$ more than it lowers its $\delta^{18}O$, producing a deviation above the 1:1 line in $\delta^{18}O$ vs. $\delta^{15}N$ space (Rafter et al., 2013) (into the blue shaded area in Figure 2.8).

For the purpose of quantifying the deviation from a 1:1 $\delta^{18}O$-to-$\delta^{15}N$ relationship (expected for pure nitrate assimilation and/or denitrification) and thus the extent to which the N and O isotopes of nitrate are decoupled, Sigman et al. (2005) developed the Δ(15,18) parameter, defined as:

$$\Delta(15,18) \equiv (\delta^{15}N - \delta^{15}N_m) - ({}^{15}\varepsilon/{}^{18}\varepsilon) * (\delta^{18}O - \delta^{18}O_m)$$

where $\delta^{15}N$ and $\delta^{18}O$ are the measured isotope values for a given nitrate sample, $\delta^{15}N_m$ and $\delta^{18}O_m$ represent the mean isotopic composition of the nitrate supplied to the system, and ${}^{15}\varepsilon/{}^{18}\varepsilon$ is the N-to-O isotope effect ratio of the nitrate-consuming process (Sigman et al., 2005; Sigman et al., 2009c); i.e., assimilation or denitrification, both of which are close to 1 according to culture studies (Granger et al., 2004; Granger et al., 2008).

Rafter et al. (2013) subsequently adopted a simpler approach using Δ(15-18), the difference between the $\delta^{15}N$ and $\delta^{18}O$ of nitrate, as an indicator of decoupling:

$$\Delta(15-18) = \delta^{15}N - \delta^{18}O$$

which is similar to the Δ(15,18) parameter, except that Δ(15-18) is not normalized to the background of deep nitrate isotopic composition. Taking the Pacific sector of the Southern Ocean as an example and using the average $\delta^{15}N$ and $\delta^{18}O$ values of UCDW (the deep nitrate source; 5.0 ± 0.1‰ and 2.0 ± 0.3‰, respectively) gives a Δ(15-18) = 5.0‰ - 2.0‰ = 3.0‰, which can be thought of as the baseline value for this parameter (rather than 0‰ in the case of Δ(15,18)) in this system (Rafter et al., 2013). In this notation, nitrate with a Δ(15-18) > 3.0‰ would represent a deviation below the 1:1 line in $\delta^{18}O$ vs. $\delta^{15}N$ space (as in the case of complete nitrate assimilation followed by nitrification; case 1 described above), while nitrate with a Δ(15-18) < 3.0‰ would represent a deviation above the 1:1 line (as in the case of either N_2-fixation or partial nitrate assimilation followed by nitrification; cases 2 and 3, respectively) (Figure 2.8).

The value of these coupled-isotope parameters (e.g., nitrate Δ(15-18)) lies in the fact that they are conserved for mixing, nitrate assimilation and denitrification (which alter $\delta^{15}N$ and $\delta^{18}O$ 'in sync'), but sensitive to the regeneration of organic matter, allowing these processes to be disentangled (Rafter et al., 2013).

A dual isotope approach was taken by DiFiore et al. (2009) in an investigation of nitrate dynamics in the upper water column of the summertime coastal PAZ. The N and O isotopes

of nitrate were found to be closely coupled, with profile data falling close to the 1:1 line in $\delta^{18}O$ vs. $\delta^{15}N$ space (i.e., nitrate Δ(15-18) remaining close to the baseline value from depth towards the surface). The data was interpreted as reflecting the dominance of nitrate assimilation in the system (which imparts a ~1:1 increase in the $\delta^{18}O$ vs. $\delta^{15}N$ of nitrate), with minimal euphotic zone nitrification (which would cause a deviation from the 1:1 relationship) (DiFiore et al., 2009).

The minor role for nitrification in the PAZ summer mixed layer indicated by this study (which could potentially disconnect sinking and sedimentary $\delta^{15}N$ from the degree of surface nitrate utilization) is good news for the interpretation of paleo-$\delta^{15}N$ records. Another important implication is for the estimation of organic carbon export in the modern ocean based on the f-ratio, the ratio of new production to primary (i.e., new plus regenerated) production. Assuming that nitrification is negligible within the surface ocean (a traditionally accepted view) has led to the use of a simplified form of the f-ratio, with nitrate uptake as an approximation for new production (Dugdale & Goering, 1967; Eppley & Peterson, 1979; Olson, 1981). If, however, some of the nitrate taken up by phytoplankton is from nitrification within the euphotic zone (i.e., regenerated *in situ* rather than newly supplied from below), use of this simplified f-ratio would lead to overestimation of organic carbon exported to the deep ocean (Dugdale & Goering, 1967; Diaz & Raimbault, 2000; Yool et al., 2007). From this point of view, the findings of DiFiore et al. (2009) (i.e., minimal euphotic zone nitrification) are also good news for previous estimates of export production in the PAZ.

Given the potential implications for both paleo- and modern-ocean work, we take on a similar dual isotope approach in our investigation of nitrate dynamics in the wintertime Atlantic sector of the Southern Ocean.

2.6 Scope of the thesis

The oceanic region south of Africa represents uncharted territory in the field of nitrate isotopes. Consequently, the first goal of this work is to provide a detailed description of nitrate isotope patterns in the Atlantic sector for comparison with previous measurements from the Indian and Pacific sectors of the Southern Ocean, offering extended insight into the circumpolar continuity of nitrate isotope dynamics and water mass evolution within the Southern Ocean.

More importantly, the data reported here are from the wintertime. As the review of previous field-based studies (section 2.4) reveals, a common limitation in estimating the isotope effect of nitrate assimilation from summertime data is uncertainty regarding the initial nitrate source; i.e., which $[NO_3^-]$ and $\delta^{15}N$ values to assume as the starting-point for assimilation in Rayleigh space. This is particularly problematic in the OAZ where the different potential source waters (namely, UCDW and the T_{min} layer) yield conflicting estimates for the isotope effect (Sigman et al., 1999a; Karsh et al., 2003; DiFiore et al., 2010). By uncovering the wintertime conditions that precede the growing season, it is hoped that the dataset reported here might contribute to resolving such questions and lead to improved estimates for the isotope effect of nitrate assimilation in the Southern Ocean. Furthermore, both the N and O isotope ratios of nitrate were measured, to assist in isolating the different biogeochemical and physical processes responsible for the observed patterns.

The present study is highly relevant to the field of paleoceanography, in that it touches on each of the three major challenges currently hindering the application of N isotopes as a paleo-nutrient proxy (highlighted in section 2.3.2); namely, defining the initial nitrate source, quantifying the isotope effect, and discerning additional N cycling processes (like nitrification) that might mask the nitrate assimilation signal. Moreover, this work may provide valuable insights into the workings of the modern-day Southern Ocean (e.g., the biological pump). It is with these motivations that this study is undertaken.

We begin with a description of the methods employed in collecting and analysing the samples from the wintertime Atlantic sector, and subsequently present the resulting nitrate and PN isotope data within the hydrographic and biogeochemical context of the region. After establishing a broad overview of the nitrate N and O isotope distributions south of Africa, we narrow our focus to the AZ where some unexpected gradients in nitrate isotope composition are noted, and consider various N cycling scenarios that might explain the observed anomalies. We end with a dual isotope synopsis of the entire depth section between South Africa and Antarctica.

3. Methods

In this chapter, we outline the sample collection procedures used at sea as well as the laboratory methods employed to analyse these samples. The resulting dataset provides a first glimpse into the distribution of the nitrogen (N) and oxygen (O) isotopes of nitrate in the sector south of Africa, and is the most extensive dataset of its kind from the wintertime Southern Ocean to date.

3.1 Sample collection

Samples were collected in July 2012 (austral winter) on the maiden scientific voyage of the R/V *S.A. Agulhas II* (VOY03). Sampling efforts were focused on the Good Hope monitoring line (Ansorge et al., 2005) between Cape Town (South Africa) and Antarctica (leg 1; Figure 3.1). Twenty-two hydrocast profile stations were performed on this transect between the subtropics (34.6°S) and the winter sea-ice edge (encountered at 56.7°S), with the southernmost station located in the sea ice at 57.8°S. Temperature and salinity profiles were obtained from a Sea-Bird Conductivity Temperature Depth (CTD) sensor mounted on the Niskin bottle rosette, as well as from 28 Underway-CTD (UCTD) deployments made on leg 1. A total of 88 Expendable Bathythermograph (XBT) deployments were made during this transect, providing additional temperature profiles. Acoustic Doppler Current Profiler (ADCP) data was also collected between CTD stations (Ansorge, 2012). These data provide the physical oceanographic context for our analyses.

The major circumpolar fronts were identified using surface and subsurface (200 m) temperature and salinity properties, based on the definitions of Belkin & Gordon (1996) and Holliday & Read (1998) (positions shown in Figure 3.1). For all casts, mixed-layer depth was determined from depth profiles of sigma-theta (σ_θ; calculated from temperature and salinity), with the mixed-layer depth at each station defined as the closest depth to the surface at which σ_θ is greater by $\geq$ 0.03 kg m^{-3} than the value at a reference depth of 32 m (the shallowest depth common to every CTD station); $\Delta\sigma_\theta$ = 0.03 kg m^{-3} being the density criterion of de Boyer Montégut et al. (2004).

Fifteen of the twenty-two CTD stations on leg 1 were sampled (red dots in Figure 3.1), seven of which reached 1000 m and eight of which extended to 2000 m or more. From each depth (see Figure 4.3 for sample depths), an unfiltered seawater sample was collected in a rinsed 60 ml HDPE bottle (filled to the bottle shoulder) for dissolved nitrate concentration ($[NO_3^-]$) and nitrate $\delta^{15}N$ and $\delta^{18}O$. Samples were immediately frozen and stored at -20°C for later analysis.

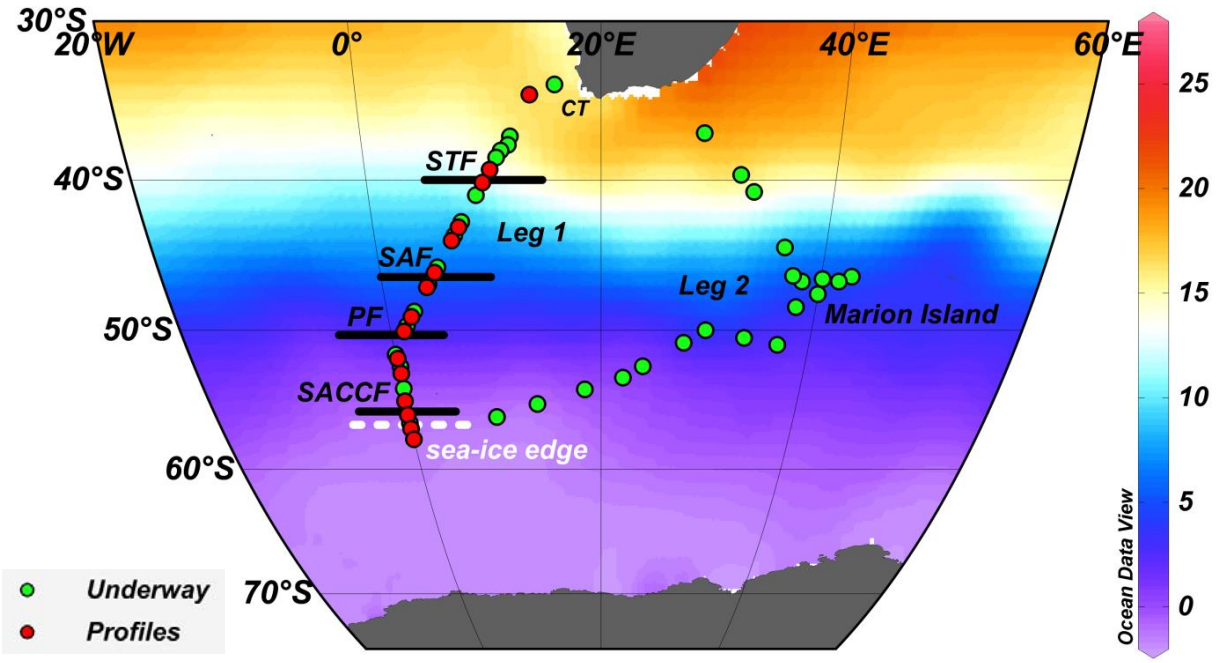

Figure 3.1 Sampling locations on the wintertime voyage (VOY03) south of Africa in July 2012. During leg 1 (the Good Hope line, between Cape Town and the Antarctic winter sea-ice edge), both CTD profile and underway collections were made; while on leg 2 (from the ice-edge to Marion Island and back to South Africa), only underway samples were collected. Green symbols represent underway stations and red dots represent profile stations. The cruise track is plotted against the *World Ocean Atlas* 2009 (WOA09) sea surface temperature (°C) climatology for July (http://www.nodc.noaa.gov/OC5/WOA09/pr_woa09.html). The thick black lines denote the latitudes of the major fronts on leg 1; from north to south, they are the Subtropical Front (STF), the Subantarctic front (SAF), the Polar Front (PF) and the Southern Antarctic Circumpolar Current Front (SACCF). The white dashed line indicates the latitude of the sea ice-edge at the time of the cruise.

Along the Good Hope Line, underway surface samples (green dots in Figure 3.1) were collected in duplicate from the ship's underway system (intake situated at ~7 m) via parallel inline filtration of seawater through 47 mm, 0.4 µm polycarbonate filters. All filtration equipment (inline filter holders, tubing, and connectors) was acid washed with 10% hydrochloric acid (HCl), followed by three rinses with de-ionized MilliQ water prior to use.

At the beginning of each underway collection, 60 ml HDPE sample bottles were rinsed, filled to the shoulder with filtrate, and immediately transferred to a -20°C freezer for later analysis of $[NO_3^-]$ and nitrate $\delta^{15}N$ and $\delta^{18}O$. Filtration was allowed to continue until (i) the filters clogged, (ii) 10 l was reached, or (iii) roughly 2 hours had passed.

After filtration was terminated, the final volumes filtered were recorded. Each polycarbonate filter was removed and stored according to the protocol of Fawcett et al. (2011) to allow for future $\delta^{15}N$ measurements of the flow cytometrically sorted components of particulate N (PN) captured on the filters. Briefly, each polycarbonate filter was folded lengthwise using ethanol-cleaned forceps and placed in an acid-washed 5 ml cryovial with approximately 4 ml of 0.2 μm-filtered seawater (with $[NO_3^-]$ ~ 2.75 μM; collected in sub-tropical waters (33°56.879'S, 16°16.305'E) at the start of the voyage). Seventy microliters of 37% formaldehyde solution (PFA) was added to achieve a final concentration of 0.5% PFA in each vial. Cryovials were sealed and gently shaken to re-suspend the particles and facilitate "fixation" by the PFA. After cooling at 4°C for 1-4 hours, which also serves to encourage fixation, the samples were transferred to a -80°C freezer for storage.

The Good Hope leg was followed by a transect from the sea-ice edge to Marion Island (46.913°S; 37.744°E), and from Marion back to South Africa (leg 2; Figure 3.1). Here, only underway samples were collected. Although the Good Hope Line forms the core of this study, these additional transects allow for a broader view of the nitrate isotope distributions south of Africa, permitting some degree of investigation into zonal continuity, and providing additional PN samples for bulk N isotope analysis.

On leg 2 of the voyage, two parallel inline filtration systems were assembled to allow duplicate polycarbonate and glass fibre filter (GF/F) particle collections to be made simultaneously, and their associated filtrates sampled. An additional unfiltered seawater sample was collected at each underway station for comparison with filtered seawater samples. No systematic difference is observed between the N and O isotope ratios of nitrate for filtered and unfiltered seawater collections at the same underway sites (see Appendix A), an important observation since underway samples were filtered while profile samples were not.

The purpose of the GF/F collections was to provide material for direct measurement of zonal gradients in the N isotope composition of bulk suspended PN. At the termination of filtration, each polycarbonate filter was stored as described above, while each GF/F was

folded in half using ethanol-cleaned forceps, wrapped in a square of ashed tinfoil, and frozen at -80°C. Both the GF/Fs and tinfoil were precombusted at 400°C for 8 hours before the voyage to remove any pre-existing organic contaminants.

Throughout the voyage, underway collections were scheduled to coincide with standard biological measurements of chlorophyll-a, particulate organic carbon and nutrients (nitrate, nitrite, phosphate, ammonium, and silicate). The same biological data (from discrete sample collections) as well as oxygen and florescence profiles (from mounted oxygen and florescence sensors) were obtained from every CTD cast. Furthermore, nitrate and ammonium uptake rates were estimated from on-deck ^{15}N tracer incubations (Dugdale & Goering, 1967; Gandhi et al., 2012). Sample water collections for these incubations were made at a total of 8 CTD stations during the voyage (6 on leg 1, and 2 on leg 2), providing uptake rates at the 1% and 55% light levels. A further 5 underway collections were made (1 on leg 1, and 4 on leg 2), providing uptake rates at the 55% light level only (Philibert et al., *in preparation*). Together, these data provide the biogeochemical context for our isotope measurements.

At the end of the voyage, the nitrate and PN samples were shipped frozen on dry ice to Princeton University where they were stored at -20°C and -80°C, respectively, for later isotope analysis.

3.2 Laboratory methods

3.2.1 Nitrate concentration

Measurements of $[NO_3^-]$ were made on board the R/V *S.A. Agulhas II* by flow injection and standard colorimetric analysis. Sample nitrate was reduced to nitrite as it was passed through a copper-cadmium column. The addition of a sulphanilamide colour reagent containing N-(1-napthyl)-ethylenediamine dihydrochloride allowed the resulting nitrite concentration ($[NO_2^-]$) (the sum of that which was originally present in the seawater and that which was converted from nitrate) to be inferred from a spectrophotometer absorbance reading (Strickland & Parsons, 1972; Eriksen, 1997).

The resulting concentrations are, therefore, a measure of nitrate plus nitrite (i.e., $[NO_3^- + NO_2^-]$). Measurements of sample $[NO_2^-]$ alone indicate deep (> 200 m) concentrations of less than

0.1 μM (< 0.5% of the combined [NO_3^- + NO_2^-] pool), and mixed-layer concentrations typically between 0.2 μM and 0.3 μM (0.75-3.0% of the combined [NO_3^- + NO_2^-] pool) across most of the hydrocast transect. Below, we refer to nitrate plus nitrite measurements as nitrate measurements (as in previous studies; e.g., Sigman et al., 1999a; DiFiore et al., 2009), except in section 3.2.4 below and Appendix B, where we explicitly address the role of the nitrite pool.

Concentration measurements obtained from colorimetric analysis were reported in units of μg N l^{-1}. Profile measurements were converted to μM (i.e., μmol l^{-1}) using potential density calculated from CTD data (salinity, temperature, and pressure), while surface underway measurements were converted to μM assuming a constant seawater density of 1.027 kg l^{-1} (as is routinely done in the literature; e.g., Sigman et al., 2000).

On-board [NO_3^-] measurements from the same stations and depths as our collected seawater samples provide information necessary for nitrate isotope analysis. The isotope measurement protocol, in turn, yields information regarding the amount of N in each sample; which, as we describe below, provides an additional means by which the sample [NO_3^-] can be determined (Altabet & Francois, 2001). It is this "back-calculated" [NO_3^-] that we use in further data analyses.

3.2.2 Nitrate isotopes: $\delta^{15}N$ and $\delta^{18}O$

A central goal of this study is to accurately resolve variations in the N and O isotopes of nitrate ($\delta^{15}N$ and $\delta^{18}O$, respectively) across the Atlantic sector of the Southern Ocean. Nitrate $\delta^{15}N$ and $\delta^{18}O$ analyses were carried out using the "denitrifier method" in conjunction with gas chromatography and isotope ratio mass spectrometry (Sigman et al., 2001; Casciotti et al., 2002). The denitrifier method involves the transformation of dissolved nitrate ($NO_{3\,(aq)}^-$) into nitrous oxide ($N_2O_{(g)}$) via naturally occurring denitrifying bacterial strains that lack an active form of the enzyme N_2O reductase (which converts $N_2O_{(g)}$ to $N_{2(g)}$); causing these strains to quantitatively convert nitrate-N to N_2O-N via the following pathway:

$$2NO_{3\,(aq)}^- \rightarrow 2NO_{2\,(aq)}^- \rightarrow 2NO_{(g)} \rightarrow N_2O_{(g)}$$

Compared with earlier methods involving the conversion of nitrate to $N_{2(g)}$, this approach is more than two orders of magnitude more sensitive, allowing for routine, high-precision analyses at 5 nmols of N. This greatly facilitated the at-sea sampling because of the reduced

sample water volumes required. Furthermore, O isotope analysis of nitrate can also be done with the denitrifier method (Casciotti et al., 2002), which is central to our study.

Preservation of the original isotope ratio relies on the complete conversion of sample nitrate to N_2O, such that the fractionation inherent in the denitrification pathway (Mariotti et al., 1981; Barford et al., 1999) is not expressed. With respect to N atoms, the process represents a mass-balance reaction. Thus, provided that the initial nitrate is fully converted and there are no 'hidden' N pools contributing to the resulting N_2O, the $\delta^{15}N$ of the product will be identical to that of the reactant (Sigman et al., 2001). In the case of O, however, only one of the six initial O atoms remains in the product N_2O, potentially subjecting sample nitrate $\delta^{18}O$ to the effects of fractionation (via preferential loss of the ^{16}O atoms during the reduction process) and exchange (with the surrounding H_2O). Fortunately, both preventative and corrective measures can be taken to address these concerns (Casciotti et al., 2002).

Two strains of denitrifying bacteria are routinely cultivated in the Sigman Laboratory at Princeton University: *Pseudomonas chlororaphis* and *Pseudomonas aureofaciens*. While *P. chlororaphis* tends to be more robust in culture and manipulations, *P. aureofaciens* has been found to exchange fewer oxygen atoms with water (typically less than 4% for this data set) and in a reproducible fashion within a given harvest of bacterial cells, making it the strain of choice for $\delta^{18}O$ measurements (Sigman et al., 2001; Casciotti et al., 2002).

Bacterial growth medium was prepared by amending Triptic Soy Broth (TSB) with potassium nitrate, dipotassium phosphate and ammonium sulphate (in the case of *P. chlororaphis*, or ammonium chloride in the case of *P. aureofaciens*), followed by autoclaving for 30 to 50 minutes. The autoclaved media bottle was then inoculated from a starter tube, containing a single colony of the appropriate bacterial strain, grown overnight on the same amended TSB medium. The inoculated bacterial medium was incubated on a rotary shaker for 6–10 days (depending on the strain of bacteria), sufficient time for any O_2 in the headspace and nitrate in the medium to be consumed (Sigman et al., 2001).

On the day of the harvest, after testing for the presence of nitrate/nitrite, the bacterial medium was divided equally among 12 sterile centrifuge tubes (~67 ml each) and centrifuged (7600 rpm) at 18°C for 10 minutes. Centrifugation results in the formation of a dense bacterial pellet at the bottom of each tube, such that the spent medium can then be decanted. Approximately 8 ml of a nitrate-free medium and one drop of Antifoam-B emulsion (Sigma

MKBH3127) was added to each tube, and the bacteria were resuspended by vortexing. The contents of all tubes were then combined to produce a homogenised, concentrated bacterial medium. After pipetting 1 ml of this concentrate into muffled glass 20 ml headspace vials (typically 80 per run), each one was fitted with a butyl septum and an aluminium top seal, and crimped to seal. The sealed vials were purged with helium on a needle rack for 3 hours to flush the headspace of any N_2O or O_2 that could contaminate the sample or interfere with the conversion of sample nitrate to N_2O (Sigman et al., 2001).

Once the vials had been removed from the needle rack, they were injected with sample nitrate using a glass barrel syringe, which was rinsed three times with de-ionized water (DIW) and three times with sample seawater before injecting. Injection volumes were calculated on an individual sample basis (using the measured $[NO_3^-]$) such that the same final quantity of N was added to each vial. Samples with $[NO_3^-]$ in the 1.8-5 μM range were run at 5 nmol of N (i.e., 1-2.8 ml added to each vial), samples with $[NO_3^-]$ in the 5-15 μM range were run at 10 nmol (i.e., 0.67-2 ml added to each vial), and samples with $[NO_3^-]$ exceeding 15 μM were run at 20 nmol (i.e., ≤1.3 ml added to each vial). The same procedure was applied to any standards that were injected and run alongside the sample vials.

Tailoring a run in this way minimizes the error introduced by any non-linear behaviour of the isotope ratio mass spectrometer at different N sample sizes. Furthermore, restricting sample injections to a specified volume range limits the range of dilutions imposed upon the bacteria within any given batch of analyses, which likely improves precision.

A typical run of 80 vials consisted of 57 seawater samples (within which some samples were duplicated), 19 standards (specifically, 8 replicates of IAEA-N3, 8 replicates of USGS-34 and 3 replicates of Deep Pacific Reference, see below), 2 backgrounds (i.e., vials containing bacterial concentrate but no sample, prepared in the same way as every other vial) and 2 blanks (i.e., vials containing bacterial concentrate and an injection (of approximately the same volume as the samples) of low-nitrate ($[NO_3^-] < 0.02$ μM) Sargasso Sea water).

IAEA-N3 and USGS-34 are international nitrate standards that were used to calibrate the measured N isotope ratios to N_2 in air, and O isotope ratios to Vienna Standard Mean Ocean Water (VSMOW). IAEA-N3 has a $\delta^{15}N$ of +4.7‰ vs. air (Gonfiantini et al., 1995) and a $\delta^{18}O$ of +25.6‰ vs. VSMOW (Böhlke et al., 2003), while USGS-34 has a $\delta^{15}N$ of -1.8‰ vs. air and a $\delta^{18}O$ of -27.9‰ vs. VSMOW (Böhlke et al., 2003). The concentrations of IAEA-N3

and USGS-34 standards used in each run were chosen to match those of the samples as closely as possible (i.e., 2 μM and 5 μM standards for 5 nmol runs, 5 μM and 15 μM standards for 10 nmol runs, and 30 μM standards for 20 nmol runs). Deep Pacific Reference (DPR) is an 'in-house' nitrate standard used to monitor inter- and intra-run variability. It has a $[NO_3^-]$ of approximately 37 μM and yielded a $\delta^{15}N$ of 5.25 ± 0.03‰ vs. air and a $\delta^{18}O$ of 2.20 ± 0.18‰ vs. VSMOW for all 20 nmol runs during the measurement period.

Once all the injections had been completed, the vials were shaken, inverted, and stored in the dark at room temperature overnight to allow for the complete conversion of nitrate to N_2O by the bacteria. After 12-18 hours, the reaction was terminated by the injection of 0.1-0.2 ml of 10N sodium hydroxide (NaOH) into each vial. In addition to lysing the bacteria, the NaOH acts to remove most of the $CO_{2(g)}$ from the headspace (by raising the pH of the medium above 12 and driving the carbonate equilibrium towards $CO_3^{2-}{}_{(aq)}$); CO_2 and N_2O generate ions with the same mass-to-charge ratio, and thus separation of the N_2O from CO_2 is a central goal of the N_2O extraction and purification (Sigman et al., 2001). Three to four drops of Antifoam-B emulsion were injected into each vial after the NaOH. An additional set of sealed vials (~16 per run of 80) were purged with helium for 15-20 minutes, and then injected with the target amount of N_2O (e.g., 20 nmol of N). These vials were interspersed regularly among the bacterial vials within the run to serve as a check on inter-run variability, and could be used to correct for any isotopic 'drift' associated with the mass spectrometer.

The N_2O in each vial was then extracted on-line by an automated sampler (using helium as a carrier-gas) and passed through a series of purification systems: first, a chilled ethanol trap (to remove water and any volatile organics); second, a Nafion drier (to remove water); and third, a chemical trap containing 'ascarite', a sodium hydroxide-coated silica (to remove CO_2), and magnesium perchlorate (to remove any residual water). What remains of the sample gas is cryogenically trapped and focused (using liquid nitrogen traps), and chromatographically separated (from any remaining CO_2) before reaching the open split of the mass spectrometer (Finnigan MAT235) (the instrumentation changes from Casciotti et al., 2002 can be found in McIlvin & Casciotti, 2011 and Foriel et al., *in preparation*). The 45/44 and 46/44 ratios of the analyte N_2O were then measured under continuous flow, relative to pulses of N_2O from a reference tank.

Before the measured ratios (45/44 and 46/44) could be calibrated using the international nitrate standards, they were corrected for the presence of the rare ^{17}O isotope, and the

contribution of the blank (i.e., any N_2O that did not derive from the injected sample/standard; Sigman et al., 2001; Casciotti et al., 2002). The size of the blank (calculated using the mass spectrometer peak areas produced by "blank" and "background" vials in each run) was typically less than 0.1 nmol of N (i.e., ≤0.5% of a 20 nmol sample, or ≤1% of a 10 nmol sample). This is a great improvement on earlier blanks which were commonly ~0.5 nmol of N (Sigman et al., 2001). A further correction was applied to the O isotope ratios to account for any exchange with H_2O in the vial (Casciotti et al., 2002; Sigman et al., 2009a). Finally, the corrected $\delta^{15}N$ and $\delta^{18}O$ values were referenced to atmospheric N_2 and VSMOW respectively, using the known and measured isotope values of IAEA-N3 and USGS-34.

Each seawater sample was analysed one to three times using *P. chlororaphis* (which provides only $\delta^{15}N$), and at least three times using *P. aureofaciens* (which provides both $\delta^{15}N$ and $\delta^{18}O$). Samples with standard deviations > 0.2‰ for $\delta^{15}N$ and > 0.5‰ for $\delta^{18}O$ (roughly four times the average sample standard deviation for all measurements, or twice the 90th percentile – see below) were identified and re-measured to ensure at least three valid measurements of $\delta^{15}N$ and $\delta^{18}O$ per sample.

After ensuring no significant discrepancies between the $\delta^{15}N$ values yielded by the two strains of bacteria (with the $\delta^{15}N$ yielded by *P. chlororaphis* being, on average, 0.05‰ higher than that yielded by *P. aureofaciens*; likely associated with the greater importance of the ^{17}O correction with *P. aureofaciens*), all valid $\delta^{15}N$ measurements for each sample were averaged. The sample standard deviation for $\delta^{15}N$ was 0.04‰ on average, and <0.08‰ for more than 90% of the samples. Since our sample averages incorporate both single and duplicate measurements from between two and five separate runs, they represent both inter- and intra-run variability. The overall precision of the denitrifier method for $\delta^{15}N$ was initially quoted as 0.2‰ (Sigman et al., 2001). The greater precision achieved in this study can be attributed to on-going laboratory method development and technological improvements in the automated system (McIlvin & Casciotti, 2011; Foriel et al., *in preparation*).

Similarly, all three to five valid $\delta^{18}O$ measurements were averaged for each sample (i.e., representing two to three different run days), resulting in a sample standard deviation of 0.14‰ on average, and <0.25‰ in 90% of cases. The higher standard deviation of $\delta^{18}O$ compared to $\delta^{15}N$ is inherent to the measurement of the O isotopes of nitrate, for which there exists greater potential for expressed fractionation as well as exchange with sample water (Casciotti et al., 2002). Nonetheless, the precision of $\delta^{18}O$ measurements reported here

signifies an improvement, with the data in Casciotti et al. (2002) yielding standard deviations of 0.34‰ on average within a run, and 0.42‰ between different runs (i.e., different days and different bacteria). This improved precision allows us to more fully investigate subtle changes in the N and O isotopes of nitrate across the Southern Ocean, particularly in the wintertime AZ (the isotope gradients of which are relatively weak).

As mentioned previously, each isotope analysis also provides a measure of the N yield (in the form of the mass spectrometer peak area), which we used to "back-calculate" the [NO_3^-] of the samples (Altabet & Francois, 2001). Although subject to injection error, repeated measurements (i.e., three to seven for each sample) reduces the standard error to 0.2 μM on average (and <0.4 μM for over 95% of the samples).

3.2.3 $\delta^{15}N$ of bulk suspended PN

The $\delta^{15}N$ of bulk suspended PN was determined from the underway GF/F collections made during leg 2 of the winter voyage (i.e., from the sea-ice edge to Marion Island and back to South Africa).

Frozen GF/Fs (samples and blanks, see below) were dried in a desiccating oven at 65°C for 24-48 hours. Two small subsamples were cored from each GF/F and transferred to 4 ml combusted Wheaton vials. The PN captured on each filter fraction was then oxidized to nitrate using the persulfate oxidation method of Knapp et al. (2005), following adaptations described in Fawcett et al. (*in review*). Briefly, 2 ml of a freshly made potassium persulfate oxidizing reagent (POR) was added to each sample vial, to triplicate vials containing two L-glutamic acid standards (USGS-40 and USGS-41; Qi et al., 2003) at a range of concentrations, and to six vials containing subsamples of GF/F through which filtered seawater (but no particles) had been passed before the GF/F was processed in the same manner as the samples (i.e., "GF/F blanks"). The POR itself was made by dissolving 2.5 g of potassium persulfate (recrystallized four times according to the protocol described by Knapp et al. (2005), after Koroleff (1983), and rinsed with methanol to remove adsorbed organic contaminants and speed up crystal drying (Higgins et al., 2009)) and 2.5 g of NaOH in 100 ml of DIW. After POR addition, the vials were capped tightly and autoclaved for 55 minutes at 121°C on a slow-vent setting.

After oxidation, sample pH was lowered to 5-8 using 12N ACS grade HCl in order to prevent the high pH of the POR from killing the denitrifying bacteria. The concentration of the

resultant nitrate was determined via chemiluminescent analysis (Garside, 1982; Braman & Hendrix, 1989), in which nitrate was reduced by vanadium(III) to nitric oxide ($NO_{(g)}$), which was quantified based on the intensity of the photoreaction with excess ozone.

The oxidised PN samples were then analysed for $\delta^{15}N$ in the same way as the seawater nitrate samples, except that only *P. chlororaphis* was used for conversion of nitrate to N_2O, and DIW- (rather than seawater-) based standards were run alongside the samples during isotope analysis. The final N content and $\delta^{15}N$ of the oxidized samples was corrected for the POR-associated N blank (which included the GF/F blank) and N content was converted to N concentration (i.e., [PN]) based on the volume filtered for each sample during the underway collections.

3.2.4. Nitrite removal from seawater samples

To this point, every seawater sample was treated as if the nitrite contribution to the nitrate plus nitrite pool was negligible. Here we outline our efforts to quantify the isotopic effect of nitrite in the upper ocean, where its concentration relative to nitrate is highest in the Southern Ocean. The N isotopic effect of nitrite depends on the relative quantity and $\delta^{15}N$ composition of nitrite simply because it represents a portion of the nitrate plus nitrite pool. The O isotopic effect is more complex. The N_2O generated from nitrite by the denitrifier method is ~25‰ lower in $\delta^{18}O$ than N_2O generated from nitrate (Casciotti et al., 2007; Rafter et al., 2013); thus, unknowingly measuring nitrite as nitrate causes one to underestimate the $\delta^{18}O$ of nitrate plus nitrite in the sample, with the error being worse for a higher ratio of nitrite to nitrate in the sample (Granger et al., 2006; Granger & Sigman, 2009).

A seawater sample from each underway station, at least one sample from the mixed layer of each CTD station, and a selection of depth profile samples (from six different CTD stations) were selected for nitrite removal. Subsequent to nitrite removal with sulphamic acid (which converts nitrite to N_2 at a pH of ~1.7), the N and O isotopes of these samples were reanalysed (Granger & Sigman, 2009).

Nitrite was removed from the selected samples on the day of the harvest as follows: After aliquoting the desired volume (5-10 ml) of sample seawater into an acid-washed HDPE bottle, 10 µl of a sulphamic acid solution (2% w/v sulphamic acid in 10% v/v HCl) was added per 1 ml of sample. Each sample was then shaken thoroughly and left to react at room temperature for 10 minutes, during which time any nitrite in the sample was reduced to N_2

(Granger & Sigman, 2009). The pH of each sample was then restored to near neutral by adding 5.5 µl of 2N NaOH per 1 ml of sample, shaking, and leaving at room temperature for 10 minutes; after which the final pH was confirmed using a pH indicator strip.

These samples, together with their untreated counterparts, were then converted to N_2O using the denitrifier method and their isotope ratios measured as described above. The process was repeated until two to five measurements of each 'nitrite-removed' sample had been obtained. The results of this nitrite removal experiment are presented and their implications discussed in Appendix B.

4. Results

4.1 Physical and biogeochemical overview

4.1.1 Hydrographic context

The wintertime hydrocast transect between South Africa and the Antarctic sea-ice edge (which represents the core of this study) encompasses a wide range of oceanic environments, from the colder (< 0°C), fresher (< 34.2 psu) surface waters of the polar ocean to the warmer (> 10°C), saltier (> 35.0 psu) waters of the subtropics (Figure 4.1a&b). Surface and subsurface (200 m) temperature and salinity properties place the Southern Antarctic Circumpolar Current Front (SACCF) at 55.7°S, the Polar Front (PF) at 50.3°S, the Subantarctic Front (SAF) at 46.4°S, and the Subtropical Front (STF) at 39.7°-40.9°S along the Good Hope line (based on the criteria of Belkin & Gordon (1996) and Holliday & Read (1998); positions indicated in Figure 3.1 and Figure 4.1a-f).

Mixed-layer depth generally increases northwards from 93-124 m in the Polar Antarctic Zone (PAZ; region south of the SACCF), to 108-137 m in the Open Antarctic Zone (OAZ; between the SACCF and the PF), to 113-153 m in the Polar Frontal Zone (PFZ; between the PF and the SAF), and 122-189 m in the Subantarctic Zone (SAZ; between the SAF and the STF). In the Subtropical Zone (STZ; north of the STF) between 35°S and 40°S, mixed layers of up to 250 m are noted in the CTD data (station at 39.3°S), and > 300 m according to XBT and UCTD data (data not shown; Ansorge, 2012).

4.1.2 Water mass identification

In the upper 100 m of the transect, equatorward increases in temperature and salinity are accompanied by decreases in oxygen (from > 7.5 ml l^{-1} in the PAZ to < 5.5 ml l^{-1} in the STZ) (Figure 4.1c) and nitrate concentration ($[NO_3^-]$; from > 28.0 µM to < 4.0 µM) (Figure 4.1d). Considering the full depth sections (0-2000 m) of temperature, salinity, oxygen and $[NO_3^-]$ together, some distinct sub-surface features emerge. These are described below.

(a) Temperature

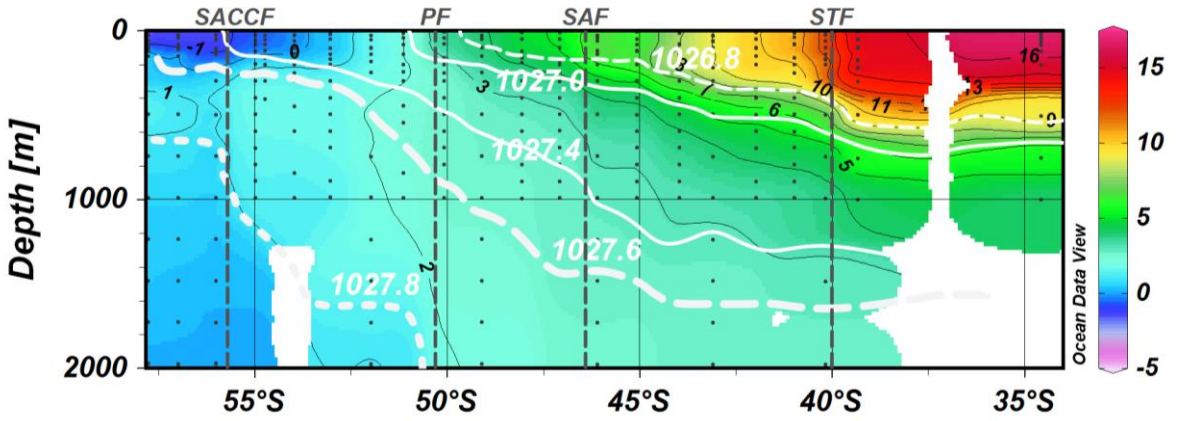

(b) Salinity

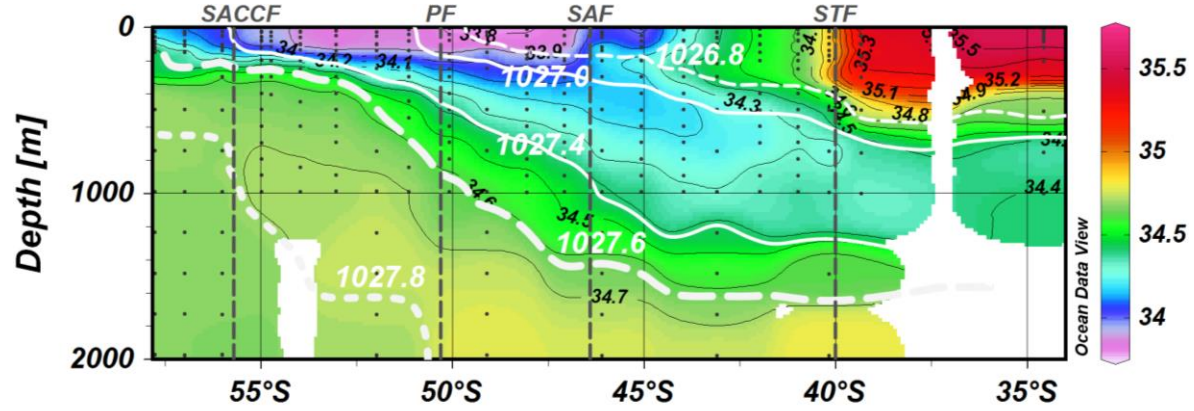

(c) Oxygen

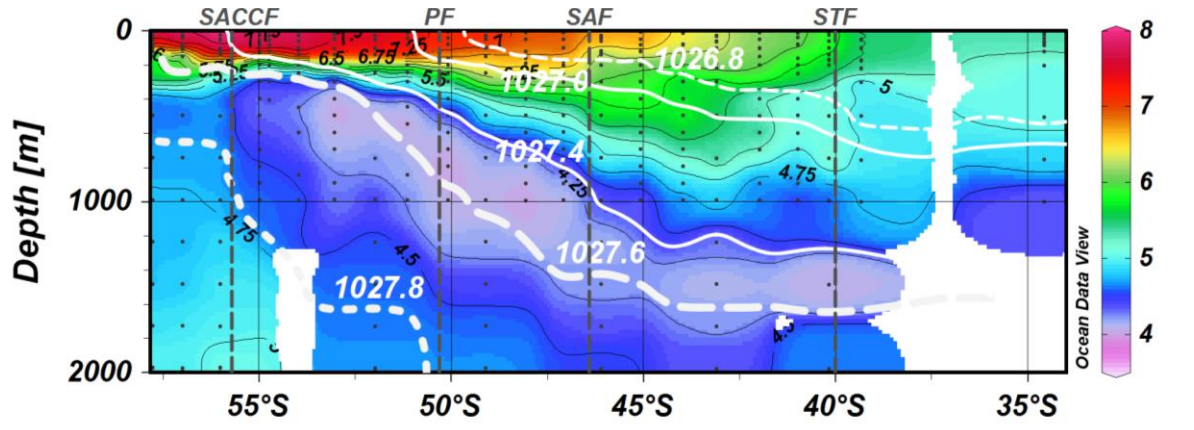

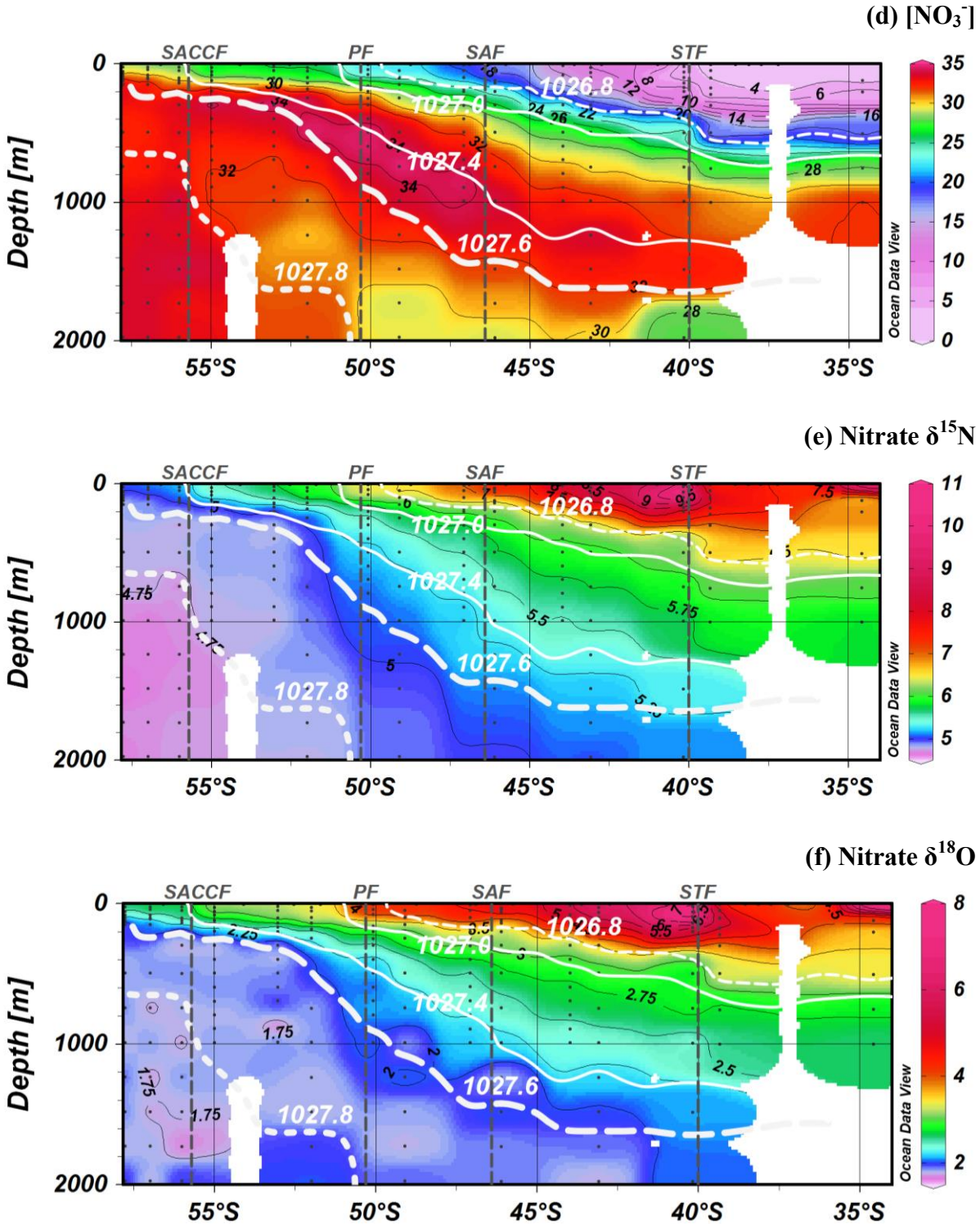

Figure 4.1 Section plots of (a) temperature (°C), (b) salinity (psu), (c) oxygen (ml l^{-1}), (d) [NO_3^-] (µM), (e) nitrate $\delta^{15}N$ (‰ vs. air), and (f) nitrate $\delta^{18}O$ (‰ vs. VSMOW) for the wintertime transect between Cape Town (33.5°S) and the Antarctic winter sea-ice edge (56.7°S). Plots incorporate both underway and profile measurements, with grey dots denoting sampling depths. Colour shading and black contours refer to the primary variable. Isopycnals are denoted by white contours and labels to assist in locating key water masses; namely LCDW (1027.8 kg m^{-3}), UCDW (1027.6 kg m^{-3}), AAIW (1027.0-1027.4 kg m^{-3}) and SAMW (1026.8 kg m^{-3}). Frontal positions are indicated by dashed grey vertical lines and labels above the sections. See text for definitions of acronyms.

One of the most prominent is a nitrate-rich (> 34.0 µM) (Figure 4.1d), oxygen-depleted (< 4.5 ml l^{-1}) (Figure 4.1c) sub-surface feature north of the SACCF (although a subsurface [NO_3^-] maximum extends further south), characteristic of Upper Circumpolar Deep Water (UCDW) (Orsi et al., 1995; Sigman et al., 1999a). The core of this water mass is roughly denoted by the 1027.6 kg m^{-3} isopycnal (Orsi et al., 1995), which rises from ~1600 m to ~100 m from north to south across the section. Beneath UCDW lies a more saline (> 34.7 psu) water mass (Figure 4.1b) with a higher oxygen content (> 4.5 ml l^{-1}) (Figure 4.1c) and generally lower [NO_3^-] (Figure 4.1d), fitting the description of Lower Circumpolar Deep Water (LCDW) (Whitworth & Nowlin, 1987; Orsi et al., 1995; Sigman et al., 1999a). The [NO_3^-] of LCDW appears to increase southwards from < 30.0 µM at ~50.5°S to > 32.0 µM at ~55.0°S along its core isopycnal of 1027.8 kg m^{-3} (Orsi et al., 1995), which rises from below 2000 m to ~600 m polewards across the Antarctic Zone (AZ; which encompasses both the OAZ and PAZ).

A pronounced subsurface salinity minimum layer (weakening northwards from < 34.2 psu at 43.5°S to > 34.3 psu at 40.0°S) (Figure 4.1b) with a relatively high oxygen content (Figure 4.1c), typical of Antarctic Intermediate Water (AAIW), appears near the SAF at ~200-600 m and deepens equatorward to ~1000 m north of the STF; roughly bounded by the 1027.0 kg m^{-3} and 1027.4 kg m^{-3} isopycnals (Whitworth & Nowlin, 1987; Belkin & Gordon, 1996; Talley, 1996; Speich et al., 2012). Above AAIW and below the mixed layer of the SAZ lies a relative salinity maximum (34.4-34.6 psu; Figure 4.1b), characteristic of Subantarctic Mode Water (SAMW), traced roughly by the 1026.8 kg m^{-3} isopycnal (McCartney, 1977; Piola & Georgi, 1982; DiFiore et al., 2006).

4.2 Nitrate isotopes and concentration

Figure 4.1e&f display the $\delta^{15}N$ and $\delta^{18}O$ of nitrate, respectively, for the wintertime section south of Africa. Both $\delta^{15}N$ and $\delta^{18}O$ increase progressively from depth towards the surface, and from south to north across Southern Ocean surface waters. The lowest $\delta^{15}N$ and $\delta^{18}O$ are observed at depth (below 800 m) within the AZ (< 4.75‰ and < 1.75‰, respectively), increasing slightly into the AZ surface (to > 5.0‰ and > 2.5‰) and reaching maximum values (> 9.5‰ and > 7.0‰) at the surface near the STF (~40.5°S). Below, we describe in detail the nitrate $\delta^{15}N$ and $\delta^{18}O$ patterns in relation to [NO_3^-], as revealed by both underway and profile measurements.

4.2.1 Underway samples

Underway surface nitrate $\delta^{15}N$ and $\delta^{18}O$ exhibit strong, negative correlations with $[NO_3^-]$ south of the STF (Figure 4.2). The overall decrease in $[NO_3^-]$ from 27.3 µM at 56.6°S to 9.8 µM at 41.0°S (near the STF) is coupled with an increase in $\delta^{15}N$ (from 5.2‰ to 8.9‰) and $\delta^{18}O$ (from 2.7‰ to 6.3‰), with linear correlation co-efficients of approximately -0.99 for both. North of the STF, however, these relationships appear to break down, and a further decrease in $[NO_3^-]$ is instead accompanied by a sudden drop in $\delta^{15}N$ and $\delta^{18}O$ (by ~1.4‰ and 2.2‰, respectively). The distinct deviation in the $\delta^{15}N$(and $\delta^{18}O$)-to-$[NO_3^-]$ relationship between 35°S and 40°S coincides with warm temperatures (> 16°C), high salinities (> 35.5 psu) and deep mixed layers (≥ 250 m) (Figure 4.1a&b). These hydrographic properties are characteristic of an Agulhas Ring (Lutjeharms & van Ballegooyen, 1988; Schmid et al., 2003), a feature that is discussed in section 5.5 below and in Appendix B.

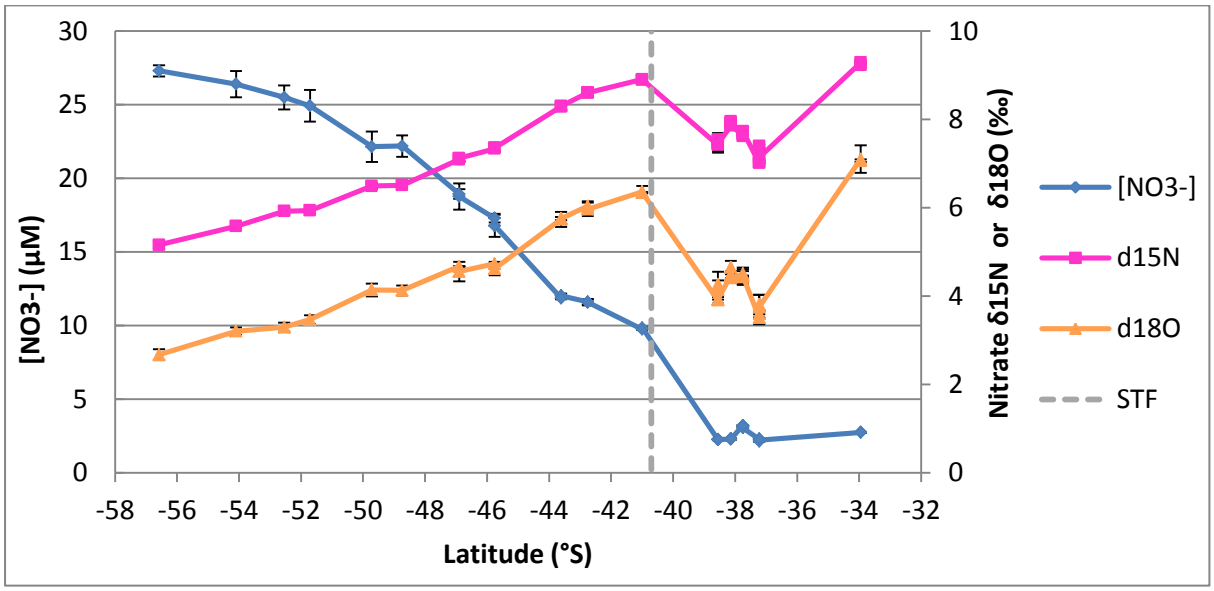

Figure 4.2 Underway surface measurements of $[NO_3^-]$ (in µM), nitrate $\delta^{15}N$ (in ‰ vs. air) and nitrate $\delta^{18}O$ (in ‰ vs. VSMOW) plotted against latitude for the wintertime transect from Cape Town (33.5°S) to the Antarctic winter sea-ice edge (56.7°S). Error bars indicate one standard deviation from the mean of replicate the measurements (n ≥ 3 for each sample). An inverse relationship between concentration and isotopic composition is noted.

4.2.2 Depth profiles

Profile measurements from the same transect as the underway collections show that the negative correlations of $\delta^{15}N$ and $\delta^{18}O$ with $[NO_3^-]$ also extend deeper through the water column (Figure 4.3). The dominant pattern revealed by the profile data is one of decreasing $[NO_3^-]$ towards the surface (Figure 4.3a) accompanied by a rise in $\delta^{15}N$ and $\delta^{18}O$ (Figure 4.3b&c). In terms of the magnitude of these vertical changes, a striking latitudinal progression is evident. Each latitudinal zone (and relevant subsurface water masses) is described in turn below.

In the PAZ, the characteristic subsurface $[NO_3^-]$ maximum of UCDW can be seen at 100-200 m with concentrations close to 34 µM, while in the OAZ, maximum concentrations of around 35 µM occur at 200-300 m (Figure 4.3a). These maxima roughly correspond with, or fall slightly shallower than, the core potential density (1027.6 kg m^{-3}) and oxygen minimum of UCDW (Orsi et al., 1995; Sigman et al., 1999a) (Figure 4.1c&d). The subsurface $[NO_3^-]$ minimum of LCDW is evident at 500-700 m (with $[NO_3^-]$ of 32-33 µM) in the PAZ, deepening northwards to around 1000-1500 m (with $[NO_3^-]$ of 30-32 µM) in the OAZ; following, or falling just shallower than, the core isopycnal at 1027.8 kg m^{-3} (Figure 4.1d). Although their concentrations differ (Figure 4.4a), UCDW and LCDW are isotopically similar throughout the sampled Antarctic Zone (AZ) interior (Figure 4.4b&c), with $\delta^{15}N$ of 4.82 ± 0.01‰ and 4.76 ± 0.01‰, and $\delta^{18}O$ of 1.87 ± 0.03‰ and 1.81 ± 0.03‰ for UCDW and LCDW, respectively (where n = 23 for UCDW and n = 30 for LCDW). Subtly lower $\delta^{15}N$ (< 4.75‰) and $\delta^{18}O$ (< 1.75‰) values are observed in the deepest, most polar waters sampled (Figure 4.1e&f). Overall, the mean nitrate $\delta^{15}N$ and $\delta^{18}O$ of the AZ interior are 4.78 ± 0.004‰ and 1.84 ± 0.02‰ respectively (where n = 53).

The PAZ profiles exhibit the smallest vertical changes from the subsurface $[NO_3^-]$ maximum (100-200 m) into the mixed layer, with $[NO_3^-]$ decreases of 4.8-5.9 µM (Figure 4.3a) associated with average $\delta^{15}N$ and $\delta^{18}O$ increases of 0.3-0.4‰ and 0.8-0.9‰ (Figure 4.3b&c), respectively. In the OAZ, a $[NO_3^-]$ decrease of 8.5-8.8 µM from the $[NO_3^-]$ maximum (200-300 m) into the mixed layer (Figure 4.3a) is accompanied by a rise in $\delta^{15}N$ and $\delta^{18}O$ of 0.7-0.9‰ and 1.2-1.4‰ (Figure 4.3b&c), respectively.

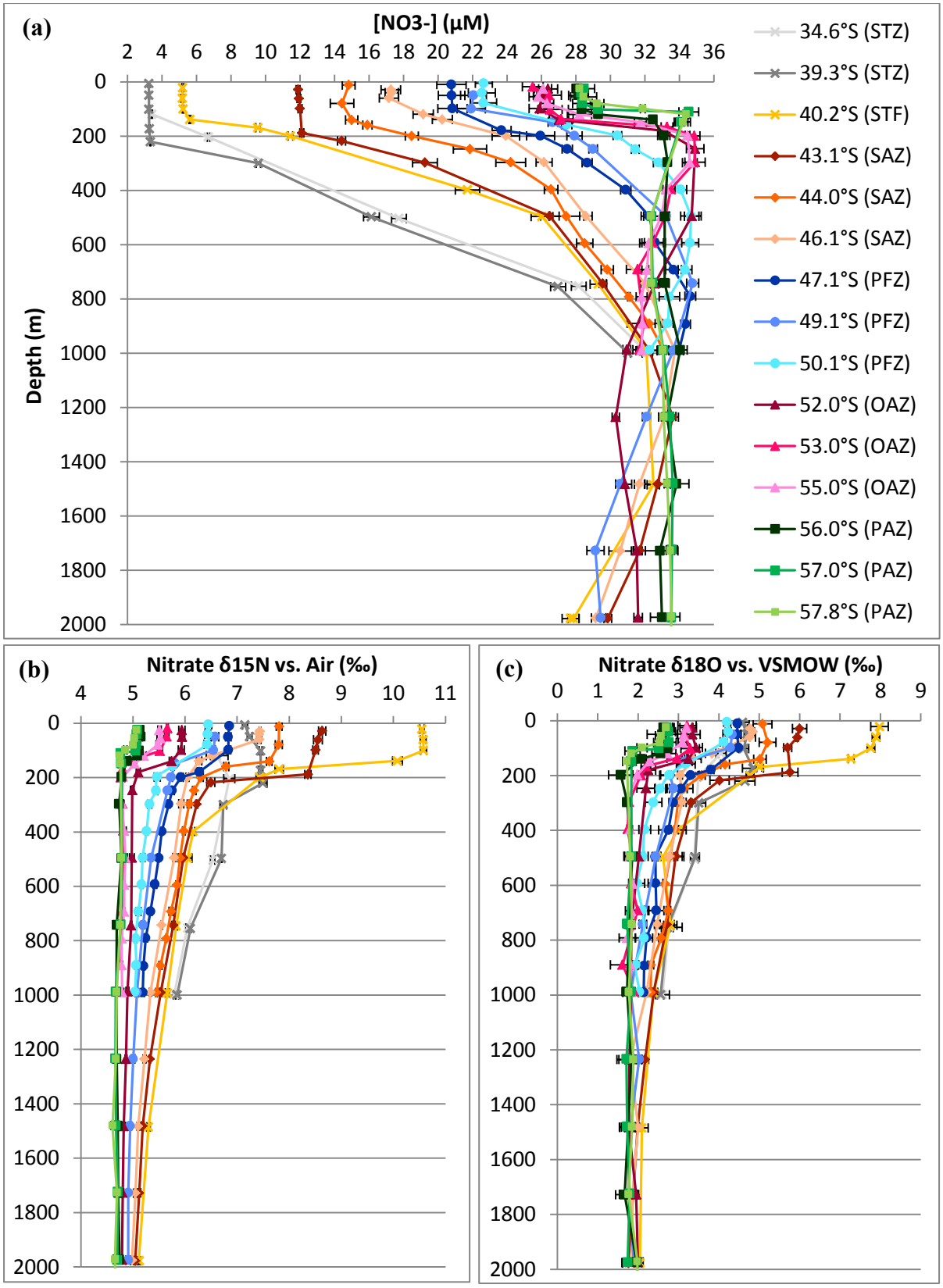

Figure 4.3 Vertical profiles of (a) [NO_3^-] (in µM), (b) nitrate $\delta^{15}N$ (in ‰ vs. air) and (c) nitrate $\delta^{18}O$ (in ‰ vs. VSMOW) for the upper 2000 m from the wintertime transect between Cape Town (33.5°S) and the Antarctic winter sea-ice edge (56.7°S). Error bars indicate one standard deviation from the mean of replicate measurements ($n \geq 3$ for each sample). The overall decrease in concentration towards the surface is mirrored by an increase in both $\delta^{15}N$ and $\delta^{18}O$.

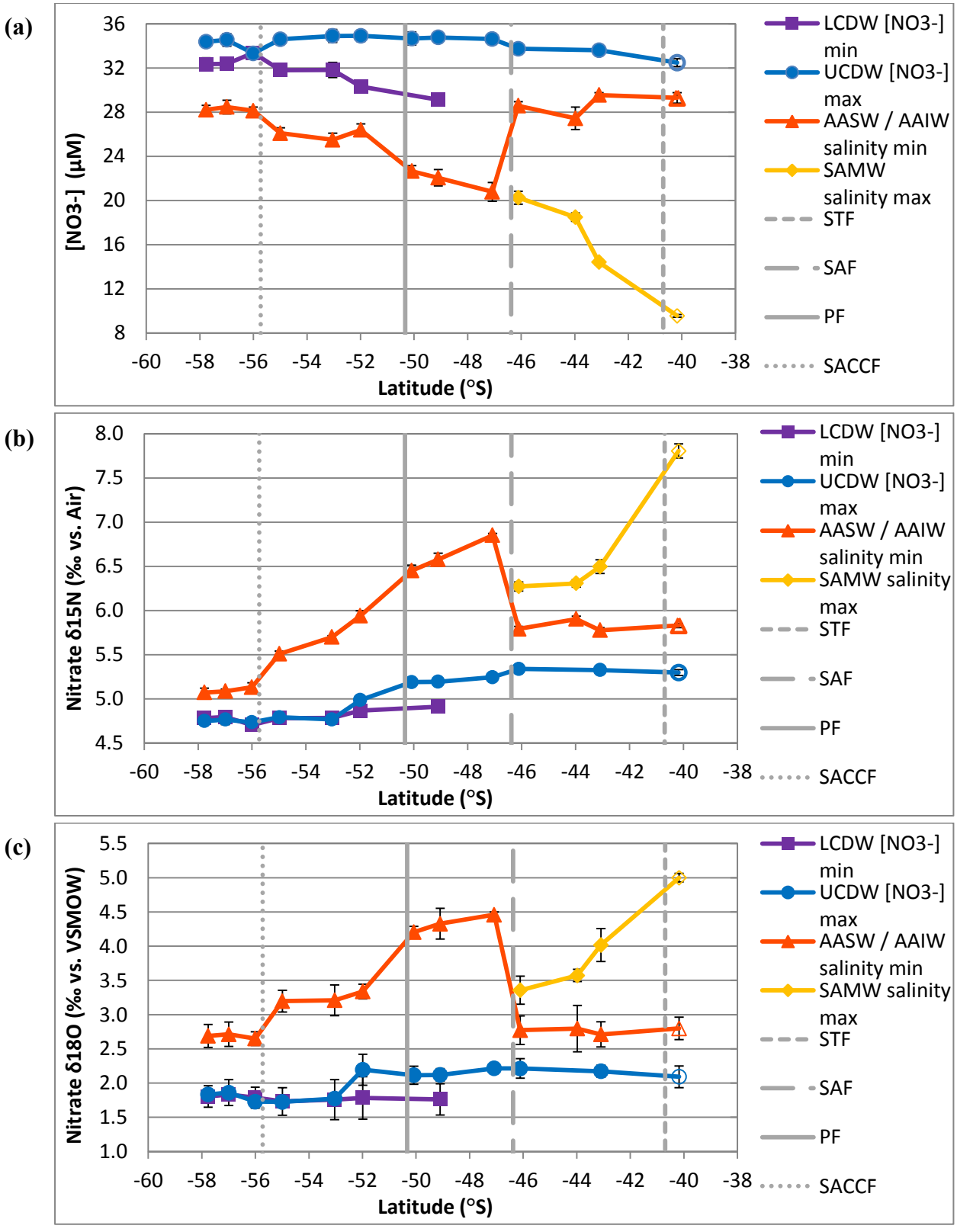

Figure 4.4 Latitudinal evolution of water mass properties across the wintertime Atlantic sector of the Southern Ocean. (a) [NO_3^-] (in µM), (b) nitrate $\delta^{15}N$ (in ‰ vs. air) and (c) nitrate $\delta^{18}O$ (in ‰ vs. VSMOW) are plotted for LCDW (deep [NO_3^-] minimum), UCDW (deep [NO_3^-] maximum), AASW/AAIW (salinity minimum) and SAMW (salinity maximum). Vertical grey lines indicate the positions of the main Southern Ocean fronts at the time of the winter transect. Error bars indicate one standard deviation from the mean of replicate measurements ($n \geq 3$).

In the PFZ, the [NO_3^-] minimum of LCDW decreases further to ~29 μM at around 1700 m (Figure 4.3a), deeper than in the AZ. Here, its $\delta^{15}N$ is slightly higher than in the AZ (4.9‰) (Figure 4.3b and Figure 4.4b), while its $\delta^{18}O$ remains relatively constant (1.8‰) (Figure 4.3c and Figure 4.4c). Further north, LCDW is typically deeper than our maximum depth of sampling. Across the PFZ, the [NO_3^-] maximum of UCDW diverges from its core isopycnal (which plunges from around 900 m to 1400 m) (Figure 4.1d), deepening from just 500 m to 800 m and maintaining concentrations in the 34-35 μM range (Figure 4.3a and Figure 4.4a). Its $\delta^{15}N$, on the other hand, increases notably to ~5.2‰ (from 4.8‰ in the AZ) (Figure 4.3b and Figure 4.4b) and its $\delta^{18}O$ increases to ~2.2‰ (from 1.8‰ in the AZ) (Figure 4.3c and Figure 4.4c).

To the north across the SAZ, the [NO_3^-] maximum (33-34 μM) deepens from 1000 m to 1200 m (Figure 4.3a), in parallel with a 200 m deepening of the 1027.6 kg m^{-3} core isopycnal (Figure 4.1d). The ~1 μM decrease in maximum concentration (relative to the adjacent PFZ) (Figure 4.3a and Figure 4.4a) is accompanied by a slight increase in $\delta^{15}N$ to 5.3‰ (Figure 4.3b and Figure 4.4b), while $\delta^{18}O$ remains unchanged at ~2.2‰ (Figure 4.3c and Figure 4.4c). AAIW deepens progressively from 500 m to 750 m as it flows northwards across the SAZ (Figure 4.1b), and is characterized by a [NO_3^-] of 27-30 μM (Figure 4.4a), a $\delta^{15}N$ of 5.8-5.9‰ (Figure 4.4b), and a $\delta^{18}O$ of 2.7-2.8‰ (Figure 4.4c).

The trend of decreasing [NO_3^-] and associated $\delta^{15}N$ and $\delta^{18}O$ rise continues up through the SAZ water column into SAMW, near the 1026.8 kg m^{-3} isopycnal (DiFiore et al., 2006). Heading north across the SAZ, its characteristic subsurface salinity maximum deepens from 140 m to 220 m (Figure 4.1b), in close correspondence with a deepening thermocline (mixed-layer depth increases from 122 m to 189 m) (McCartney, 1977; Piola & Georgi, 1982). The [NO_3^-] associated with the salinity maximum decreases from around 20 μM to 14 μM (Figure 4.4a), while $\delta^{15}N$ increases from 6.3‰ to 6.5‰ (Figure 4.4b) and $\delta^{18}O$ increases from 3.4‰ to 4.0‰ (Figure 4.4c).

Overall, [NO_3^-] decreases by 16-22 μM from the deep [NO_3^-] maximum of the SAZ upwards into the surface mixed layer (Figure 4.3a), over which interval $\delta^{15}N$ and $\delta^{18}O$ increase by 2.1-3.2‰ (Figure 4.3b) and 2.6-3.7‰ (Figure 4.3c), respectively. While the concentration decrease occurs gradually from great depth (≥ 1000 m), the rise in $\delta^{15}N$ and $\delta^{18}O$ is largely focussed at the base of the mixed layer in the SAZ; this in contrast to the AZ where the sharpest vertical gradients in both concentration and isotopes occur near the base of the

mixed layer. PFZ profiles appear largely transitional between the SAZ and the AZ, although more similar to the SAZ in this regard. In the PFZ, profiles exhibit a 12-14 μM decrease from the subsurface [NO_3^-] maximum (at 500-800 m) into the mixed layer (Figure 4.3a), together with $\delta^{15}N$ and $\delta^{18}O$ increases of 1.2-1.6‰ (Figure 4.3b) and 2.1-2.3‰ (Figure 4.3c), respectively.

As seen in the underway data (Figure 4.2), profiles north of the STF deviate in their relationship of [NO_3^-] with $\delta^{15}N$ and $\delta^{18}O$ from the latitudinal progression observed across the rest of the transect (Figure 4.3). While [NO_3^-] either decreases or remains constant through the upper 200 m towards the surface (Figure 4.3a), the corresponding nitrate $\delta^{15}N$ decreases (Figure 4.3b) and $\delta^{18}O$ is variable (Figure 4.3c).

4.3 PN $\delta^{15}N$ and concentration

Underway collections of bulk suspended particulate nitrogen (PN) from leg 2 of the winter voyage (from the ice-edge to Marion Island and back to South Africa) reveal an overall increasing trend in surface PN concentration ([PN]) from polar waters (< 0.2 μM at 56.1°S) to subtropical waters (within the 0.3-0.5 μM range north of 40.5°S) (Figure 4.5a). The $\delta^{15}N$ of PN exhibits an increase from low values in polar waters (between -4.8‰ and -0.7‰ south of 52.0°S) to a maximum (4.9‰ at 46.3°S) within the PFZ near Marion Island (46.9°S), and a subsequent decrease into the subtropics (0.8-1.0‰ north of 40.5°S). Although not from the same leg as our profile data, these PN measurements provide an additional constraint on nitrate isotope dynamics in the region south of Africa, which we make use of in section 5.4.2 to assess the feasibility of different mixed-layer N-cycling scenarios in explaining our nitrate isotope data.

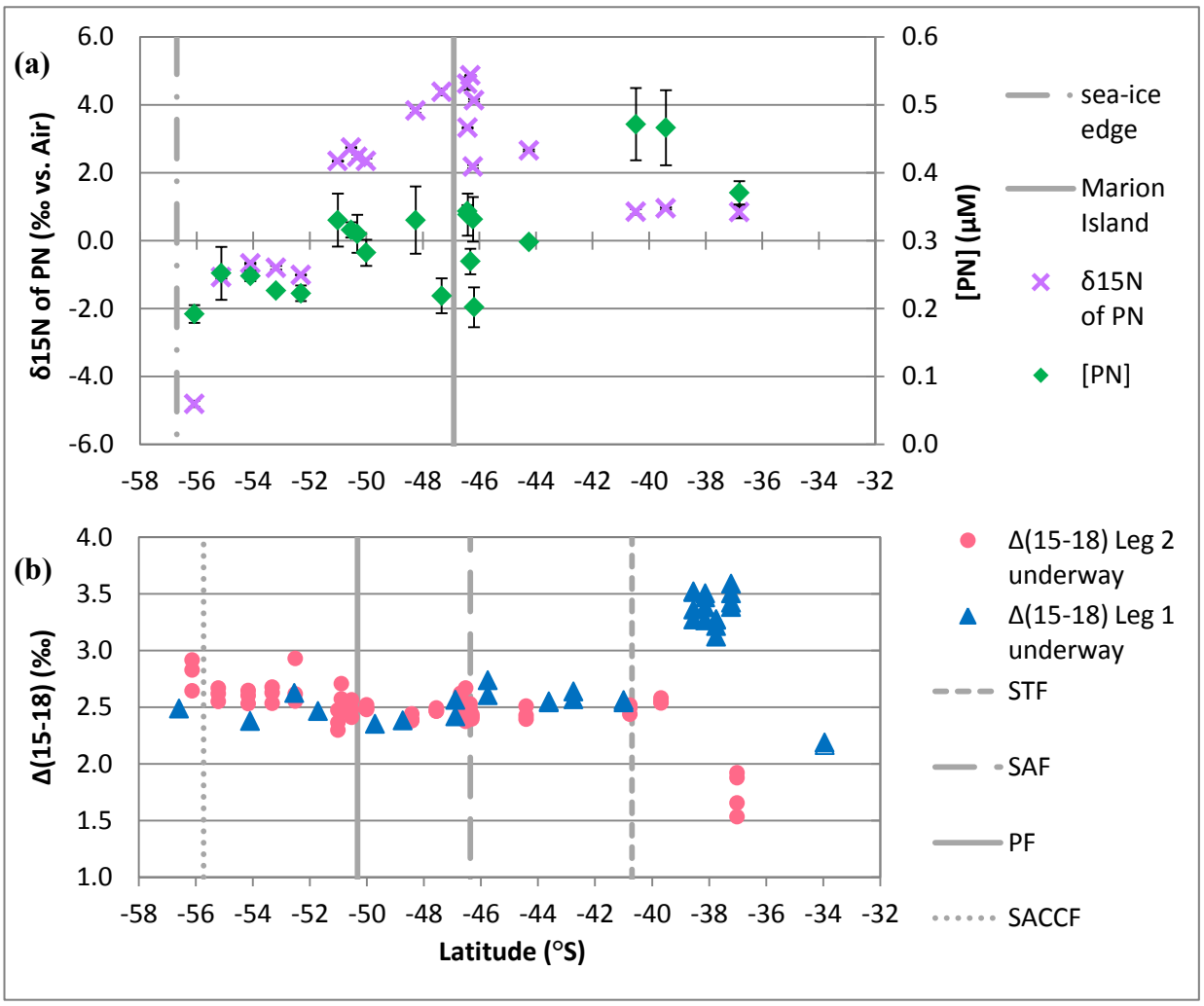

Figure 4.5 (a) Underway surface measurements of bulk suspended [PN] (in µM) and the $\delta^{15}N$ of PN (in ‰ vs. air) plotted against latitude for leg 2 of the winter voyage, from the sea ice-edge (at 56.7°S; indicated by the dotted grey line) to Marion Island (at 46.9°S; indicated by the solid grey line) and back to South Africa. Error bars represent one standard deviation from the mean for two subsamples (i.e., n = 2) of the same glass fibre filter (GF/F), each oxidised and analysed separately in duplicate/triplicate. Measurement (i.e., denitrifier) error was so small that it was not included in the standard deviation (< 0.05‰ for n ~ 3).

(b) Underway surface nitrate Δ(15-18) in ‰ units plotted against latitude for both legs 1 and 2 of the winter voyage, for comparison with [PN] in panel (a) above (as discussed in section 5.5). Vertical grey lines denote the frontal positions on leg 1.

5. Discussion

The clear negative correlation that we observe between the nitrate isotopes ($\delta^{15}N$ and $\delta^{18}O$) and nitrate concentration ($[NO_3^-]$) reflects the dominant effect of nitrate assimilation by phytoplankton on nitrate isotope distributions in the Southern Ocean – even in mid-winter. Preferential assimilation of the lighter isotopes (^{14}N and ^{16}O) causes the $\delta^{15}N$ and $\delta^{18}O$ of the remaining nitrate pool to increase, an effect that strengthens with the increasing degree of consumption (Mariotti et al., 1981; Altabet & Francois, 1994a; Sigman et al., 1999a; DiFiore et al., 2009). The relationship between surface nitrate consumption and isotopic elevation, at least in part, accounts for the observed northward increase in $\delta^{15}N$ and $\delta^{18}O$ (as nitrate consumption increases northwards) and for the weaker isotopic elevation of the wintertime surface (5.1‰-8.9‰ for $\delta^{15}N$) compared with summertime observations (typically 6‰-14‰ for $\delta^{15}N$), when nitrate consumption is more complete (Sigman et al., 1999a; DiFiore et al., 2006; DiFiore et al., 2009).

Closer inspection, however, reveals depth and spatial gradients in nitrate isotopic composition that cannot be explained solely by the relationship described above. Deviations from a single nitrate consumption/nitrate $\delta^{15}N$ relationship, both in the mean and in terms of seasonal changes, have been investigated most intensively in the Subantarctic Zone (SAZ), and appear to speak largely to the effect of mixing between nitrate-rich and nitrate-poor waters (Sigman et al., 1999a; DiFiore et al., 2006). Deviations in the nitrate $\delta^{15}N$-to-$\delta^{18}O$ relationship from that expected from nitrate assimilation alone has been shown to result from an internal cycle within the SAZ that includes summertime partial nitrate assimilation in the surface, remineralization of sinking N in the thermocline, and resupply of thermocline nitrate to the surface during winter mixing (Rafter et al., 2013).

The data reported here provide by far the most comprehensive view to date of wintertime nitrate isotopes in the Antarctic Zone (AZ) of the Southern Ocean. As shown below, the data share features observed in the summertime Antarctic that do not fit with nitrate assimilation alone and which have so far defied explanation (Sigman et al., 1999a; DiFiore et al., 2010). Explaining such anomalies (i.e., deviations from the expected isotope/concentration relationship) is crucial to the accurate interpretation of paleoceanographic records, and may also yield valuable insights into the present-day workings of the Southern Ocean's biological pump. Our predominant goal below is to provide new insight into these anomalies.

In order to provide context for our findings, we first discuss the properties of potential source water masses to the AZ and their spatial evolution. Thereafter, we examine the N and O isotope gradients of nitrate in the AZ, individually, before taking on a dual isotope approach to explore potential mechanisms behind the observations. After reflecting on the implications of the findings from the wintertime AZ, we consider the transect as a whole within a dual isotope framework, providing a Southern Ocean synthesis.

5.1 Sub-surface water mass properties and evolution

The nitrate $\delta^{15}N$ depth profiles show a subtle but detectible latitudinal progression (with lower $\delta^{15}N$ in the south, increasing to the north), even at the deepest depths sampled (Figure 4.3b). This suggests some sensitivity of nitrate N isotopes to spatially varying deep-water properties.

Across the entire transect, the nitrate $\delta^{15}N$ of Upper Circumpolar Deep Water (UCDW) and Lower Circumpolar Deep Water (LCDW) fall within the range of 5.0 ± 0.5‰ that is typical of global deep ocean nitrate below 2 km (Sigman et al., 2000; Sigman et al., 2009a) (Figure 4.1e and Figure 4.4b). The isotopic homogeneity of the AZ interior is striking, with both UCDW and LCDW characterized by a $\delta^{15}N$ close to 4.8‰ (i.e., 4.82 ± 0.01‰ and 4.76 ± 0.01‰, respectively). Although such similarity between these two water masses within the AZ has been seen previously in the east Indian sector, UCDW $\delta^{15}N$ was found to be slightly higher than LCDW $\delta^{15}N$ (by < 0.4‰; Sigman et al., 2000). This $\delta^{15}N$ difference was seen to grow northwards to 0.7‰ in the SAZ, without any noticeable rise in LCDW $\delta^{15}N$. We observe a similar trend of isotopic divergence in the Atlantic sector, although our LCDW data extend only as far north as the Polar Frontal Zone (PFZ). At the corresponding latitude in the east Indian sector, the $\delta^{15}N$ elevation of UCDW above LCDW was around 0.2-0.5‰ (Sigman et al., 2000). This is comparable to the 0.3‰ difference that we observe in the Atlantic PFZ. In the Atlantic data, this difference occurs despite a slight (~0.1‰) rise in the $\delta^{15}N$ of LCDW from the AZ into the PFZ (Figure 4.4b).

The northward increase of UCDW $\delta^{15}N$ across the Southern Ocean was explained by Sigman et al. (2000) as a balance between two opposing forces: lateral exchange with high-$\delta^{15}N$ intermediate-depth waters (a remote denitrification signal from the eastern Pacific and western Indian basins) acting to elevate the $\delta^{15}N$ from the north, and the remineralization of

low-$\delta^{15}N$ particulate nitrogen (PN) sinking out of polar surface waters (where nitrate utilization is low, producing PN with $\delta^{15}N \sim 0‰$; Altabet & Francois, 2001) acting to lower Antarctic deep nitrate $\delta^{15}N$.

If these same processes govern the properties of UCDW in the Atlantic sector, the lower $\delta^{15}N$ of SAZ UCDW (5.3‰ compared to ~5.5‰ in the east Indian sector) (Sigman et al., 2000), and perhaps also the lack of any $\delta^{15}N$ elevation of UCDW over LCDW in the AZ, could be interpreted as a result of being further from the major water column denitrification zones in the context of the circumpolar circulation. A weaker influence of denitrification zones would lead to less $\delta^{15}N$-elevated nitrate reaching the study region south of Africa.

The implied damped communication between the Atlantic sector of the Southern Ocean and the Pacific and Indian basins is also consistent with the weaker [NO_3^-] maximum of UCDW south of Africa (34-35 μM (Figure 4.4a) compared to ~36 μM in the east Indian and east Pacific sectors) (Sigman et al., 2000), since it is communication with these basins (specifically, the nitrate-rich deep waters of the western Indian and eastern South Pacific) that actually gives rise to the concentration maximum of UCDW (Callahan, 1972; Park et al., 1993; Orsi et al., 1995).

Similarly, the latitudinal evolution of LCDW $\delta^{15}N$ might be the product of the interplay between (i) the sinking and remineralization of low-$\delta^{15}N$ PN in the south and (ii) exchange with (a) North Atlantic Deep Water (NADW), which is observed to have a nitrate $\delta^{15}N$ of 4.85‰ in the subtropical North Atlantic (Marconi et al., *in preparation*), and (b) Indo-Pacific waters that, as with UCDW, are weakly contaminated with high-$\delta^{15}N$ nitrate from the denitrification zones. The influence of NADW in the Atlantic sector is evident in the lower [NO_3^-] minimum of LCDW (decreasing northwards from ~32 μM in the AZ to < 30 μM north of the Polar Front (PF) (Figure 4.4a), compared to ~33 μM in the east Indian and east Pacific sectors), reflecting closer communication between LCDW and low-nitrate NADW south of Africa (Mantyla & Reid, 1983; Whitworth & Nowlin, 1987).

Vertical mixing works to homogenize biogeochemical properties (e.g., the concentration and isotopic composition of nitrate) in stacked water masses away from the regions that generated their differences (Sigman et al., 2000). The observed depth offset between the [NO_3^-] maximum and the core isopycnal of UCDW, for instance, may be a reflection of this (Figure 4.1d), with the low-nitrate waters of LCDW eroding the nitrate-rich waters of UCDW from

below. Thus, perhaps mixing also has some part to play in the isotopic convergence of UCDW and LCDW in the AZ.

In sum, while UCDW and LCDW are pulled apart isotopically by their disparate northern endmembers, both remineralization of low-$\delta^{15}N$ sinking PN and vertical mixing may act to draw them together in the south.

The O isotopes of nitrate add a new dimension to the discussion. Our Atlantic sector UCDW and LCDW $\delta^{18}O$ data (1.7-2.2‰) (Figure 4.1f and Figure 4.4c) overlap with those reported by Sigman et al. (2009) for the abyssal ocean (1.8-2.0‰), and by DiFiore et al. (2009) for deep (> 300 m) Antarctic coastal waters (2.2 ± 0.1‰).

The $\delta^{18}O$ of UCDW exhibits a similar gradient to its $\delta^{15}N$, although slightly weaker. While the $\delta^{18}O$ and $\delta^{15}N$ of nitrate are equally elevated by denitrification (Granger et al., 2008) and equally altered by mixing (Rafter et al., 2013), the regeneration of sinking PN can decouple them (i.e., lowering deep $\delta^{15}N$ more than it lowers deep $\delta^{18}O$) (Sigman et al., 2003; Granger et al., 2008; Sigman et al., 2009a). This is because the $\delta^{15}N$ of the newly regenerated nitrate depends on the $\delta^{15}N$ of the PN being remineralized, while its $\delta^{18}O$, instead, depends primarily on the $\delta^{18}O$ of ambient water (Casciotti et al., 2002; Sigman et al., 2009a).

It follows that the two isotopic gradients of nitrate within a deep water mass (i.e., the $\delta^{15}N$ gradient and the $\delta^{18}O$ gradient over the same interval) can provide constraints on remineralization and the extent to which regenerated nitrate contributes to the observed distributions of $\delta^{15}N$. Applying this idea to UCDW – assuming that nitrification adds new nitrate with a $\delta^{15}N$ of 0‰ (inferred from the low $\delta^{15}N$ of PN sinking out of polar surface waters due to less complete nitrate assimilation there; Altabet & Francois, 2001) and a $\delta^{18}O$ of 1.1‰ (as estimated by Sigman et al., 2009) – suggests that ~0.25‰ of the ~0.6‰ decrease in UCDW $\delta^{15}N$ from the SAZ to the Polar Antarctic Zone (PAZ) (Figure 4.4b&c) is due to *in situ* regeneration of sinking PN.

5.2 N isotope gradients of the Antarctic Zone mixed layer

First, it is worth noting that there *are* nitrate isotope and concentration gradients from the subsurface into the winter mixed layer of the AZ (Figure 4.3). Thus, either wintertime mixing is not adequately deep or vigorous to reset the AZ surface to deep source (e.g.,

UCDW) values, completely erasing the summertime assimilation signal, and/or nitrate assimilation by phytoplankton in the wintertime is not negligible. The significance of this observation for summertime estimates of the isotope effect is discussed in section 5.4.3.

There is strong support for the first explanation (given above) in that the mixed-layer depth in the AZ during the time of the cruise is 93-137 m (116 m on average) and not deeper. We illustrate this with the following calculation. For the summertime AZ we assume a mixed-layer depth of 75 m (commonly observed during summer voyages in the region; Joubert et al., 2011; Swart et al., 2012), a $[NO_3^-]$ of 24.7 μM (from the *World Ocean Atlas* 2009 (WOA09) climatology for January) and a nitrate $\delta^{15}N$ of 5.9‰ (assuming summertime Rayleigh consumption with an isotope effect of 5‰, and the AZ winter mixed layer as the initial nitrate source). Deepening a summer mixed layer with these properties to 116 m by mixing with underlying UCDW would yield a winter mixed layer with a $[NO_3^-]$ and $\delta^{15}N$ of 27.8 μM and 5.4‰, respectively; these predictions are very close to our observations of the wintertime AZ mixed layer, averaging 27.3 μM and 5.4‰, respectively.

As mentioned earlier (section 2.2.1), the Rayleigh model best describes closed-system nitrate isotope dynamics (Mariotti et al., 1981; Sigman et al., 1999a). Given the lower uptake and higher resupply rates of nitrate relative to the summer season, the wintertime AZ clearly violates the closed-system condition. However, violation of this condition is less problematic for the interpretation of data at the very high $[NO_3^-]$ and weak $[NO_3^-]$ gradients that characterize the AZ (Sigman et al., 1999a). In any case, the Rayleigh model provides a useful reference point for identifying and interpreting deviations from this 'ideal state'.

Plotting our AZ profile data in Rayleigh space (i.e., $\delta^{15}N$ vs. $\ln([NO_3^-])$; Figure 5.1) reveals the general trend that we expect for nitrate assimilation: as concentration decreases towards the surface, so $\delta^{15}N$ increases (Sigman et al., 1999a; Altabet & Francois, 1994a; Altabet & Francois, 2001), with the Open Antarctic Zone (OAZ) profiles exhibiting a greater degree of consumption (and thus isotopic elevation) than the PAZ profiles. The slopes of these lines in Rayleigh space (from the deep nitrate source to the surface) are commonly used to estimate the isotope effect of nitrate assimilation (Sigman et al., 1999a; Altabet & Francois, 2001; DiFiore et al., 2009). Applying this to our wintertime profiles (using data down to the $[NO_3^-]$ maximum; i.e., assuming an UCDW source) yields slopes, and thus isotope effect estimates, of 1.6-2.2‰ in the PAZ and 2.5-3.3‰ in the OAZ (Figure 5.2).

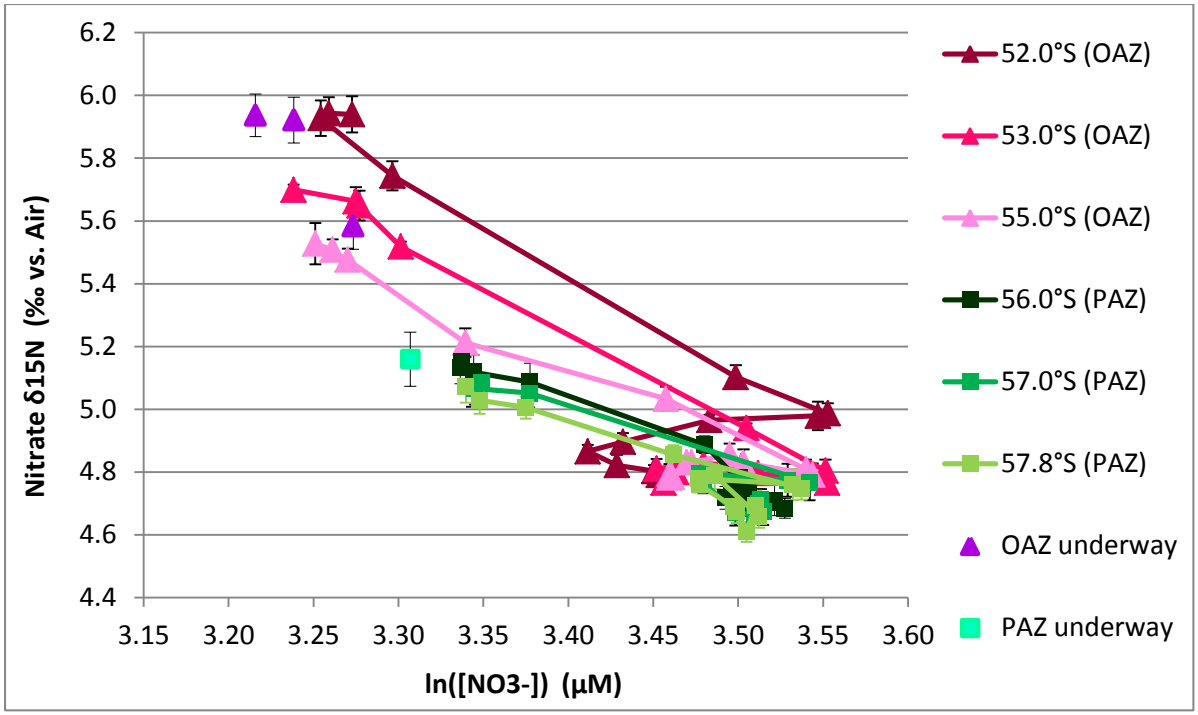

Figure 5.1 Full-depth (0-1000 m or 0-2000 m) AZ profiles (and underway surface data) plotted in Rayleigh space (nitrate $\delta^{15}N$ vs. $\ln([NO_3^-])$). OAZ data (shown in shades of pink) exhibit greater isotopic enrichment and nitrate depletion towards the surface than PAZ data (in shades of green). Error bars indicate the measurement standard deviation for each sample.

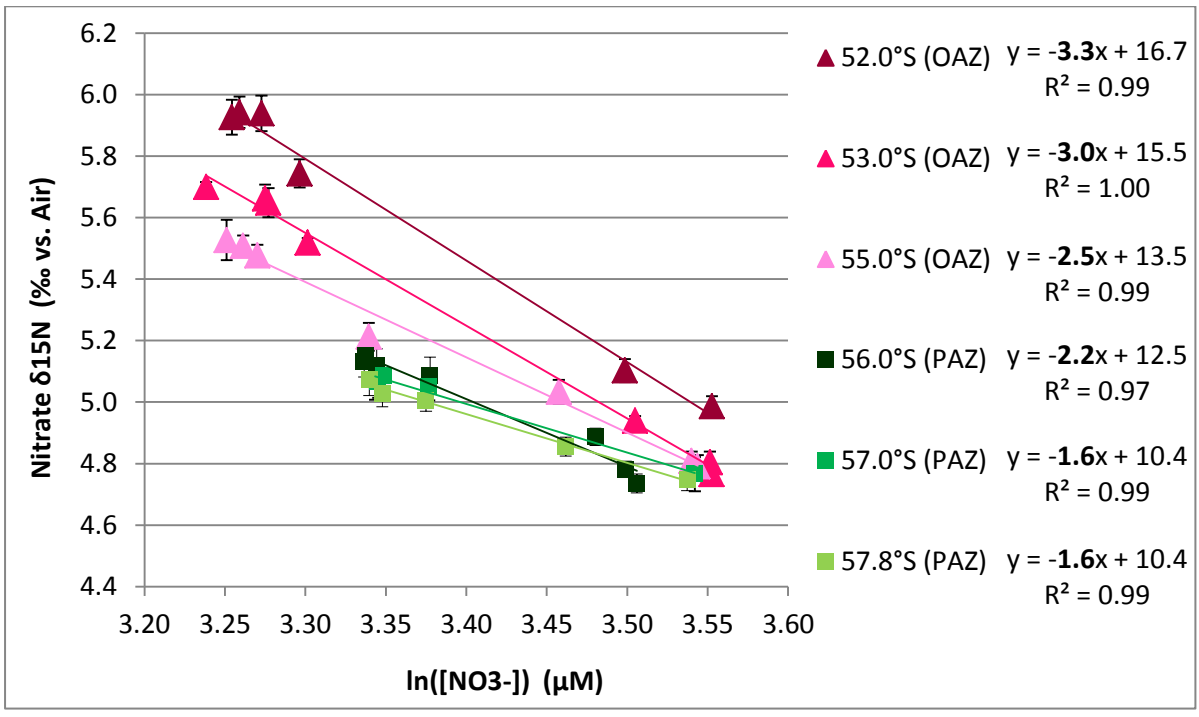

Figure 5.2 OAZ (pink) and PAZ (green) profile data plotted in $\delta^{15}N$ vs. $\ln([NO_3^-])$ space, from the surface to the depth of the $[NO_3^-]$ maximum of UCDW. The slopes of the linear trendlines (bold text in the legend) in Rayleigh space provide an estimate of the isotope effect of nitrate assimilation at each station. Error bars indicate measurement standard deviation.

These values are remarkably low compared to those suggested by culture studies and summertime data from the AZ. Although the nitrate assimilation isotope effect suggested by culture experiments is highly variable (0-20‰) (Wada & Hattori, 1978; Montoya & McCarthy, 1995; Granger et al., 2008), most of the data suggest a mean value near 5-6‰ for diatoms (Waser et al., 1998; Needoba et al., 2003; Needoba & Harrison, 2004; Needoba et al., 2004; Granger et al., 2010). Field estimates from the AZ range from 4‰ to as high as 10‰ (Sigman et al., 1999a; Altabet & Francois, 2001; Karsh et al., 2003; DiFiore et al., 2009). In the OAZ, as described below, the greatest source of uncertainty in isotope effect estimates is whether the summertime T_{min} (i.e., the remains of the winter mixed layer) should be taken as a measure of the initial [NO_3^-] and $\delta^{15}N$ that is then modified by summertime phytoplankton drawdown (Sigman et al., 1999a; DiFiore et al., 2009). Nevertheless, a nitrate assimilation isotope effect of 2-3‰ can be ruled out for the Southern Ocean summertime (Sigman et al., 1999a; Karsh et al., 2003; DiFiore et al., 2009) as well as for the North Pacific and other regions (e.g., Wu et al., 1997; Altabet, 2001).

One interpretation of the low slopes suggested by our data is that the actual isotope effect of nitrate assimilation expressed by phytoplankton in the AZ during winter is around 2-3‰, less than half of the summertime isotope effect. That is, the degree of isotope fractionation expressed by the phytoplankton in the environment is smaller in the winter than in summer (e.g., due to some change in environmental conditions or phytoplankton community composition). This, however, would be contrary to our current understanding of the relationship between the isotope effect, light and mixed-layer depth (Needoba & Harrison, 2004; Needoba et al., 2004; DiFiore et al., 2010; Karsh, 2013). In the winter, incident sunlight at these latitudes is lower and mixed layers are deeper, so that phytoplankton spend less time near the surface where light conditions are favourable for photosynthesis. Under such conditions, it is predicted that phytoplankton will efflux proportionally more of the isotopically-elevated intracellular nitrate into the environment, resulting in a larger expressed isotope effect (Needoba et al., 2004; Needoba & Harrison, 2004). This is the opposite of what we observe.

An alternative dynamic that may lower the net wintertime isotope effect, however, involves phytoplankton growth within sea-ice. When assimilation takes place in sea-ice, diffusion of the remaining ^{15}N-enriched nitrate pool into the seawater below the ice is inhibited, potentially causing under-expression of the organism-level assimilation isotope effect in the ocean (Fripiat et al., *accepted*). If this were the reason for the low isotope effects suggested

by our $\delta^{15}N$ profiles, however, we would expect to observe the same effect in the $\delta^{18}O$ profiles; which, as we discuss below, is not the case.

As described above, the Rayleigh model applies in the case of consumption of an isolated substrate pool, with which wintertime deep mixing is inconsistent. The possibility thus exists that the Rayleigh slope of the winter AZ profile data derives from this violation of the Rayleigh model. One approach for evaluating this possibility is to analyse the data in a simple model that includes continuous resupply of nitrate: the "steady-state" model (Hayes, 2002). This reanalysis will indeed raise the isotope effect from the predicted Rayleigh utilization trend (Sigman et al., 1999a).

The difference in isotope effect that would be estimated from the profile data under the distinct assumptions of the Rayleigh and steady-state models is illustrated here as follows. We calculate the difference between the Rayleigh- and steady-state-predicted nitrate $\delta^{15}N$ at the same degree of nitrate depletion (i.e., the *f* value, calculated based on the sample $[NO_3^-]$ and the subsurface maximum $[NO_3^-]$), assuming an isotope effect of 5‰. This $\delta^{15}N$ difference is then added to the $\delta^{15}N$ of each mixed layer sample data point, effectively removing the approximate effect of dilution with subsurface nitrate that the steady-state model includes but the Rayleigh model does not. This modification of the data appears to resolve only part of the deviation, raising the isotope effects to just 2.0-2.6‰ in the PAZ and 3.1-4.0‰ in the OAZ (Appendix C, Figure C.1a-f). The reason that this effect is modest is that at the low nitrate utilization levels characteristic of the wintertime AZ (< 30%), the Rayleigh and steady-state models provide very similar estimates of the isotope effect (Sigman et al., 1999a). The surface and deep water masses are not different enough in their $[NO_3^-]$ and $\delta^{15}N$ for their mixing to produce a deviation from a pure utilization trend (Sigman et al., 1999a) that is sufficiently large to explain our data.

An important indication as to the significance of the low Rayleigh slopes in the wintertime profile data comes from Rayleigh model analysis of the AZ mixed-layer data alone (Figure 5.3). In principle, the slope of the regression line through these data should yield an additional estimate of the assimilation isotope effect (Sigman et al., 1999a), provided that all these mixed-layer samples derive from the same deep nitrate source (or at least have the same nitrate $\delta^{15}N$-to-$[NO_3^-]$ relationship). Because the northernmost AZ profile (at 52.0°S) appears to stem from a nitrate source with a ~0.2‰ higher $\delta^{15}N$ than the others (see Figure

5.1 for original profile) these data and nearby underway samples have been excluded from the analysis.

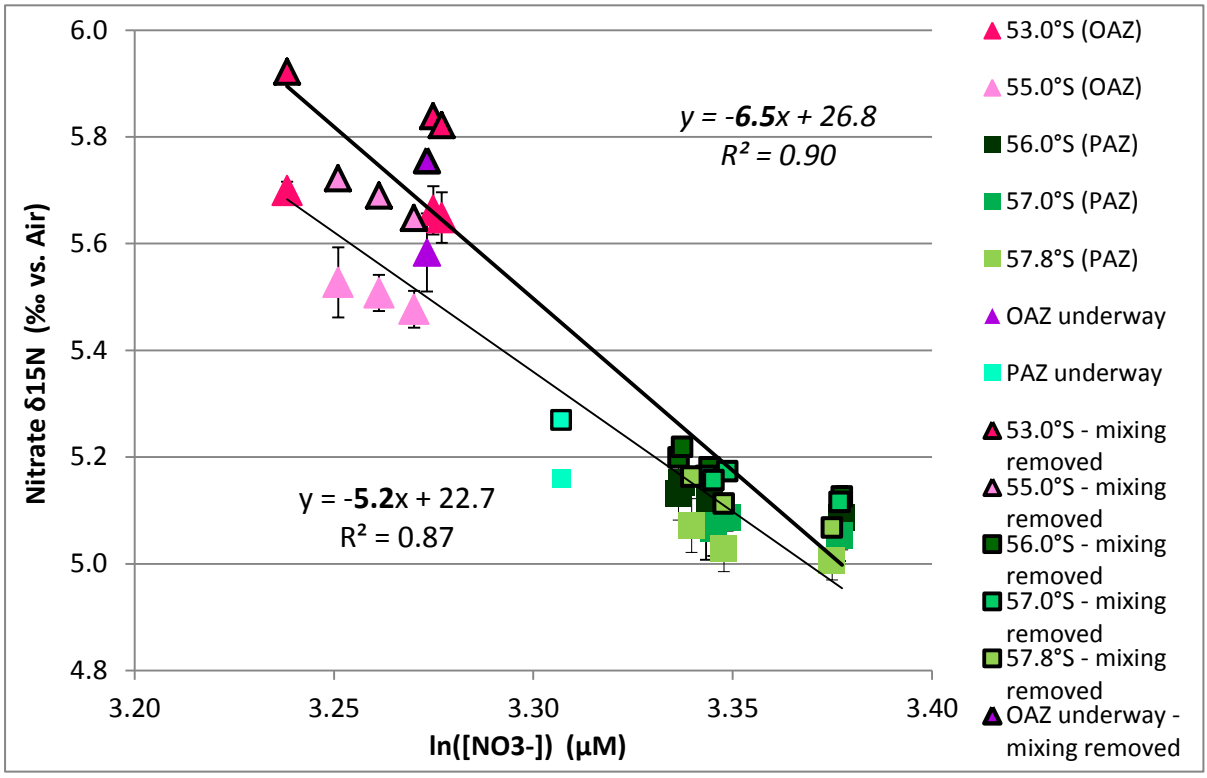

Figure 5.3 All AZ mixed-layer (profile and underway) data from south of 53.0°S plotted in $\delta^{15}N$ vs. $\ln([NO_3^-])$ space. Plain symbols represent the original measurements (yielding a regression slope of -5.2), while black-outlined symbols illustrate the effect of removing the 'steady-state dilution' component from the original data (yielding a regression slope of -6.5). The profile at 52.0°S and nearby underway samples have been excluded from the regressions as they appear to derive from a different subsurface source.

The slope in Figure 5.3 implies an isotope effect of 5.2‰ for nitrate assimilation in the mixed layer; higher than estimates deriving from the profile data but in much better agreement with summertime estimates from the AZ. If we correct for a possible steady-state dilution effect in the mixed-layer data, as done above in the context of the depth profiles, this serves to raise the isotope effect to 6.5‰ (Figure 5.3), putting it in still greater disagreement with the profile-based isotope effect estimates. The disagreement between the mixed layer- and depth profile-based isotope effect estimates is consistent with an additional process modifying the wintertime depth profile relationships, and it is this possibility that further analysis supports, as described below.

This is not the first time that such low slopes have been observed in AZ profile data. Sigman et al. (1999a) found the T_{min} layer of summertime profiles (i.e., the base of the winter mixed

layer) from the Indian and Pacific sectors to be an anomaly in Rayleigh space, falling well below the expected utilization trend between underlying UCDW and the surface mixed layer (Figure 5.4). The low slopes connecting UCDW with the T_{min} layer in their summer profiles are thus analogous with our wintertime UCDW-to-mixed-layer slopes. Previous investigations into the T_{min} anomaly south of Australia neither invoked a summer-winter difference in the isotope effect to account for its existence, nor could they explain the full extent of the deviation as a mixing effect with UCDW below (Sigman et al., 1999a; DiFiore et al., 2010). Instead, it was concluded that the influence of low-$\delta^{15}N$ LCDW, via lateral exchange between the T_{min} and T_{max} layers (the latter of which is fed by LCDW from below), was largely responsible for the anomalous character of the T_{min} (DiFiore et al., 2010).

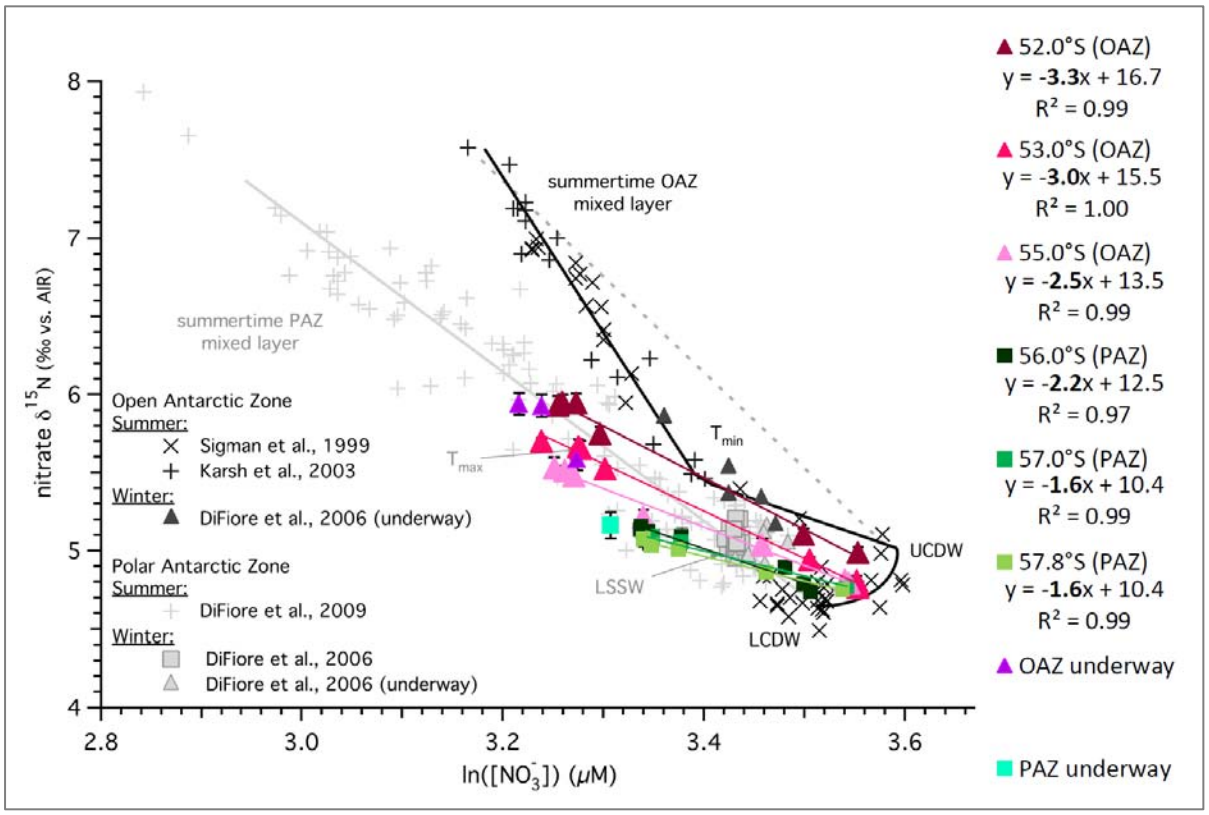

Figure 5.4 Comparison between our wintertime AZ data south of Africa (OAZ in pink, PAZ in green) and a compilation of winter and summer AZ data from the region south of Australia (OAZ in black, PAZ in grey). Atlantic sector profiles are plotted down to the $[NO_3^-]$ maximum, with linear trendline equations provided for each in the right-hand legend. For all data, solid symbols represent winter measurements, while summer measurements are denoted by crosses and x's. The solid grey and black lines indicate the depth progression through the data, along which key water masses are labelled (see text for definitions of acronyms). The dashed grey line indicates the expected trajectory for OAZ profiles under conditions of pure Rayleigh assimilation of UCDW nitrate. The anomalously low slopes of our AZ profiles are reminiscent of those connecting UCDW with the summer T_{min} (remnant winter mixed layer) in the data from the Australian sector. Original data sources indicated bottom left. [source: figure modified from DiFiore et al., 2010]

However, it appears that contamination of the T_{min} with LCDW nitrate cannot explain the low Rayleigh slopes in the Atlantic AZ winter profile data reported here. The failure of this explanation derives from the similarity between UCDW and LCDW [NO_3^-] and $\delta^{15}N$ in the Atlantic sector AZ. Considering the simplified, extreme case where the AZ winter mixed layer is fed solely by LCDW (Figure 5.5), the regression line through the average LCDW values and the average of the mixed-layer data at each station does produce steeper slopes. However, only in the case of the northernmost profile (at 52.0°S) does this achieve an estimate for the isotope effect that is greater than 5‰, yet the mixed layer at 52.0°S is the least likely to be directly supplied by LCDW (given its greater distance from the latitude at which LCDW might be imported directly into the wintertime mixed layer). The isotope effects implied by all the other slopes (2.3-2.9‰ in the PAZ and 3.5-4.3‰ in the OAZ) are still substantially lower than expected for the AZ.

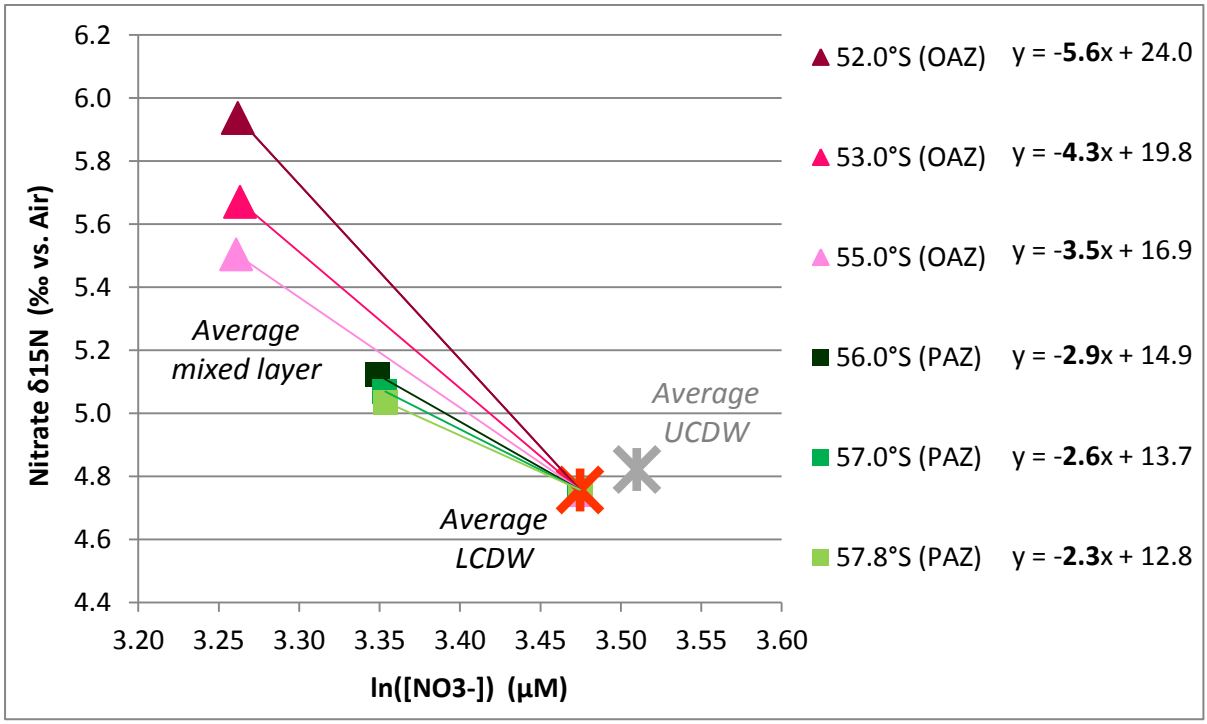

Figure 5.5 A simplified $\delta^{15}N$ vs. ln([NO_3^-]) plot demonstrating the effect of a pure LCDW source on profile-based estimates of the AZ isotope effect. Regression lines are passed from the average LCDW values through the average mixed-layer values at each station (OAZ in pink, PAZ in green), with their resulting slope values highlighted in bold in the right-hand legend. For comparison, the average position of UCDW in this space is indicated in grey.

Comparing the positions of LCDW and UCDW in Rayleigh space reveals why even a complete change in the choice of source cannot fully explain the low implied isotope effects. The two water masses are too similar, particularly in $\delta^{15}N$ (both close to 4.8‰), to make a

large enough difference. To lower the slopes from a utilization trajectory of 5‰ or 6‰ to the observed 2-4‰ by mixing alone would require a water mass with a much lower $\delta^{15}N$ and/or a much lower $[NO_3^-]$ than that of LCDW. For example, source water with the $[NO_3^-]$ of LCDW (~32 μM) would need to have a $\delta^{15}N$ of ~4.4‰ to yield slopes in the 5-6‰ range (or 5-7‰ if we include the northernmost AZ profile). We see no evidence for such a water mass in our data.

Comparing our profile data with those compiled by DiFiore et al. (2010) (Figure 5.4), on the other hand, explains why a LCDW influence would have a substantial effect on the T_{min} layer of the east Indian sector, south of Australia (and likewise the mixed layer of our northernmost AZ profile). In that region, UCDW and LCDW appear as distinct water masses in Rayleigh space, in terms of both concentration and isotopic composition (Figure 5.4).

This observation raises the question of how much these inter-basin differences in deep water mass properties contribute to the surface differences between sectors. While the form of our Atlantic AZ profiles is reminiscent of the Indian *OAZ* profiles (where UCDW-to-T_{min} slopes are typically 2-3‰), they derive from a source that is lower in $[NO_3^-]$ and $\delta^{15}N$, more similar to that of the Indian *PAZ* (i.e., LCDW) (except in the northernmost AZ profile) (Figure 5.4). As described above, this subsurface difference likely derives from the greater influence of NADW and reduced influence of Indo-Pacific denitrification in the Atlantic sector. The differences between the Indian OAZ T_{min} and the AZ winter mixed layer, in terms of their actual $\delta^{15}N$ and $[NO_3^-]$ values, are consistent with being at least partly driven by the difference in deep nitrate source properties. This carry-over of deep source water properties to the surface would also explain why we do not see the same kind of 'regime shift' in our profiles from the PAZ to the OAZ, as is observed south of Australia (where the two zones are fed by distinct water masses) (DiFiore et al., 2010).

In any case, it seems that we require an alternative to the hydrographic explanation of DiFiore et al. (2010) to explain the anomalously low isotope effects implied by the $\delta^{15}N$ profiles of the AZ south of Africa. Some other mechanism is required that acts to lower the $\delta^{15}N$ of nitrate in the winter mixed layer. Furthermore, the question of how the AZ mixed-layer and profile data can yield such different estimates for the isotope effect of nitrate assimilation remains unanswered. We now turn to the O isotope data to pursue these questions.

5.3 O isotope gradients of the Antarctic Zone mixed layer

Plotting the nitrate O isotope data in Rayleigh space reveals a similar trend of isotopic elevation with increasing nitrate consumption towards the AZ surface (Figure 5.6). The isotope effects implied by the $\delta^{18}O$ profile slopes (from the deep $[NO_3^-]$ maximum of UCDW to the mixed layer), however, fall within a smaller range of 4.2-4.5‰ (with the exception of one station at 56.0°S that suggests an isotope effect of 5.8‰) and are all notably higher than those yielded by the $\delta^{15}N$ profiles (Figure 5.7).

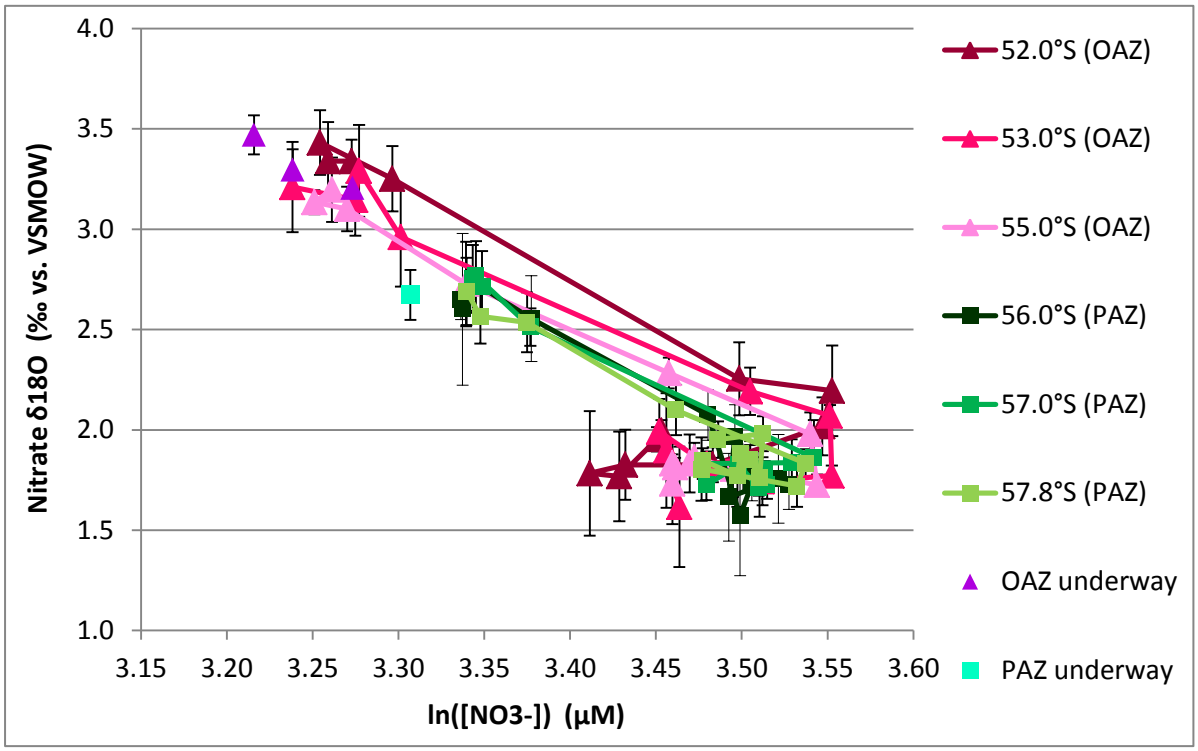

Figure 5.6 Full AZ depth profiles (and underway surface data) plotted in Rayleigh space (nitrate $\delta^{18}O$ vs. $\ln([NO_3^-])$). OAZ data (shown in shades of pink) exhibit greater isotopic enrichment and nitrate depletion towards the surface than PAZ data (in shades of green). Error bars indicate the measurement standard deviation for each sample. Error bars indicate the standard deviation for replicate measurements.

Although nitrate $\delta^{18}O$ data from the Southern Ocean are still relatively rare, existing studies indicate an O isotope effect of assimilation close to 5‰ for the AZ; for instance, 4.7 ± 0.1‰ in the PAZ (DiFiore et al., 2009). If the steady-state dilution effect is removed from our $\delta^{18}O$ profiles (in the same way as described above for $\delta^{15}N$), the revised isotope effects (4.7-5.2‰, and 6.2‰ for the profile at 56.0°S) are very similar to these previous estimates (Appendix C, Figure C.2a-f).

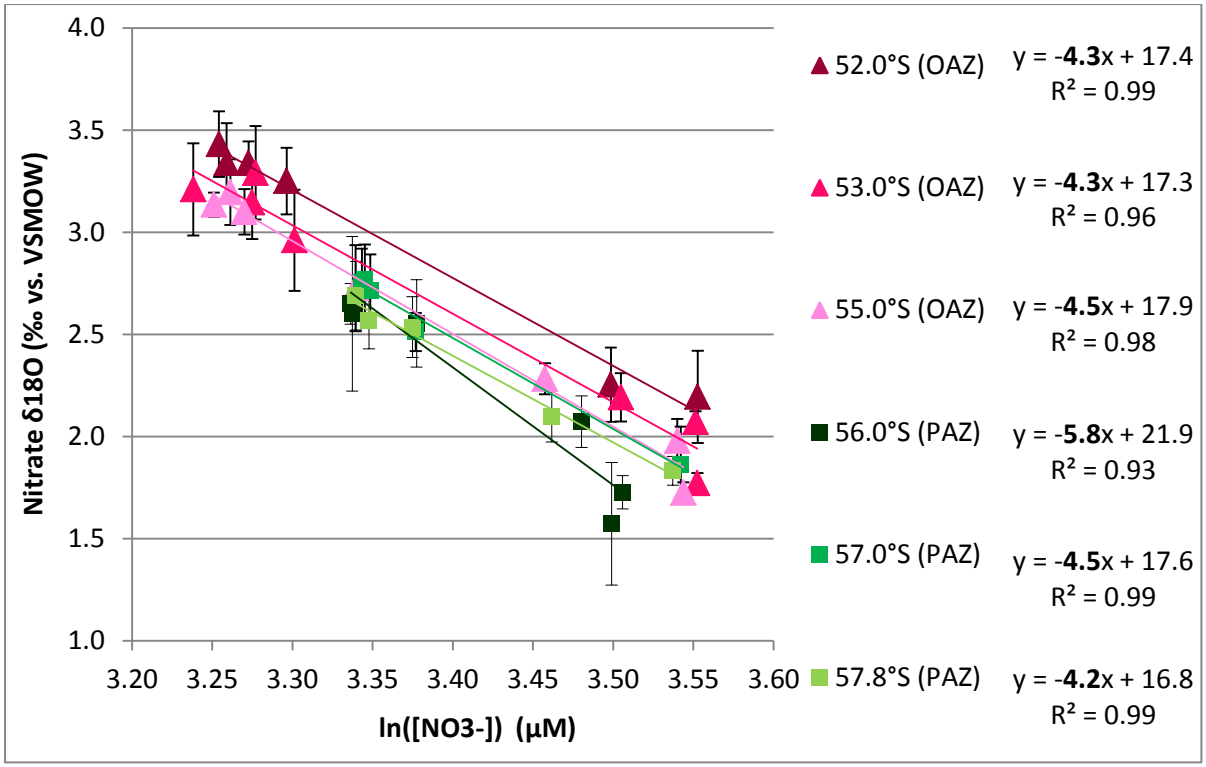

Figure 5.7 OAZ (pink) and PAZ (green) profile data plotted in $\delta^{18}O$ vs. $\ln([NO_3^-])$ space, from the surface down to the $[NO_3^-]$ maximum of UCDW. The slopes of the linear trendlines (values in bold in the legend) in Rayleigh space provide an estimate for the isotope effect of nitrate assimilation at each station. Error bars indicate measurement standard deviation.

Unlike the $\delta^{15}N$ profiles which suggest increasingly higher isotope effects from south to north across the AZ (Figure 5.2), the $\delta^{18}O$ profiles show no clear latitudinal progression (Figure 5.7). This may be partially attributable to the larger measurement error for $\delta^{18}O$ than $\delta^{15}N$, but could also derive from the decoupling of nitrate N and O isotopes during the remineralization of bulk suspended PN. We elaborate on this in section 5.4 below.

Interestingly, the O isotope data do not suggest as much of a discrepancy between profile- and mixed-layer-based estimates of the isotope effect. Isolating and running a regression line through only the mixed-layer data (excluding the profile at 56.0°S and its most closely associated underway sample, which seem to derive from a different source) implies an isotope effect of 6.1‰ (1.6-1.9‰ higher than the profile-based estimates) (Figure 5.8). With the steady-state dilution effect removed, this estimate rises to 7.2‰ (2.0-2.5‰ higher than the profile-based estimates). For comparison, mixed-layer-based estimates observed in the N isotope data are 1.9-3.6‰ and 2.4-4.3‰ higher than profile-based estimates, with and without dilution effects, respectively. The significance of the greater amplitude of the O

isotope effect and the greater similarity between the mixed-layer and profile estimates is explored next.

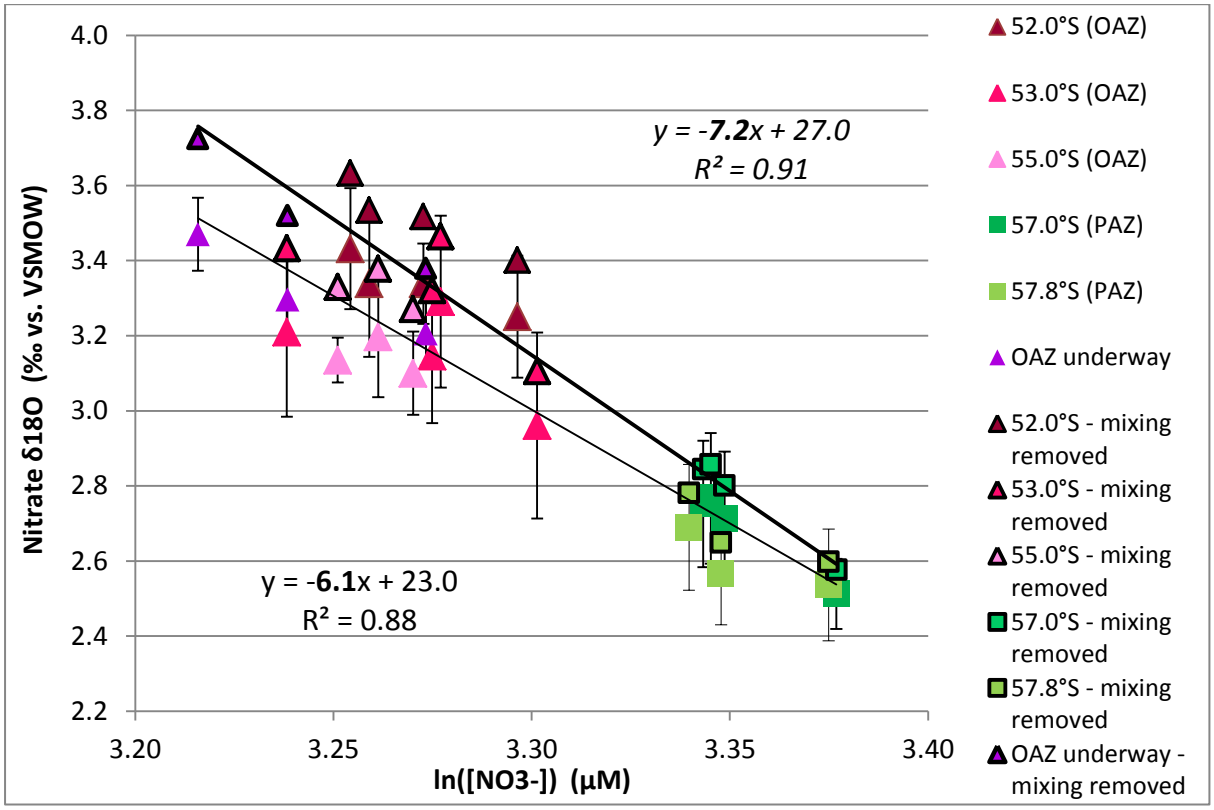

Figure 5.8 All AZ mixed-layer (profile and underway) data plotted in $\delta^{18}O$ vs. $\ln([NO_3^-])$ space (excluding the profile at 56.0°S and its most closely associated underway sample, which appear to derive from a different subsurface source). Plain symbols represent original measurements (yielding a regression slope of -6.1), while black-outlined symbols show the effect of removing the 'steady-state dilution' component from the original data (yielding a regression slope of -7.2).

5.4 The dual isotopes of nitrate in the Antarctic Zone

5.4.1 Mixed-layer nitrification indicated by the decoupling of nitrate N and O isotopes

In order to assess the relationship between the N and O isotopes of nitrate in the wintertime AZ, we consider the profiles in $\delta^{18}O$ vs. $\delta^{15}N$ space (Figure 5.9). Culture studies have shown that nitrate assimilation produces roughly equal elevations in both the $\delta^{15}N$ and $\delta^{18}O$ of nitrate; such that the N isotope effect of assimilation ($^{15}\varepsilon_{assim}$) is roughly equal to the O isotope effect of assimilation ($^{18}\varepsilon_{assim}$) (Granger et al., 2004). Thus, if the only biological process acting upon nitrate in the AZ profiles was assimilation, we would expect all the data

to fall along a 1:1 line in $\delta^{18}O$ vs. $\delta^{15}N$ space (extending from the average $\delta^{18}O$ and $\delta^{15}N$ of the deep nitrate source). However, as we trace the AZ profiles from their deep source to surface, there is a clear deviation above the 1:1 line.

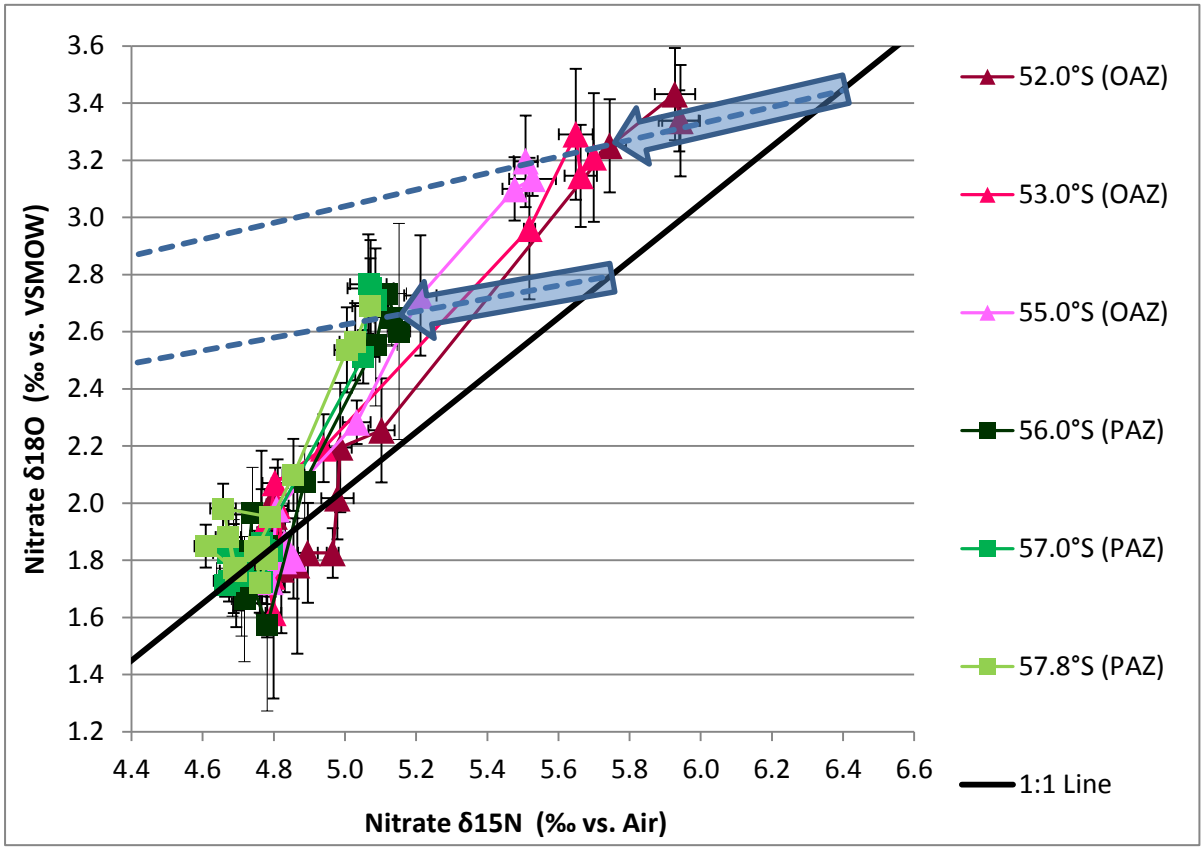

Figure 5.9 OAZ (pink) and PAZ (green) profiles plotted in $\delta^{18}O$ vs. $\delta^{15}N$ space. The solid black line is a 1:1 line passing through the average $\delta^{18}O$ and $\delta^{15}N$ values of the deep nitrate source (assumed here to be UCDW), and illustrates the trajectory that the profiles would follow if nitrate assimilation was the only process occurring in the mixed layer. The blue arrows indicate the effect that *in situ* nitrification has on the AZ mixed-layer samples in this space. The blue dashed lines project towards the approximate $\delta^{18}O$ and $\delta^{15}N$ values of newly nitrified nitrate (1.1‰ and -1.7‰ respectively; the latter being the average $\delta^{15}N$ of PN available for regeneration in the wintertime AZ surface – see Figure 4.5a). Vertical error bars represent the standard deviation of $\delta^{18}O$ measurements and horizontal error bars represent the standard deviation of $\delta^{15}N$ measurements.

Two major processes are known to produce such a deviation; firstly, N_2 fixation, and secondly, partial nitrate assimilation coupled with nitrification.

N_2-fixing organisms (e.g. *Trichodesmium*) convert atmospheric N_2 ($\delta^{15}N$~0‰) to ammonium with a small isotope effect, producing PN with a $\delta^{15}N$~-1-0‰ (Hoering & Ford, 1960; Carpenter et al., 1997; Karl et al., 2002). Remineralization of this low-$\delta^{15}N$ PN in the

underlying thermocline thus introduces anomalously low-$\delta^{15}N$ nitrate (relative to its $\delta^{18}O$, which is set by the $\delta^{18}O$ of nitrification) (Liu et al., 1996; Karl et al., 2002; Sigman et al., 2005; Knapp et al., 2008). Given its high energy requirements, N_2 fixation typically occurs in high-light, warm-water, N-impoverished environments such as the oligotrophic subtropical gyres (Dugdale et al., 1961; Carpenter & Capone, 1992; Karl et al., 2002). Given that light levels are low and nitrate is abundant in the AZ winter mixed layer, it is unlikely that N_2 fixation accounts for the observed deviation of $\delta^{15}N$ and $\delta^{18}O$ from 1:1.

Interestingly, *Trichodesmium* was observed at one station along the transect, although at ~40°S (close to the Subtropical Front; STF) (Verheye 2013, *pers. comm.*). Furthermore, the presence of *Trichodesmium* alone does not necessitate active N_2 fixation, as they are facultative organisms, capable of assimilating other forms of N when conditions are unfavourable for N_2 fixation (Mulholland & Capone, 1999). It is possible, however, that the low-$\delta^{15}N$ signal of N_2-fixation could be advected into the Southern Ocean from the subtropics. If so, we might expect to see this signal in the SAZ, but it would be unlikely to extend as far south as the AZ. The smaller deviation of SAZ profiles from the 1:1 line (i.e., less pronounced decoupling of N and O) compared to AZ and PFZ profiles (described below in section 5.5) also argues against the notion of a transport signal from the north.

A more feasible explanation for the decoupling of the N and O isotopes of nitrate in the wintertime AZ is partial nitrate assimilation followed by *in situ* nitrification. PN produced in the AZ surface is low in $\delta^{15}N$ due to the modest degree of nitrate utilization that occurs in this region (Sigman et al., 1999a; Sigman et al., 2009a). When this PN is regenerated, its low-$\delta^{15}N$ signal is preserved in the resulting nitrate, while the $\delta^{18}O$ of the nitrate is reset to the nitrification value (estimated to be ~1.1‰ higher than ambient water by Sigman et al., 2009). Because the regenerated nitrate has a combined $\delta^{15}N$ and $\delta^{18}O$ that lies above the 1:1 line (the point towards which the blue dashed lines project in Figure 5.9), its effect on the partially-assimilated (and thus ^{15}N- and ^{18}O-enriched) mixed-layer nitrate pool (via mixing) is to lower its $\delta^{18}O$ less than it lowers its $\delta^{15}N$, driving the mixed-layer samples off the 1:1 line in the direction indicated by the blue arrows.

The decoupling of N and O by nitrification is likely responsible for some of the differences between $\delta^{15}N$ and $\delta^{18}O$ gradients observed in the wintertime AZ. For instance, the smaller range of estimates for the isotope effect across the AZ suggested by the $\delta^{18}O$ profile data (which the $\delta^{15}N$ profiles estimate to increase from south to north) (compare Figure 5.7 with

Figure 5.2) likely reflect the independence of $\delta^{18}O$ (unlike $\delta^{15}N$) from the isotopic composition of the PN being regenerated at different latitudes (due to varying degrees of nitrate consumption), with lower-$\delta^{15}N$ PN at higher latitudes due to a lower degree of nitrate consumption (Figure 4.5a).

The difference in the offset between mixed-layer- and profile-based estimates of the isotope effect from N compared to O isotopes (i.e., larger for N than for O) may be another manifestation of the decoupling. The offset itself, in the case of both N and O, is likely a result of the different timescales recorded by lateral versus vertical gradients. The mixed-layer sample sets capture the assimilation-driven meridional gradient in mixed-layer nitrate isotopes, which is erased by lateral exchange of surface waters on a time scale of less than a year. In contrast, the vertical gradients in nitrate isotopes integrate over periods longer than a year, as it takes years for mixed-layer nitrate to be replaced by exchange with underlying deep water nitrate. Nitrification in the mixed layer would act to dampen the assimilation signal in both N and O isotope profiles (producing lower apparent isotope effects), although more so for N than for O since the ambient nitrate $\delta^{15}N$ is lowered more by *in situ* nitrification than is $\delta^{18}O$.

In contrast to our findings, a dual isotope investigation carried out by DiFiore et al. (2009) in the summertime coastal PAZ found the N and O isotopes of nitrate to be tightly coupled; with all profiles lying close to the 1:1 line in $\delta^{18}O$ vs. $\delta^{15}N$ space. They interpret this as indicating minimal nitrification ($\leq$ 6% of the nitrate assimilation rate according to their one-box geochemical model). This lack of summertime nitrification is consistent with the ability of phytoplankton to compete for ammonium in sunlit surface waters as well as the evidence for light inhibition of nitrifiers (Olson, 1981; Ward, 2005). We presume that wintertime nitrification would also have occurred in the coastal PAZ studied by DiFiore et al. (2009). Given that the coastal PAZ has neither a summertime T_{min} layer nor a decrease in nitrate concentration into the upper ocean during the winter (DiFiore et al., 2009), the lack of an upper ocean nitrification signal in this region is likely explained by dilution with deep nitrate due to extremely deep winter mixing characteristic of the region.

5.4.2 Explaining the anomalously low $\delta^{15}N$ of the Antarctic Zone winter mixed layer: Three N-cycling scenarios

Based on the evidence for nitrification in the AZ winter mixed layer, we consider three different scenarios of N cycling in the mixed layer (in order of increasing complexity) and explore their potential to account for the anomalously low $\delta^{15}N$ of mixed-layer nitrate in the wintertime AZ which ultimately leads to underestimation of the isotope effect from profile data. The goal is to establish the conditions under which nitrification is capable of producing deviations as substantial as those we observe in the AZ $\delta^{15}N$ profiles.

Scenario 1

The first scenario we consider is a simplified mixed-layer N cycle, depicted by Figure 5.10, in which the nitrate taken up by phytoplankton (i.e., PN) is ultimately returned to the nitrate pool via remineralization of PN to ammonium and then nitrification of that ammonium to nitrate *in situ*. Each step occurs with some fractionation of the N isotopes (indicated by the $^{15}\varepsilon$ value next to each arrow). In this scenario we assume that $^{15}\varepsilon_{Remin}$ = 0‰ and that there is no export of PN from the mixed layer.

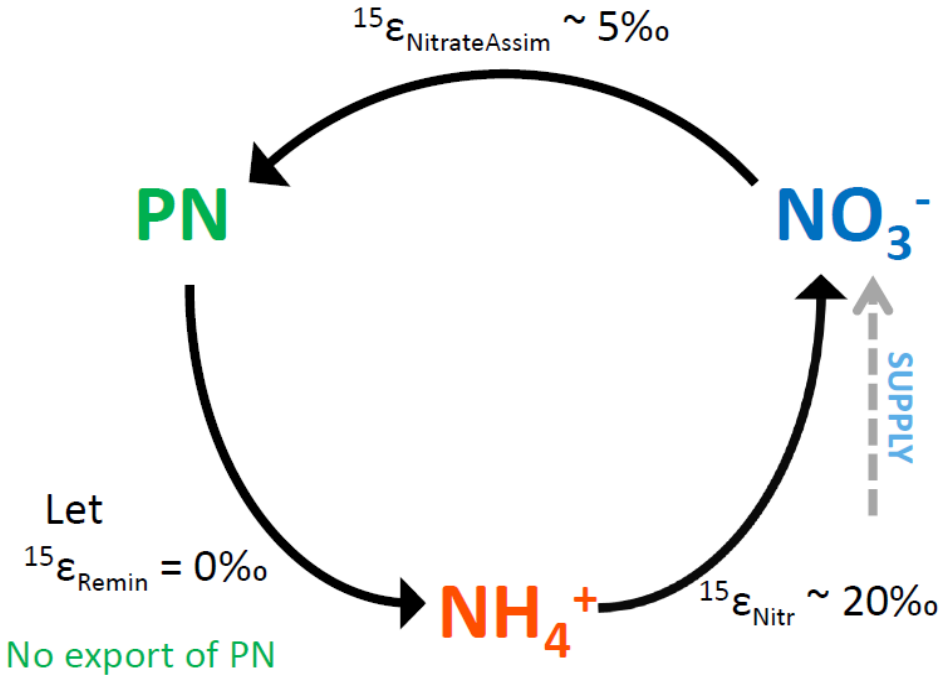

Figure 5.10 A simplified mixed-layer N cycle (scenario 1) where nitrate (NO_3^-), supplied from below the mixed layer, is taken up by phytoplankton (PN) with an isotope effect ($^{15}\varepsilon_{NitrateAssim}$) of ~ 5‰ (Sigman et al., 1999a). This PN is remineralized to ammonium (NH_4^+) with no fractionation (assuming $^{15}\varepsilon_{Remin}$ = 0‰), and then nitrified back to nitrate *in situ* with an overall isotope effect ($^{15}\varepsilon_{Nitr}$) of ~ 20‰ (Casciotti et al., 2003). In this case, we assume no export of PN from the mixed layer.

The cycling depicted in Figure 5.10, due to the nitrification step, acts to decouple the N and O isotopes of nitrate (Sigman et al., 2005; Sigman et al., 2009a), consistent with our nitrate isotope data from the AZ. This loop alone, however, cannot explain the anomalously low $\delta^{15}N$ of the AZ winter mixed layer. As noted by Sigman et al. (1999a), *in situ* PN regeneration (i.e., within the same parcel of water as the partially-consumed nitrate pool from which the PN formed) gradually lowers the total mixed-layer-nitrate $\delta^{15}N$ along a trajectory that falls only slightly below the utilization trend in Rayleigh space (analogous to a mixing curve between the 'initial' and 'final' nitrate pools). Once the PN has been completely regenerated, the $\delta^{15}N$ of mixed-layer nitrate converges on that of the original source. Thus, at any stage in the regeneration process, the deviation below a Rayleigh line with $\varepsilon_{NitrateAssim}$ = 5‰ will be minor (particularly at low levels of utilization), such that regeneration alone cannot account for the anomalously low slopes in Rayleigh space generated by our wintertime AZ profiles. We, therefore, look to the second scenario.

Scenario 2

Figure 5.11 depicts the same mixed-layer N cycling regime as Figure 5.10, with the addition of a second pathway for ammonium (i.e., direct assimilation into the PN pool). The added potential of this scenario to explain our observations lies in the co-occurrence of nitrification and ammonium assimilation, each with a different isotope effect.

The isotope effect of ammonium assimilation ($^{15}\varepsilon_{AmAssim}$) appears to increase with increasing ammonium concentration ($[NH_4^+]$) (Hoch et al., 1992; Pennock et al., 1996; Waser et al., 1998; Vo et al., 2013). At $[NH_4^+]$ of 5 μM, the isotope effect of ammonium assimilation for a marine bacterium was found to be 4‰ (Hoch et al., 1992). Although variable, ambient concentrations in the AZ mixed layer are typically much lower than 5 μM. Indeed, on-board measurements of $[NH_4^+]$ ranged from 0.1-1.8 μM for the AZ (Philibert et al., *in preparation*). To be conservative, however, we use $^{15}\varepsilon_{AmAssim} \sim 4‰$ in our discussion.

Nitrification consists of three main steps: (1) the ammonia/ammonium equilibrium, (2) the oxidation of ammonium to nitrite, and (3) the oxidation of nitrite to nitrate. The first and second have a combined isotope effect of 14-38‰ (Casciotti et al., 2003), while the third occurs with an inverse isotope effect of around -12‰, although its expression in the environment is largely supressed under low ambient nitrite concentration ($[NO_2^-]$) (Casciotti, 2009; DiFiore et al., 2009). On-board measurements of $[NO_2^-]$ from the AZ mixed layer fall

in the 0.2-0.3 µM range. For our purposes, it is sufficient to consider the overall fractionation imparted by the nitrification process ($^{15}\varepsilon_{Nitr}$), which we take to be ~ 20‰.

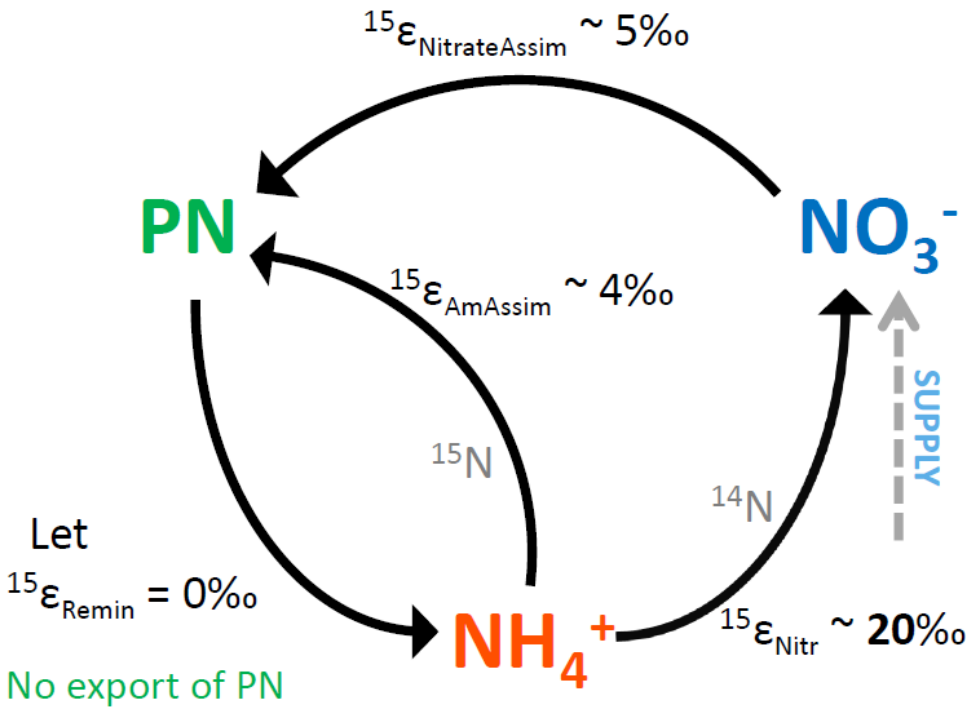

Figure 5.11 The second mixed-layer N-cycling scenario, including co-occurring ammonium assimilation (with $^{15}\varepsilon_{AmAssim}$ ~ 4‰; Hoch et al., 1992) and nitrification (with $^{15}\varepsilon_{Nitr}$ ~ 20‰); where the differing isotope effects of the two branches result in the accumulation of ^{14}N in the NO_3^- pool.

Because the isotope effect of nitrification (~20‰) is greater than the isotope effect of ammonium assimilation (~4‰), ^{14}N will be preferentially channelled into the nitrate pool, lowering its $\delta^{15}N$; while ^{15}N will be preferentially channelled into the PN pool, causing its $\delta^{15}N$ to rise (DiFiore et al., 2009) (Figure 5.11). This "branching ammonium effect" can, in principle, lower the $\delta^{15}N$ of mixed-layer nitrate and produce low slopes in the AZ profiles (and thus low isotope effects).

At steady state, the $\delta^{15}N$ of the PN pool would be 16‰ (i.e., 20‰ - 4‰; the difference between the two branching isotope effects) higher than the $\delta^{15}N$ of the nitrate pool. To fit our observations of the AZ winter mixed layer with an average nitrate $\delta^{15}N$ of 5.4‰ would, therefore, require the PN pool to have a $\delta^{15}N$ of 21.4‰ (i.e., 5.4‰ + 16‰), which is much higher than the -6-0‰ range indicated by our bulk suspended PN measurements from the region (Figure 4.5a).

In order for the branching ammonium mechanism to be feasible, a substantially large PN pool is required, such that it can retain enough of the ^{15}N diverted to it to noticeably lower the $\delta^{15}N$ of the nitrate pool. Bulk suspended PN measurements from the AZ, however, indicate concentrations to be low during winter ([PN] ~ 0.2-0.4 μM; Figure 4.5a), limiting its influence on a nitrate pool so much larger than itself ($[NO_3^-]$ ~ 25-29 μM within the AZ mixed layer). Furthermore, a large PN pool in the AZ would require extensive wintertime production to sustain it, which nitrate uptake rates from the region suggest to be unlikely. Depth-integrated nitrate uptake rates obtained from on-board tracer incubations during the winter cruise fall in the 0.20-0.45 mmol m^{-2} d^{-1} range within the AZ (Philibert et al., *in preparation*), while previous summertime measurements from the same region indicate rates of 3.39 ± 1.9 mmol m^{-2} d^{-1} (Joubert et al., 2011). Thus, winter nitrate uptake rates in the AZ are roughly 3 to 26 times lower than during summer.

Therefore, it appears that another mechanism, which does not require an unfeasibly high PN-$\delta^{15}N$ or an unfeasibly large wintertime PN pool (and thus high productivity during winter), is needed to account for the anomalously low nitrate $\delta^{15}N$ of the AZ winter mixed layer.

Scenario 3

The third scenario we consider entails an additional mechanism for lowering the $\delta^{15}N$ of mixed-layer nitrate, namely, a sinking PN flux together with some degree of fractionation during remineralization (as illustrated by Figure 5.12).

The cumulative isotope effect of remineralization (ε_{Remin}) expressed in the ocean is thought to be relatively small, around 3‰ (Altabet et al., 1999; Lehmann et al., 2002; DiFiore et al., 2009). However, if the remineralization of PN to ammonium occurs with any fractionation, the export of that PN will preferentially remove high-$\delta^{15}N$ N from the mixed layer; lowering the $\delta^{15}N$ of total mixed-layer N, including that of the nitrate pool. In this scenario, the $\delta^{15}N$ of PN remaining in the mixed layer can be progressively lowered; both because of the physical removal of high-$\delta^{15}N$ PN into the ocean interior, and the continual re-assimilation of low-$\delta^{15}N$ ammonium (into which ^{14}N is being diverted). The return of this "anomalously" low-$\delta^{15}N$ PN and ammonium to the ambient mixed-layer nitrate pool is thus capable of lowering its $\delta^{15}N$ far more than the simple case of nitrate assimilation coupled to regeneration (as in Figure 5.10) would allow.

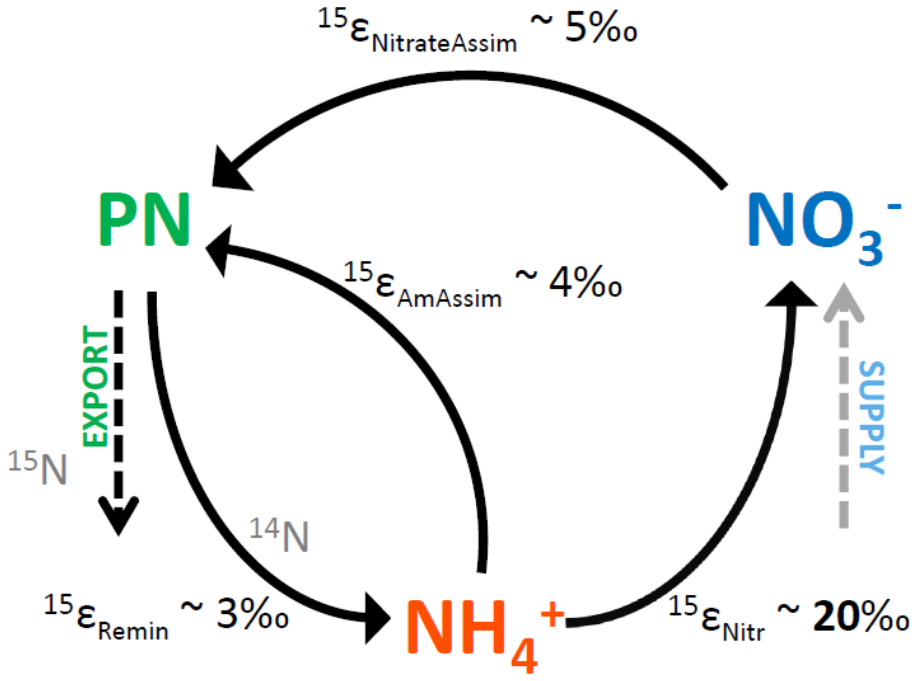

Figure 5.12 The third N-cycling scenario for the AZ mixed layer, the same as Figure 5.11, but with the addition of a PN export flux and non-zero fractionation during remineralization of PN to NH_4^+ ($^{15}\varepsilon_{Remin}$ ~ 3‰; Altabet et al., 1999; Lehmann et al., 2002); which would preferentially export ^{15}N from the mixed layer and lower the $\delta^{15}N$ of the remaining mixed-layer N.

The mechanism described above (a sinking PN flux coupled with fractionation during remineralization) is more powerful than the branching ammonium effect alone (scenario 2; Figure 5.11), as it does not require a large PN pool to substantially lower the $\delta^{15}N$ of the AZ winter mixed-layer nitrate and produce isotope effects in the range that we observe.

Seasonal synthesis

In reality, the processes involved in scenario 3 (depicted by Figure 5.12) may not occur continuously, all year round (i.e., at steady state). Instead, it is likely that there exists some form of seasonal succession, with different mechanisms coming into play at different times. It has been hypothesized that euphotic zone nitrification could be more important in the Southern Ocean during winter than in summer (Sanders et al., 2007). This is in good agreement with our findings (which suggest significant levels of nitrification within the AZ winter mixed layer) and those of DiFiore et al. (2009) (which advocate a minor role for nitrification in the summertime PAZ). If this is the case, we might expect the proposed mechanisms for lowering mixed-layer nitrate $\delta^{15}N$ to play out as follows on a seasonal timescale.

During the summer, PN in the AZ surface is low in $\delta^{15}N$; not only because of the modest degree of nitrate utilization, but also because of the assimilation of low-$\delta^{15}N$ recycled N (i.e., ammonium) (Altabet & Francois, 1994b; Sigman et al., 1999a; Lourey et al., 2003). If the remineralization of PN to ammonium occurs with some fractionation, sinking PN will remove relatively high $\delta^{15}N$ material from the mixed layer (although the fractionation during nitrate assimilation still causes this N to be substantially lower than the $\delta^{15}N$ of the deep nitrate supply), and the $\delta^{15}N$ of ammonium available for assimilation will be lower still. By the end of the summer season, the PN remaining in surface waters will be low in $\delta^{15}N$ which, once remineralized and nitrified in the wintertime mixed layer, lowers the $\delta^{15}N$ of the ambient nitrate beyond Rayleigh or steady-state predictions.

The addition of a nitrification pathway to the mixed-layer system during winter, by default, introduces the branching ammonium effect, which could lower the $\delta^{15}N$ of the mixed-layer nitrate in its own right. Factors such as the extent to which summer PN is remineralized during winter, the magnitude of the associated isotope effect (ε_{Remin}), and the $\delta^{15}N$ of the PN being remineralized will all influence how much of a role the branching ammonium effect must play to produce the observed decrease in winter mixed-layer nitrate $\delta^{15}N$.

In order to determine the relative importance of the two primary mechanisms proposed (i.e., the branching ammonium effect, and sinking PN coupled with a remineralization isotope effect) and better understand their interactions, we plan to employ a numerical model of nitrate isotope dynamics in the mixed layer (similar to that of DiFiore et al. (2009)) in future work.

5.4.3 Specific implications of Antarctic Zone findings

Our investigation into the wintertime AZ of the Atlantic sector has revealed two key findings: (1) the isotopic similarity between the winter mixed layer and the summertime T_{min}, and (2) isotopic evidence for nitrification in the surface ocean. Beyond their specific implications for understanding present-day nitrate isotope dynamics in the Southern Ocean, these findings are also of relevance for paleoceanographers and the broader oceanographic community.

1. Isotopic similarity between the winter mixed layer and the summertime T_{min}

Even though this study was conducted in the winter, our findings imply a higher isotope effect for summertime nitrate assimilation than initially estimated for the AZ. As mentioned

previously, the anomalously low $\delta^{15}N$ of the T_{min} layer (the remnant winter mixed layer observed in summer profiles) has complicated estimation of the isotope effect in this region (Sigman et al., 1999a; Karsh et al., 2003; DiFiore et al., 2010). For example, in the absence of winter data, Sigman et al. (1999a) assumed that UCDW was the ultimate nitrate source to the summertime surface, yielding isotope effect estimates in the 4-6‰ range for the OAZ. However, our data agree better with those of DiFiore et al. (2010), suggesting that the T_{min} layer, or ideally the winter mixed layer itself (to avoid the effects of summertime modification of the T_{min}), is the ultimate source to the summer AZ. Using winter mixed-layer [NO_3^-] and $\delta^{15}N$ values (as opposed to those of UCDW) as an approximation for the starting point of summertime nitrate assimilation, yields isotope effects ~1.2‰ higher than those estimated initially by Sigman et al. (1999a) for OAZ profiles south of Australia (DiFiore et al., 2010).

Knowing the isotope effect of nitrate assimilation is essential for the accurate interpretation of N-isotope variations recorded in Southern Ocean sediments (Altabet & Francois, 1994b; Sigman et al., 1999a). The higher the isotope effect we apply in interpreting the ~4‰ $\delta^{15}N$ increase in glacial sediments compared to today (assuming the isotope effect is temporally constant), the lower the inferred glacial nitrate utilization and the more tightly it is constrained (i.e., the closer together the upper and lower limits of utilization provided by the Rayleigh integrated and instantaneous equations, respectively; see section 2.3.1). A change from ε = 5‰ to ε = 6.2‰ (i.e., ~1.2‰ higher isotope effects suggested by DiFiore et al. (2010), which our study support) in the AZ, however, appears only to have a modest effect on inferred glacial nitrate utilization (i.e., ~5% less utilization required to produce the same ~4‰ elevation in sedimentary $\delta^{15}N$). Thus it remains that the greater concern for paleo-interpretations is a temporally varying isotope effect (e.g., due to environmental changes involving light, mixed-layer depth and/or sea-ice) which could alternatively explain the glacial-interglacial variations in sedimentary $\delta^{15}N$ (rather than changes in nitrate utilization) (Sigman et al., 1999a; Sigman et al., 1999b; Karsh et al., 2003; DiFiore et al., 2010).

2. Mixed-layer nitrification

That nitrification is occurring in the wintertime AZ mixed layer is evident from the decoupling of the N and O isotopes of nitrate in the upper water column of this region. This too can complicate the inference of nitrate utilization from paleo-records, as sedimentary $\delta^{15}N$ will reflect not only the deep-source nitrate (and the isotope effect with which it was

assimilated) but also the newly nitrified nitrate. We have seen first-hand the potential for nitrification to obscure the manifestation of the nitrate assimilation isotope effect in the mixed-layer nitrate $\delta^{15}N$; an effect which could be passed on to the PN $\delta^{15}N$ (DiFiore et al., 2009). That is, the anomalously low $\delta^{15}N$ of mixed-layer nitrate that we observe could become anomalously low-$\delta^{15}N$ sinking and sedimentary PN when assimilated by phytoplankton. Consequently, sediments underlying waters that host significant levels of mixed-layer nitrification, either today or in the past, might be vulnerable to underestimation of nitrate utilization (since lower sedimentary PN-$\delta^{15}N$ could be misinterpreted as a lower degree of nitrate utilization in surface waters).

Furthermore, this finding has important implications for estimating organic carbon export from surface waters in the modern ocean, and also for our understanding of the conditions that favour nitrification.

The f-ratio, defined as the ratio of new production to primary (i.e., new plus regenerated) production, is conventionally used to quantify the strength of the biological pump, with high f-ratios suggesting an ecosystem supported largely by 'new' nutrients from below the euphotic layer (rather than nutrients recycled within surface waters) and characterized by substantial export (Eppley & Peterson, 1979). Traditionally, nitrification was regarded as a sub-euphotic zone phenomenon; either due to light inhibition of nitrifying bacteria (Olson, 1981), or competition for substrate with photosynthesising ammonium assimilators (Ward, 2005). Assuming that nitrification is vertically separated from primary production within the water column has led to the use of a simplified form of the f-ratio, with nitrate uptake as an approximation for new production (Dugdale & Goering, 1967; Eppley & Peterson, 1979). If, however, nitrification does occur at significant levels within the euphotic zone, some of the nitrate taken up is actually regenerated; leading to the over-estimation of new production, the f-ratio, and thus the extent of organic carbon export into the ocean interior (Dugdale & Goering, 1967; Diaz & Raimbault, 2000; Yool et al., 2007).

Several studies indicate that nitrification is possible within the euphotic zone (Ward, 1987; Dore & Karl, 1996; Diaz & Raimbault, 2000; Clark et al., 2008). A modelling study even concluded that around half of global surface nitrate is supplied by *in situ* nitrification rather than upwelling into the euphotic zone (Yool et al., 2007).

Although our AZ data speak to nitrification at significant levels in the surface ocean, the fact that this is observed in winter but not in summer (DiFiore et al., 2009) suggests sensitivity to seasonal changes in the Southern Ocean. Perhaps the low light-levels and deep mixed layers of the wintertime AZ give nitrifiers a competitive advantage, such that nitrification should be expected in this environment in the winter. The importance of wintertime nitrification in the AZ surface warns against dismissing the nitrification contribution in a particular region (whether in the estimation of carbon export from f-ratios or the interpretation of paleo-records) simply on the basis of summertime measurements. This is especially relevant for Southern Ocean studies where wintertime measurements are still relatively scarce.

5.5 Dual nitrate isotope distribution across the entire Southern Ocean depth section

Up until this point, we have focused our attention on the AZ. Here we consider the transect as a whole within a dual isotope framework, providing a broader Southern Ocean context for our existing findings and a glimpse into future directions for this work.

Figure 5.13 displays all the wintertime Atlantic sector profiles in $\delta^{18}O$ vs. $\delta^{15}N$ space. North of the PF, profiles continue to exhibit stronger deep-to-surface gradients in $\delta^{18}O$ than in $\delta^{15}N$, evident as a deviation of the mixed-layer samples above the 1:1 line. This deviation persists into and across the SAZ, although to a lessening degree.

The nitrate $\delta^{15}N$ and $\delta^{18}O$ data can be compared on a spatial basis as a depth section of $\Delta(15\text{-}18)$ (Figure 5.14), where the difference between the $\delta^{15}N$ and the $\delta^{18}O$ of nitrate is plotted at every sampling point (Rafter et al., 2013) as follows:

$$\Delta(15-18) = \delta^{15}N - \delta^{18}O$$

$\Delta(15\text{-}18)$ is similar to the $\Delta(15,18)$ parameter adopted by Sigman et al. (2005), with the difference that $\Delta(15\text{-}18)$ is not normalized to the background of deep nitrate isotopic composition. Therefore, using our average deep nitrate source values gives $\Delta(15\text{-}18)$ = 4.8‰ - 1.8‰ = 3.0‰, which can be thought of as the baseline value for this parameter (rather than 0‰ in the case of $\Delta(15,18)$). A study on nitrate $\Delta(15\text{-}18)$ evolution within the Pacific basin observed the same $\Delta(15\text{-}18)$ value of 3.0‰ for Circumpolar Deep Water

upwelling into the Pacific AZ surface (Rafter et al., 2013). In this notation, a low Δ(15-18) (i.e., < 3.0‰) falls above the 1:1 line in Figure 5.13, while a high Δ(15-18) (i.e., > 3.0‰) falls below the 1:1 line. The further the Δ(15-18) from the baseline value of 3.0‰ in either direction, the greater the apparent decoupling of the N and O isotopes of nitrate relative to the nitrate imported to the upper ocean from Antarctic deep waters.

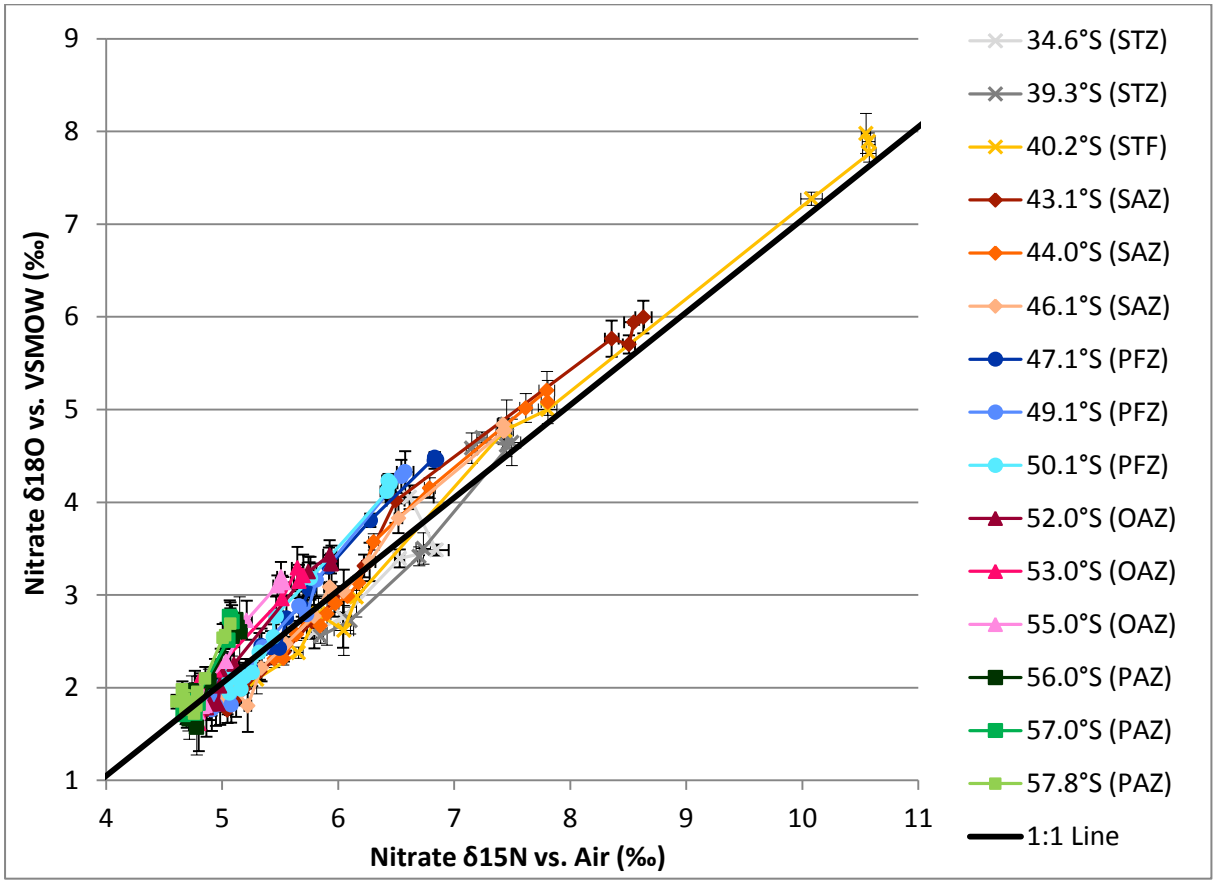

Figure 5.13 All wintertime Atlantic sector profiles plotted in $\delta^{18}O$ vs. $\delta^{15}N$ space. The solid black line is a 1:1 line passing through the average $\delta^{18}O$ and $\delta^{15}N$ values of the deep nitrate source (assumed here to be UCDW), the trajectory that the profiles would follow under conditions of nitrate assimilation alone. PAZ, OAZ and PFZ mixed-layer samples fall above the 1:1 line, a deviation that decays across the SAZ towards the STF. Vertical error bars represent the standard deviation of $\delta^{18}O$ measurements and horizontal error bars represent the standard deviation of $\delta^{15}N$ measurements.

Viewing the data in this space confirms that the low $\delta^{15}N$-to-$\delta^{18}O$ relationship in the winter mixed layer is not confined to the AZ, but extends across the Southern Ocean (Figure 5.14). Mixed-layer Δ(15-18) is less than 2.7‰ throughout the transect, with values as low as 2.2‰ near the PF. At depth, we detect a low Δ(15-18) signal in LCDW that appears to intensify

downward into waters below the salinity maximum of LCDW (compare with Figure 4.1b). As NADW appears to have a Δ(15-18) of 3.0‰ or greater (Sigman et al., 2009a), the low Δ(15-18) of the deep Atlantic Antarctic likely reflects at-depth regeneration of low-δ^{15}N PN produced in polar surface waters (Sigman et al., 2000).

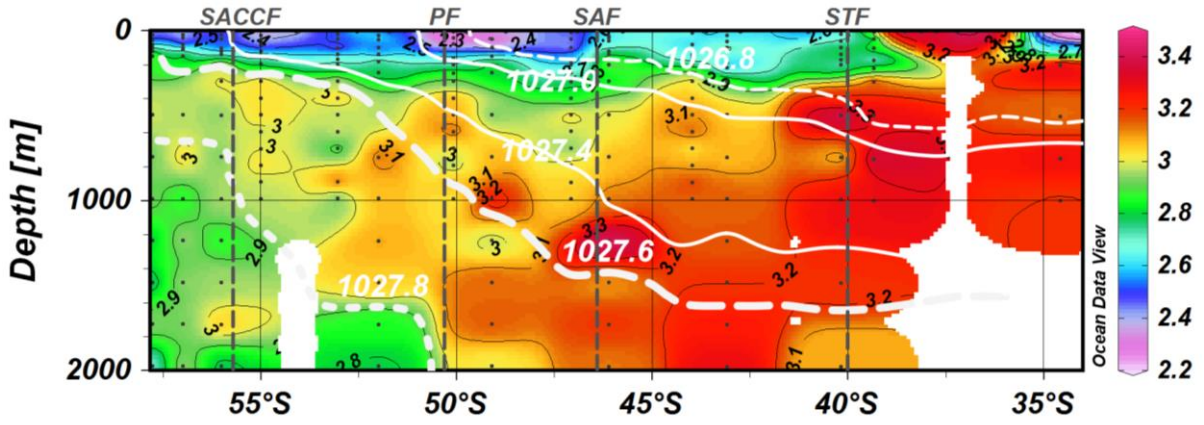

Figure 5.14 Section plot of nitrate Δ(15-18) in ‰ units for the entire wintertime transect between Cape Town (33.5°S) and the Antarctic winter sea-ice edge (56.7°S). Both underway and profile measurements are incorporated, with grey dots denoting each sampling location. Colour shading and black contours refer to Δ(15-18). White isopycnals and labels are provided for key water masses; LCDW (1027.8 kg m^{-3}), UCDW (1027.6 kg m^{-3}), AAIW (1027.0-1027.4 kg m^{-3}) and SAMW (1026.8 kg m^{-3}). Frontal positions are indicated by dashed grey vertical lines and labels above the panel. A low Δ(15-18) signal appears to be a feature of the winter mixed layer across the Southern Ocean, not only in the AZ.

The low Δ(15-18) of LCDW in the Atlantic sector raises the possibility that the Δ(15-18) minimum (i.e. anomalously low nitrate δ^{15}N) of the winter mixed layer could simply be a circulation feature. More specifically, the low Δ(15-18) of the wintertime surface might result from the upwelling of LCDW or denser water into the PAZ mixed layer and advection northward across the Southern Ocean, as proposed for the Antarctic region south of Australia by DiFiore et al. (2010). There are several arguments against circulation being the sole driver of the observed Δ(15-18) minima. For instance, the Δ(15-18) of the winter mixed layer reaches substantially lower values (e.g., 2.2‰ in the PFZ) than we observe in the deep Antarctic. It is possible, that a water mass with a lower Δ(15-18) exists further south or at greater depth than was sampled. However, in the case of northward advection of low Δ(15-18) nitrate, we would expect an increase in Δ(15-18) (i.e., a weakening anomaly) from south to north, which is not observed.

In detail, surface Δ(15-18) has local minima at around 55°S, 51°-48°S and possibly 41°S; close to the Southern Antarctic Circumpolar Current Front (SACCF), the PF (or much of the PFZ) and the STF respectively (Figure 5.14; also refer to Figure 4.5b for underway Δ(15-18) from legs 1 and 2). These locations also correspond with local maxima in [PN] (refer to Figure 4.5a). The high levels of summertime production (Wefer & Fischer, 1991; Moore & Abbott, 2000) or the physical accumulation/retention (and thus longer residence times) of PN at the fronts (Franks, 1992) may foster higher rates of *in situ* regeneration at these locations during winter, thus adding a larger amount of low-Δ(15-18) newly nitrified nitrate.

Nevertheless, our interpretation of the data as indicating *in situ* nitrification is related to the hydrographic explanation proposed by DiFiore et al. (2010) to account for the anomalously low $\delta^{15}N$ of the T_{min} layer south of Australia (i.e., exchange with LCDW). The same process (namely, partial nitrate assimilation followed by regeneration) is responsible for the feature in both mechanisms, except that regeneration of PN is focused at different depths – within the wintertime mixed layer as proposed here for the Atlantic sector versus in the deep ocean as proposed by DiFiore et al. (2010) for the Antarctic south of Australia.

In the Pacific sector, while Rafter et al. (2013) observed only a slight (~0.3‰) Δ(15-18) decrease into the AZ summer T_{min} layer, they found a much lower Δ(15-18) in the SAZ thermocline, with values as low as 1.6‰. They attributed this low $\delta^{15}N$-to-$\delta^{18}O$ relationship to the regeneration of low-$\delta^{15}N$ PN in the SAZ thermocline, deep wintertime mixing (replenishing surface nitrate), and subsequent summertime assimilation from a lower starting Δ(15-18) (Rafter et al., 2013). In this way, Δ(15-18) can be driven to progressively lower values over multiple seasons. The absence of a concentrated Δ(15-18) minimum within the Atlantic SAZ may relate to the fact that the Atlantic sector does not host active Subantarctic Mode Water (SAMW) formation, unlike the Indian and Pacific sectors (McCartney, 1977; Sallée et al., 2006; Speich et al., 2012).

As with the SAMW anomaly of the Pacific sector (Rafter et al., 2013), we suspect that the low Δ(15-18) feature of the Southern Ocean mixed layer is not generated anew each winter; rather, it is likely the product of multiple annual cycles of partial nitrate assimilation (and ammonium recycling) in summer, followed by deep mixing and *in situ* nitrification in winter, with these processes working together to lower the Δ(15-18) of mixed-layer nitrate across the wintertime AZ. Summertime measurements from the same transect may allow us to test this hypothesis of seasonal switches in upper-ocean N cycling and to differentiate between

regionally-caused differences and seasonally-driven changes in the nitrate isotope distributions.

UCDW in the Atlantic sector carries a relatively high Δ(15-18) signal of up to 3.3‰ (Figure 5.14). A high $\delta^{15}N$-to-$\delta^{18}O$ relationship can be produced by complete nitrate assimilation followed by regeneration, as occurs in the low latitudes. In this case, the $\delta^{15}N$ of the nitrate added by regeneration is similar to the ambient, deep source nitrate $\delta^{15}N$; while its $\delta^{18}O$ is reset to the nitrification value (Sigman et al., 2009a; Casciotti et al., 2002; Rafter et al., 2013). The decoupling can be further augmented if the nitrate consumed at the surface has already been elevated in $\delta^{15}N$ and $\delta^{18}O$ by denitrification or partial assimilation elsewhere (Sigman et al., 2009c; Rafter et al., 2013). Thus, the higher Δ(15-18) of UCDW is likely a vestige of its low-latitude origins, and its southward decrease towards the baseline value of 3.0‰, is likely a consequence of the accumulating signal from the regeneration of low-$\delta^{15}N$ sinking PN.

A striking mesoscale feature emerges in Figure 5.14 between 35°S and 40°S. The warm temperatures (> 16°C), high salinities (> 35.5 psu) (Figure 4.1a&b), and anticyclonic circulation (revealed by the ADCP data; not shown; Ansorge, 2012) identify it as an Agulhas Ring (Schmid et al., 2003). These warm-core eddies periodically detach from the Agulhas Current retroflection, carrying heat and salt from the Indian Ocean into the Atlantic basin (Gordon, 1986; Lutjeharms & van Ballegooyen, 1988). Underway sampling across the Agulhas Ring shows nitrate with an average concentration of 2.5 μM ($[NO_3^-+NO_2^-]$; refer to Appendix B, Figure B.2 and Figure B.3), $\delta^{15}N$ of 7.6‰ and $\delta^{18}O$ of 4.2‰. The resulting Δ(15-18) of 3.4‰ implies a high $\delta^{15}N$-to-$\delta^{18}O$ relationship; reminiscent of a low-latitude complete-assimilation-regeneration signal (Sigman et al., 2009a; Rafter et al., 2013). Given that Agulhas Rings are associated with deep mixed layers (≥ 250 m in this case) and vigorous mixing (Boebel et al., 2003; Donners et al., 2004; Speich et al., 2012), the high Δ(15-18) that we observe in the surface could be the result of exchange with the high Δ(15-18) waters below.

Taken as a whole, the wintertime nitrate isotope distributions across the Southern Ocean surface appear to suggest three prevailing modes, which characterize the three major zones of the transect. In the AZ, nitrification is the dominant process. Within this zone, the bulk of the deviation above the 1:1 line in Figure 5.13 is achieved, accompanied by only minor assimilation-induced elevations in $\delta^{15}N$ and $\delta^{18}O$. Here, mixed-layer Δ(15-18) is as low as

2.4‰, accounting for 0.6‰ of the total 0.8‰ decrease from the baseline value of 3.0‰. In the PFZ, both nitrification and assimilation appear to play important roles. In this zone, the minimum Δ(15-18) of 2.2‰ is reached (by a further 0.2‰ lowering), while $\delta^{15}N$ and $\delta^{18}O$, together, experience further elevation by assimilation. In the SAZ, the effects of mixing and assimilation seem to prevail. This is evident in the migration of surface samples back towards the 1:1 line heading north in Figure 5.13 (perhaps caused by mixing with the higher Δ(15-18) waters below), in the context of large increases in both the $\delta^{15}N$ and $\delta^{18}O$ of nitrate (consistent with more complete nitrate consumption at these latitudes).

6. Conclusions

In essence, the objectives of this study were, firstly, to characterize and, secondly, to account for the wintertime nitrate N and O isotope distributions in the region south of Africa. The wintertime patterns revealed by the data suggest that the assimilation of nitrate by phytoplankton remains a dominant control on the N and O isotope distributions of nitrate in the Southern Ocean through the winter season (evident in the strong correlation between nitrate isotopes ($\delta^{15}N$ and $\delta^{18}O$) and concentration ($[NO_3^-]$) from the subsurface into the mixed layer, and across the Southern Ocean surface), rather than having its signal overwhelmed by deep wintertime mixing.

Although the higher resupply rates relative to uptake during winter prevent us from producing accurate estimates of the isotope effect using the closed-system Rayleigh model, analysing the data within a Rayleigh framework has proven useful for identifying and interpreting deviations from the predicted nitrate utilization trend. In particular, the Antarctic winter mixed layer is observed to have an anomalously low $\delta^{15}N$-to-$[NO_3^-]$ relationship in Rayleigh space, similar to that of the T_{min} layer observed previously in summertime depth profiles from the Antarctic. This observation substantiates the claim that the summer T_{min} is more representative of the initial nitrate source (i.e., the starting point for assimilation) than the underlying Upper Circumpolar Deep Water (UCDW), and thus indirectly provides support for a higher summertime isotope effect than initially estimated for the Antarctic under the assumption of a UCDW source.

Comparison between the N and O isotope gradients of nitrate in Antarctic depth profiles demonstrates the decoupling of the two isotopes in the upper water column, with $\delta^{15}N$ exhibiting substantially weaker increases from the deep nitrate source into the mixed layer than $\delta^{18}O$. We interpret this decoupling as evidence for significant *in situ* nitrification within the Antarctic winter mixed layer. We put forward two potential mechanisms to explain the anomalously low $\delta^{15}N$ of Antarctic winter mixed-layer nitrate. The first involves the co-occurrence of nitrification and ammonium assimilation, where the isotope effect of nitrification is greater than the isotope effect of ammonium assimilation (causing ^{14}N to be preferentially channelled into the nitrate pool and lowering its $\delta^{15}N$). The second involves a sinking PN flux, coupled with fractionation during remineralization (preferentially removing high-$\delta^{15}N$ N from the mixed layer and lowering the $\delta^{15}N$ of total mixed-layer N, including

that of the nitrate pool). In order to test these hypotheses and quantify the rate of nitrification, a numerical model is required, which we plan to develop in future work.

The existence of active nitrification within Antarctic surface waters has important repercussions for our understanding of the Southern Ocean's biological pump. In order to accurately estimate the export of organic carbon to the deep ocean based on nutrient uptake rates, the contribution of *in situ* nitrification to the ambient mixed-layer nitrate pool must be accounted for. Failing to do so for environments of the Southern Ocean where euphotic zone nitrification is significant could lead to overestimating the strength of the present-day biological pump. Furthermore, both of the key findings outlined above (a higher summertime isotope effect, and wintertime mixed-layer nitrification) address unknowns that are central to the use of N isotopes as a proxy for changing biological nutrient utilization in the Antarctic through past glacial-interglacial cycles.

7. Appendices

Appendix A: Comparison between filtered and unfiltered samples

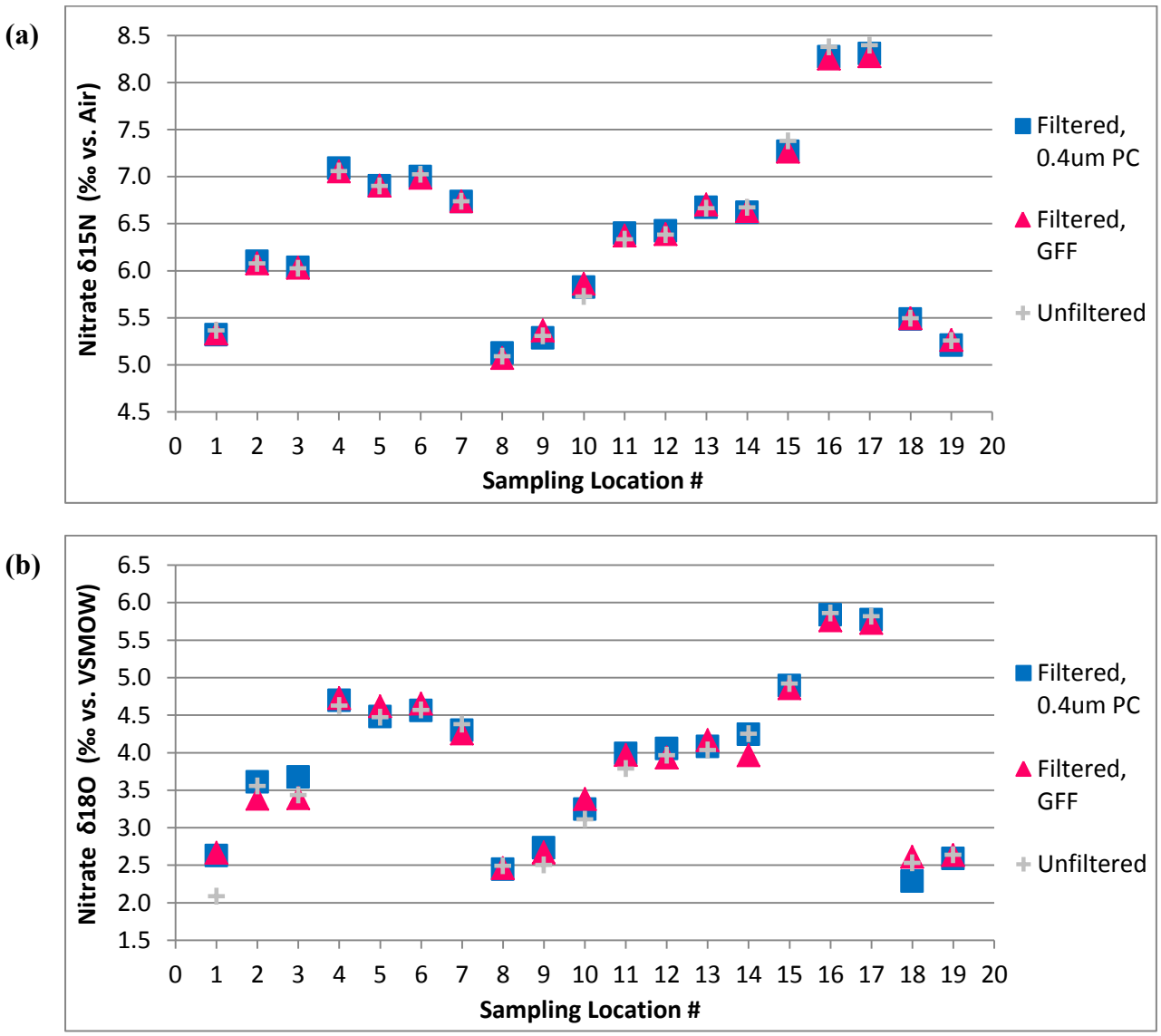

Figure A.1 Comparison between filtered and unfiltered seawater nitrate (a) $\delta^{15}N$ (in ‰ vs. air) and (b) $\delta^{18}O$ (in ‰ vs. VSMOW) measurements. Both filtered and unfiltered samples were collected at 19 different underway sampling locations on leg 2 of the winter voyage (from the Antarctic sea-ice edge (56.7°S) to Marion Island (46.9°S) and back to South Africa). Blue squares denote seawater samples filtered through 0.4 µM polycarbonate (PC) filters, pink triangles indicate samples filtered through combusted glass fibre filters (GF/Fs) and grey crosses denote unfiltered samples. All symbols represent analysis means.

Appendix B: The influence of nitrite on $\delta^{15}N$ and $\delta^{18}O$ measurements

B.1 Rationale

A potential complication in the measurement of nitrate isotopes using the denitrifier method is the presence of nitrite (Casciotti et al., 2007). The isotopic influence of nitrite on the nitrogen (N) isotope measurements depends on the relative quantity and $\delta^{15}N$ composition of nitrite, simply because it represents a portion of the nitrate plus nitrite pool. The isotopic influence of nitrite on the oxygen (O) isotope measurements is more complex. The conversion of nitrate (NO_3^-) to nitrous oxide (N_2O) represents a greater fractional loss of O atoms (two out of three) to water than the conversion of nitrite (NO_2^-) to N_2O (one out of two). Because of fractionation during the reduction process (preferential loss of ^{16}O), N_2O produced from NO_3^- will contain proportionally more ^{18}O than N_2O produced from NO_2^-. As a result, if there is any significant amount of NO_2^- present in the original seawater sample, it will yield a lower measured $\delta^{18}O$ value than if it contained purely NO_3^- (Casciotti et al., 2007; Granger & Sigman, 2009).

In previous studies of this kind, there is commonly no attempt made to correct for the presence of nitrite on the grounds of low ambient concentrations (e.g. Sigman et al., 1999a; DiFiore et al., 2009). As noted previously (section 3.2.1), on-board measurements of nitrite concentration ($[NO_2^-]$) made during the winter voyage (VOY03) indicate deep (> 200 m) concentrations of less than 0.1 µM (< 0.5% of the combined nitrate plus nitrite pool), and mixed-layer concentrations typically between 0.2 µM and 0.3 µM (0.75-3.0% of the combined nitrate plus nitrite pool) across most of the hydrocast transect. These concentrations were regarded low enough to neglect the presence of nitrite in these samples for the remainder of the study. According to Casciotti et al. (2007), however, a $[NO_2^-]$ constituting any more than 2% of the total nitrate plus nitrite pool (i.e., $[NO_3^- + NO_2^-]$) produces a detectable error in the measured $\delta^{18}O$. Here we present the results of the nitrite removal experiment (described in section 3.2.4) to test our assumption, and subsequently discuss the implications for our key findings.

B.2 Results of the nitrite removal experiment

Figure B.1 displays the $\delta^{15}N$ and $\delta^{18}O$ of all the selected seawater samples, measured before and after nitrite removal. The samples include both depth profile and underway surface collections spanning a wide range of concentrations, with $[NO_3^- + NO_2^-]$ between 1.8 µM and 34.7 µM. The effect of nitrite removal is to raise both $\delta^{15}N$ and $\delta^{18}O$ relative to untreated samples, although in general, the effect on $\delta^{18}O$ is greater (an average increase of 0.5‰) than the effect on $\delta^{15}N$ (an average increase of 0.4‰). Overall, the removal of nitrite has a greater influence on the measured isotopic composition of samples with lower concentrations (i.e., lower $[NO_3^- + NO_2^-]$). Samples with $[NO_3^- + NO_2^-]$ in the 10-35 µM range exhibit $\delta^{15}N$ and $\delta^{18}O$ increases of 0.0-0.7‰ and 0.0-0.9‰, respectively, when nitrite is removed, while samples with $[NO_3^- + NO_2^-]$ in the 1.8-10 µM range exhibit larger $\delta^{15}N$ and $\delta^{18}O$ increases of 0.1-1.8‰ and 0.1-2.3‰, respectively (with the resulting $\delta^{15}N$ and $\delta^{18}O$ increases growing towards lower concentrations).

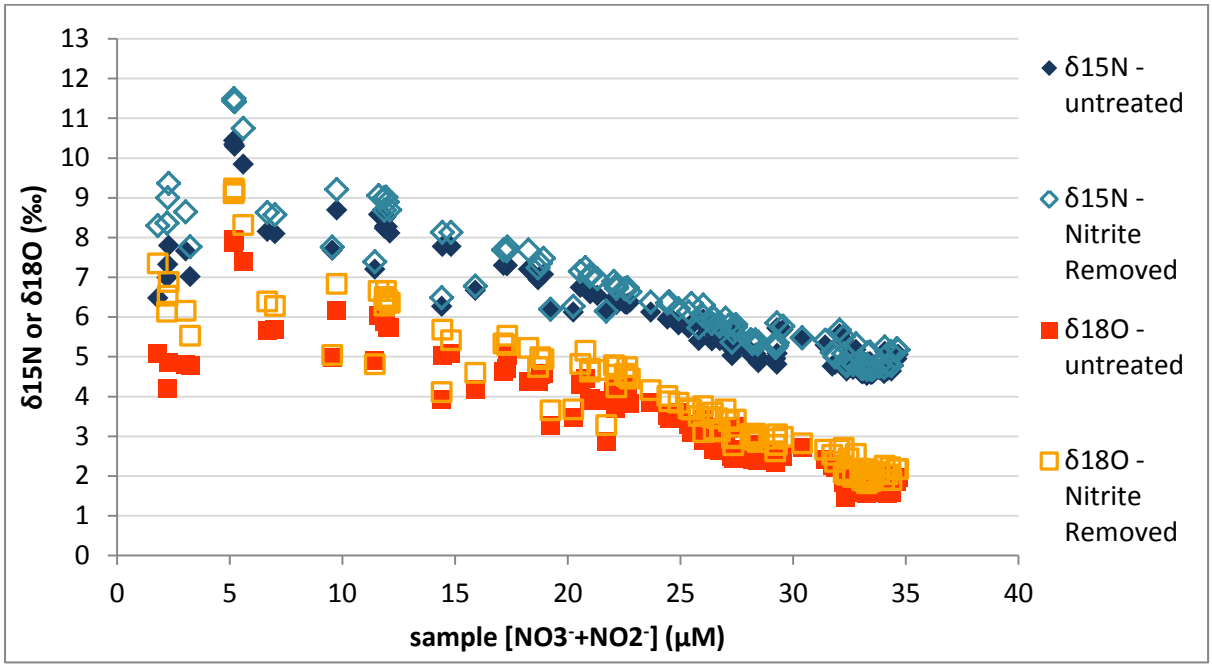

Figure B.1 The measured $\delta^{15}N$ (in ‰ vs. air; blue symbols) and $\delta^{18}O$ (in ‰ vs. VSMOW; orange symbols) of all seawater samples selected for the nitrite removal experiment, before (solid symbols) and after nitrite removal (open symbols), plotted against sample concentration (i.e., $[NO_3^- + NO_2^-]$ in µM units).

Below, these results are presented in the context of the surface and depth profile views of the wintertime Atlantic sector provided earlier in this study.

B.2.1 Underway samples

Figure B.2 exhibits the same trends described in Figure B.1, with samples containing nitrate only (i.e., nitrite removed samples) having higher $\delta^{15}N$ and $\delta^{18}O$ than those containing both nitrate and nitrite (i.e., untreated samples), with the magnitude of the offset increasing towards lower latitudes where surface concentrations are lower. The largest changes in measured isotopic composition caused by the removal of nitrite are observed in the Agulhas Ring feature (which has a $[NO_3^- + NO_2^-]$ of 2.5 µM) to the north of the Subtropical Front (STF), identified previously to be a distinct deviation in the $\delta^{15}N$(and $\delta^{18}O$)-to-$[NO_3^-]$ relationship between 35°S and 40°S (section 4.2.1). After removing nitrite, however, the feature is not as anomalous, with the average $\delta^{15}N$ increasing from 7.6‰ to 8.8‰ and the average $\delta^{18}O$ increasing from 4.2‰ to 6.4‰. As a result of the nitrite removal, the average Δ(15-18) (i.e., $\delta^{15}N$ minus $\delta^{18}O$) of the Agulhas Ring decreases from 3.4‰ to 2.4‰ (Figure B.3).

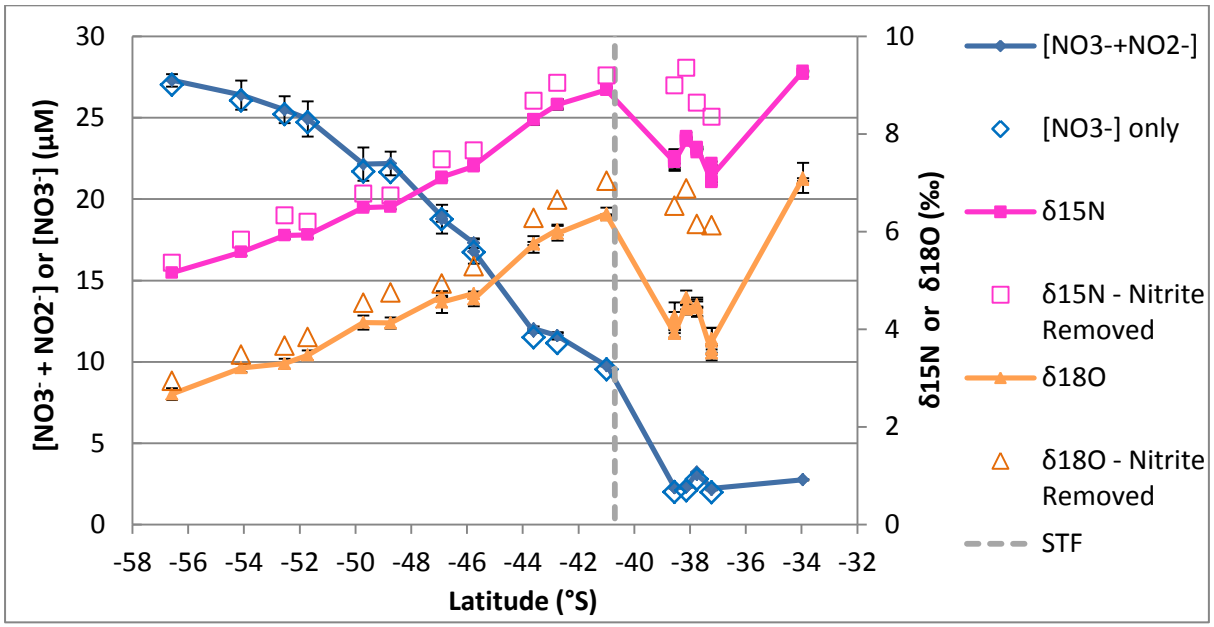

Figure B.2 Underway surface measurements of $\delta^{15}N$ (in ‰ vs. air), $\delta^{18}O$ (in ‰ vs. VSMOW), and concentration ($[NO_3^- + NO_2^-]$ or $[NO_3^-]$, in µM), before (solid symbols) and after nitrite removal (open symbols), plotted against latitude for the wintertime transect from Cape Town (33.5°S) to the Antarctic winter sea-ice edge (56.7°S). The grey dashed line denotes the position of the STF at the time of the voyage.

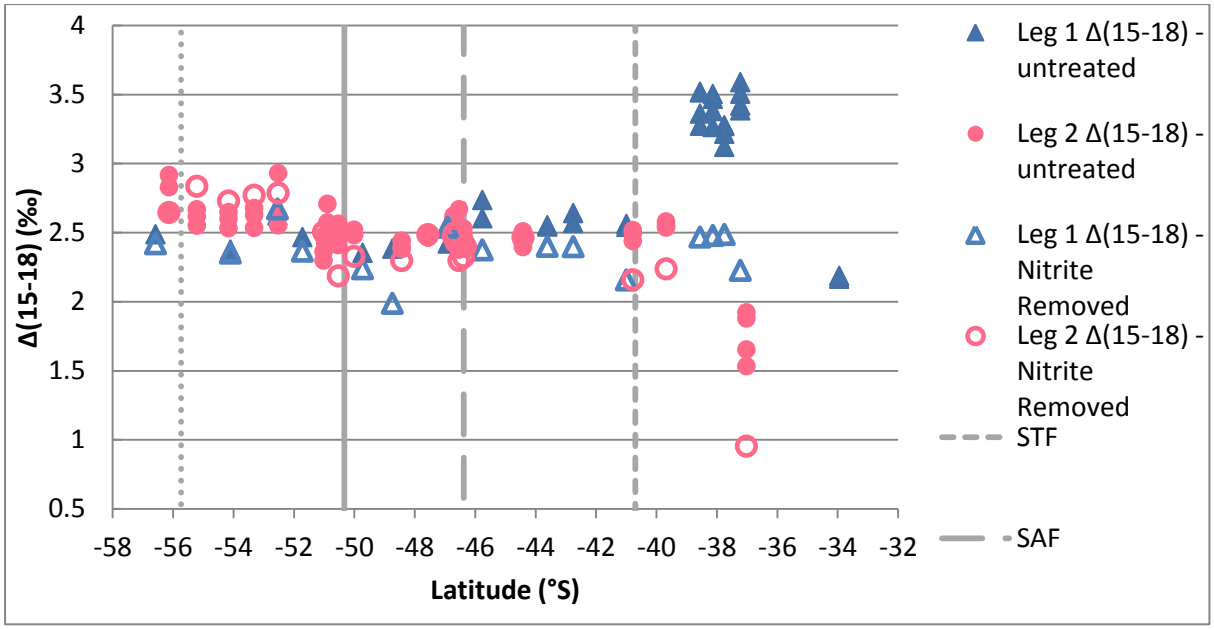

Figure B.3 Underway surface Δ(15-18) in ‰ units, before (solid symbols) and after nitrite removal (open symbols), plotted against latitude for leg 1 (in blue) and leg 2 (in pink) of the winter voyage. Vertical grey lines denote the frontal positions on leg 1.

B.2.2 Depth profiles

Plotting the available nitrite removal profile data from the wintertime Antarctic Zone (AZ) in Rayleigh space ($\delta^{15}N$ or $\delta^{18}O$ versus the natural log of concentration) for comparison with the original profile data reveals that shallower samples are generally more greatly affected by the removal of nitrite (experiencing greater increases in $\delta^{15}N$ and $\delta^{18}O$) than deeper samples (Figure B.4 and Figure B.5, respectively). Consequently, the 'nitrate only' data yield steeper slopes in Rayleigh space than the original 'nitrate plus nitrite' data for both the N and O isotopes. This is best illustrated by the Polar Antarctic Zone (PAZ) profiles, where every sample was measured with and without nitrite. In terms of the N isotopes, the slopes of the PAZ profiles in Rayleigh space (from the deep nitrate source to the surface) increase from 1.6-2.2‰ to 2.7-3.7‰ as a result of removing nitrite, while in terms of the O isotopes, PAZ profile slopes increase from 4.2-5.8‰ to 5.0-6.3‰ when nitrite is removed.

Plotting the same AZ profile data (with and without nitrite removed) in $\delta^{18}O$ vs. $\delta^{15}N$ space (Figure B.6) demonstrates the overall tendency of nitrite removal to raise the $\delta^{18}O$ of the re-measured sample slightly more than it raises its $\delta^{15}N$ (relative to untreated samples), leading to a greater deviation of mixed-layer samples above the 1:1 line than previously noted.

In the following section, we discuss the implications of these observations for the key findings presented in this study.

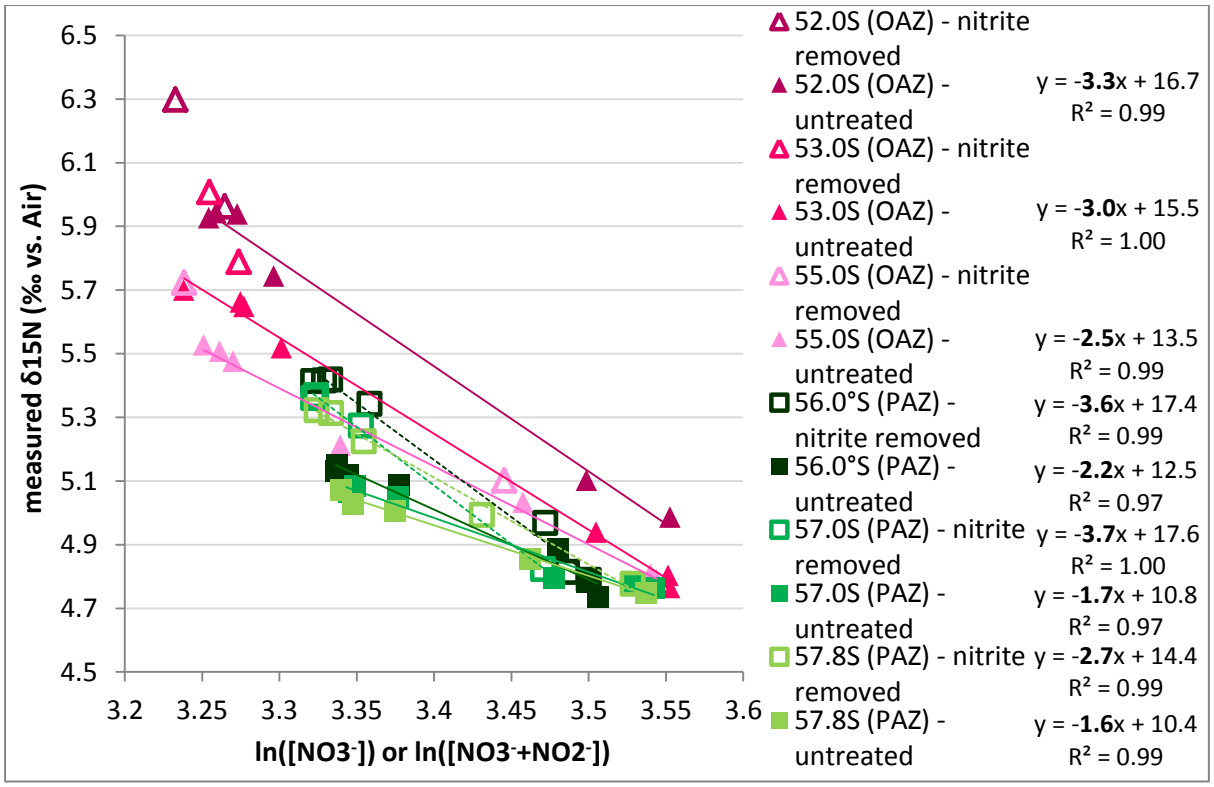

Figure B.4 The original (i.e., untreated) PAZ (solid green symbols) and OAZ (solid pink symbols) N isotope profile data are plotted in Rayleigh space ($\delta^{15}N$ versus the log of the sample concentration), from the surface to the depth of the [NO_3^-] maximum of UCDW. The available corresponding data from the nitrite removal experiment (every PAZ profile sample, and two near-surface samples from each of the OAZ profiles) are plotted for comparison (open green and pink symbols, respectively). Where full profiles are available, trendlines are plotted (solid lines for untreated samples; dotted lines for 'nitrite removed' samples) and their equations are provided in the right-hand legend (slopes are in bold text).

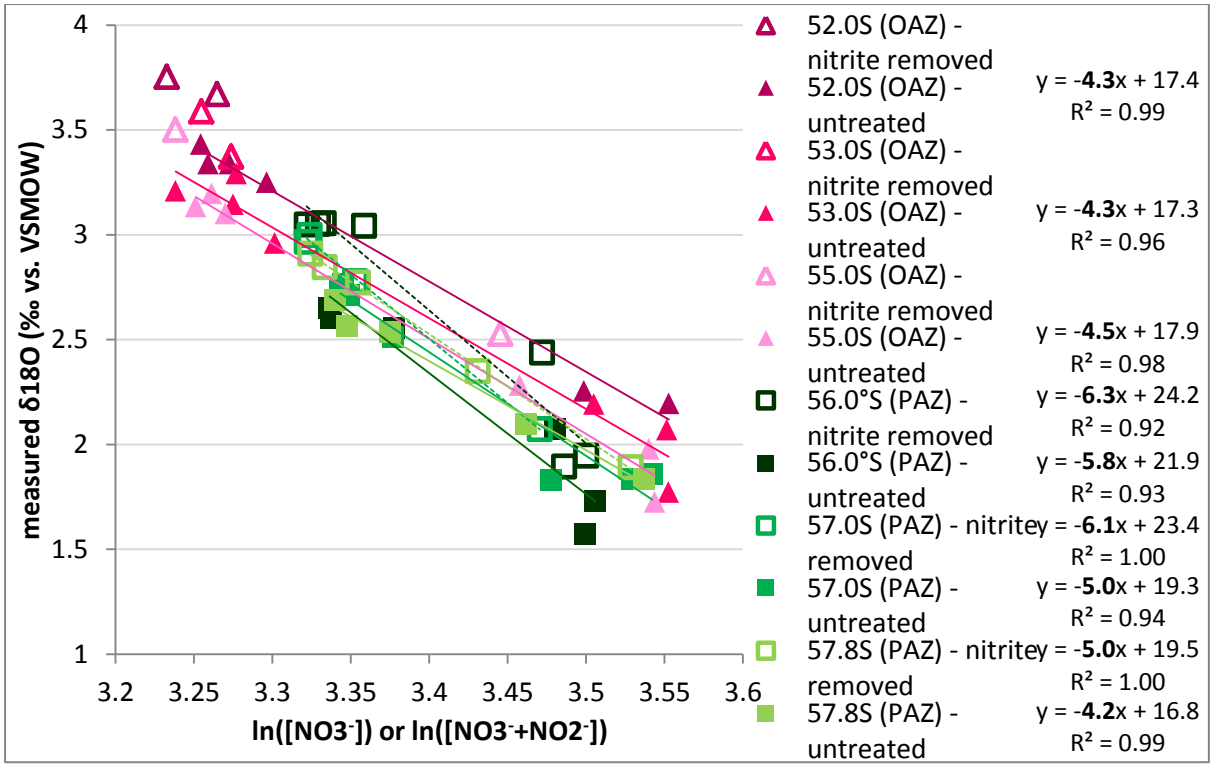

Figure B.5 The original (i.e., untreated) PAZ (solid green symbols) and OAZ (solid pink symbols) O isotope profile data are plotted in Rayleigh space ($\delta^{18}O$ versus the log of the sample concentration), from the surface to the depth of the [NO_3^-] maximum of UCDW. The available corresponding data from the nitrite removal experiment (every PAZ profile sample, and two near-surface samples from each of the OAZ profiles) are plotted for comparison (open green and pink symbols, respectively). Where full profiles are available, trendlines are plotted (solid lines for untreated samples; dotted lines for 'nitrite removed' samples) and their equations are provided in the right-hand legend (slopes are in bold text).

B.3 Implications

Although not central to the outcomes of this study, the marked effect of nitrite removal on the inferred isotopic composition of nitrate in the Agulhas Ring (inducing average $\delta^{15}N$ and $\delta^{18}O$ increases of 1.2‰ and 2.2‰, respectively; Figure B.2) serves to illustrate the importance of removing nitrite from samples where it constitutes a substantial portion of the total nitrate plus nitrite pool. Instead of having a high $\delta^{15}N$-to-$\delta^{18}O$ relationship (i.e., $\Delta(15\text{-}18) > 3$‰) as it first appeared (interpreted as a low-latitude complete-assimilation-regeneration signal acquired by mixing with the high $\Delta(15\text{-}18)$ waters below; see section 5.5), after nitrite removal the feature has a low $\delta^{15}N$-to-$\delta^{18}O$ relationship (i.e., $\Delta(15\text{-}18) < 3$‰), more similar to the Southern Ocean surface waters (as seen in Figure B.3).

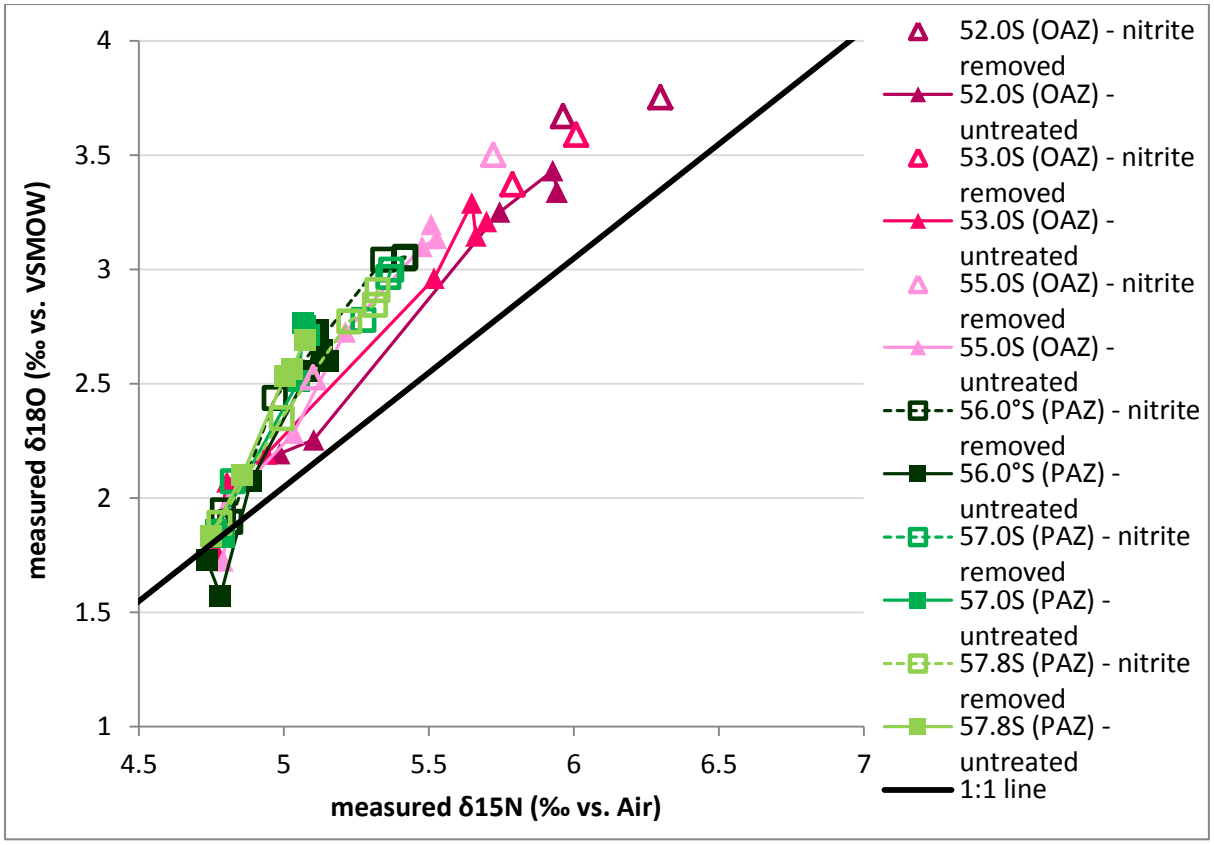

Figure B.6 The original (i.e., untreated) PAZ (solid green symbols) and OAZ (solid pink symbols) profiles plotted in $\delta^{18}O$ vs. $\delta^{15}N$ space. The available corresponding data from the nitrite removal experiment (every PAZ profile sample, and two near-surface samples from each of the OAZ profiles) are plotted for comparison (open green and pink symbols, respectively). The solid black line is a 1:1 line passing through the average $\delta^{18}O$ and $\delta^{15}N$ values of the deep nitrate source (assumed here to be UCDW).

There are two major implications of the nitrite removal experiment for the key findings of this study. The first is that the N isotope effect estimates yielded by the winter AZ profiles are not as anomalously low as implied by the original data (i.e., without nitrite removed; Figure B.4). Existing profile measurements, however, suggest that even the N isotope effects yielded by the 'nitrate only' data are lower than commonly observed in the summertime AZ (i.e., profile slopes in Rayleigh space are still less than 5), supporting the earlier conclusion that the summertime T_{min} layer (i.e., the remnant winter mixed layer) is a better approximation of the initial nitrate source to the summertime AZ surface than the underlying deep waters (see discussion in section 5.4.3, part 1).

The second major implication of the nitrite removal results is that, in most cases, the N and O isotopes of nitrate in the AZ winter mixed layer are even more decoupled than initially

suggested by the 'nitrate plus nitrite' data. This is illustrated by the greater deviation of mixed-layer samples above the 1:1 line in $\delta^{18}O$ vs. $\delta^{15}N$ space (i.e., a lower $\Delta(15\text{-}18)$) after nitrite removal, providing even stronger evidence for nitrification in the AZ winter mixed layer (see discussion in section 5.4.3, part 2). In fact, the very presence of a significant nitrite pool in the mixed layer supports the notion of ongoing *in situ* nitrification, in that it suggests that the $NH_4^+ \rightarrow NO_2^- \rightarrow NO_3^-$ pathway is active.

The original $\delta^{15}N$ data presented in this study (i.e., without nitrite removed) are, for some paleoceanographic applications, more useful than the $\delta^{15}N$ of nitrate alone, since it is the total N pool (comprising both nitrate and nitrite) that is consumed by phytoplankton which ultimately determines the $\delta^{15}N$ of the sinking flux and is, thus, relevant to the interpretation of sedimentary $\delta^{15}N$. Furthermore, given that it has been standard practice not to remove or correct for the presence of nitrite, the original isotope data presented in this study provide the most appropriate comparison with prior studies.

Appendix C: Correcting for a steady-state dilution effect in Antarctic depth profiles

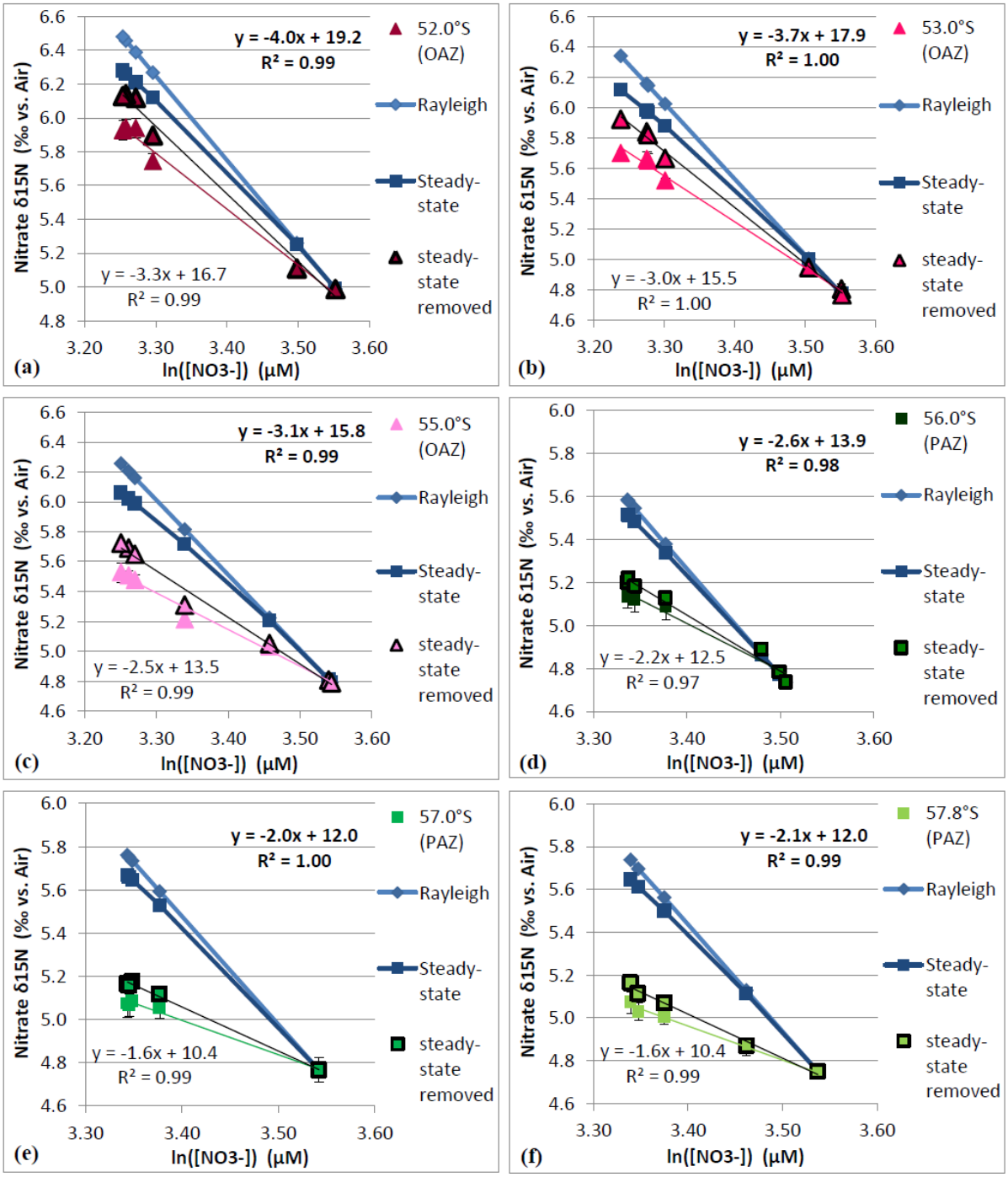

Figure C.1 Individual depth profiles from (a) 52.0°S, (b) 53.0°S, (c) 55.0°S, (d) 56.0°S, (e) 57.0°S, (f) 57.8°S plotted in $\delta^{15}N$ vs. ln($[NO_3^-]$) space, down to the $[NO_3^-]$ maximum of UCDW (original linear trendline equation given in the bottom-left of each panel). In each case, the theoretical Rayleigh and steady-state model predictions for the $\delta^{15}N$ of the substrate are plotted for comparison, based on the measured $[NO_3^-]$ and assuming an isotope effect of 5‰. The $\delta^{15}N$ difference between the two models is added to the original profile data to obtain a new profile with the 'steady-state dilution' component removed ('steady-state removed'; black-outlined symbols; new linear trendline equation shown in bold, top-right).

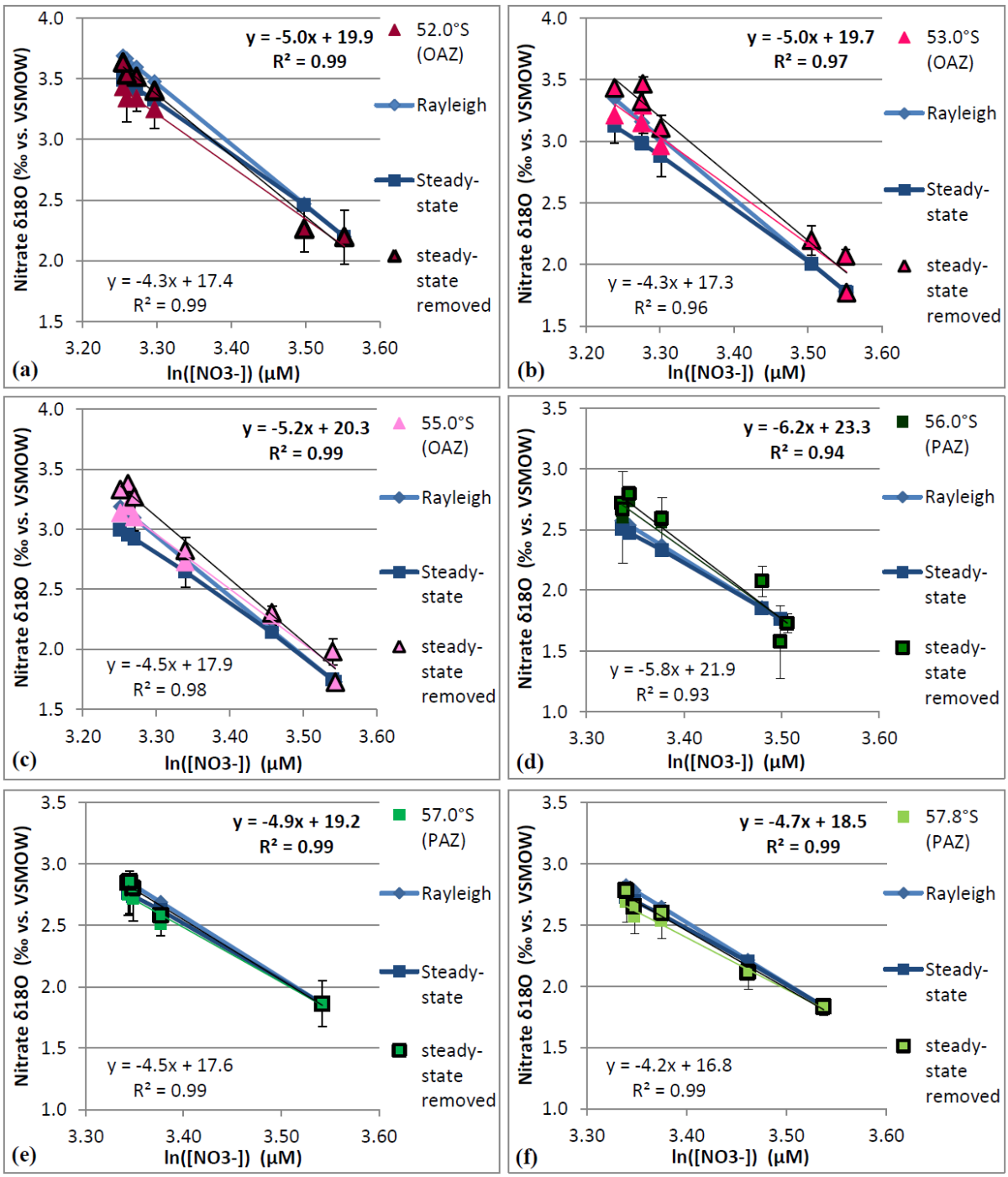

Figure C.2 Individual depth profiles from (a) 52.0°S, (b) 53.0°S, (c) 55.0°S, (d) 56.0°S, (e) 57.0°S, (f) 57.8°S plotted in $\delta^{18}O$ vs. ln([NO_3^-]) space, down to the [NO_3^-] maximum of UCDW (original linear trendline equation given in the bottom-left of each panel). In each case, the theoretical Rayleigh and steady-state model predictions for the $\delta^{18}O$ of the substrate are plotted for comparison, based on the measured [NO_3^-] and assuming an isotope effect of 5‰. The $\delta^{18}O$ difference between the two models is added to the original profile data to obtain a new profile with the 'steady-state dilution' component removed ('steady-state removed'; black-outlined symbols; new linear trendline equation shown in bold, top-right).

8. References

Altabet, M. 2001. Nitrogen isotopic evidence for micronutrient control of fractional NO_3^- utilization in the equatorial Pacific. *Limnology and Oceanography*, **46**(2), 368–380.

Altabet, M. A., & Francois, R. 1994a. *Carbon Cycling in the Glacial Ocean: Constraints on the Ocean's Role in Global Change*. NATO ASI Series, vol. 17. Springer Berlin Heidelberg. Chap. The Use of Nitrogen Isotopic Ratio for Reconstruction of Past Changes in Surface Ocean Nutrient Utilization, pages 281–306.

Altabet, M. A., & Francois, R. 1994b. Sedimentary nitrogen isotopic ratio as a recorder for surface ocean nitrate utilization. *Global Biogeochemical Cycles*, **8**(1), 103–116.

Altabet, M.A. 1988. Variations in nitrogen isotopic composition between sinking and suspended particles: Implications for nitrogen cycling and particle transformation in the open ocean. *Deep Sea Research I*, **35**, 535–554.

Altabet, M.A., & Francois, R. 2001. Nitrogen isotope biogeochemistry of the Antarctic Polar Frontal Zone at 170W. *Deep-Sea Research II*, **48**, 4247–4273.

Altabet, M.A., & McCarthy, J.J. 1985. Temporal and spatial variations in the natural abundance of ^{15}N in PON from a warm-core ring. *Deep Sea Research I*, **32**, 755–772.

Altabet, M.A., Deuser, W.G., Honjo, S., & Stienen, S. 1991. Seasonal and depth-related changes in the source of sinking particles in the N. Atlantic. *Nature*, **354**, 136–139.

Altabet, M.A., Pilskaln, C., Thunell, R., Pride, C., Sigman, D., Chavez, F., & Francois, R. 1999. The nitrogen isotope biogeochemistry of sinking particles from the margin of the Eastern North Pacific. *Deep-Sea Research I*, **46**, 655–679.

Ansorge, I.J. 2012. *Monitoring the oceanic flow between Africa and Antarctica: Preliminary report on an early winter transect to study the impacts of seasonality on the Antarctic Circumpolar Current*. VOY03 cruise report. South African Southern Ocean Community (SASOC).

Ansorge, I.J., Speich, S., Lutjeharms, J.R.E., Göni, G.J., Rautenbach, C.J. de W., Froneman, P.W., Rouault, M., & Garzoli, S. 2005. Monitoring the oceanic flow between Africa and

Antarctica: Report of the first GoodHope cruise. *South African Journal of Science*, **101**, 29–35.

Barford, C.C., Montoya, J.P., Altabet, M.A., & Mitchell, R. 1999. Steady-State Nitrogen Isotope Effects of N_2 and N_2O Production in Paracoccus denitrificans. *Applied and Environmental Microbiology*, **65**(3), 989–994.

Belkin, I.M., & Gordon, A.L. 1996. Southern Ocean fronts from the Greenwich meridian to Tasmania. *Journal of Geophysical Research*, **101**(C2), 3675–3696.

Boebel, O., Lutjeharms, J., Schmid, C., Zenk, W., Rossby, T., & Barron, C. 2003. The Cape Cauldron: A regime of turbulent inter-ocean exchange. *Deep Sea Research II*, **50**, 57–86.

Böhlke, J.K., Mroczkowski, S.J., & Coplen, T.B. 2003. Oxygen isotopes in nitrate: new reference materials for ^{18}O:^{17}O:^{16}O measurements and observations on nitrate-water equilibration. *Rapid Communications in Mass Spectrometry*, **17**, 1835–1846.

Boyd, P., LaRoche, J., Gall, M., Frew, R., & McKay, R.M.L. 1999. Role of iron, light, and silicate in controlling algal biomass in subantarctic waters SE of New Zealand. *Journal of Geophysical Research*, **104**(C6), 13395–13408.

Braman, R.S., & Hendrix, S.A. 1989. Nanogram nitrite and nitrate determination in environmental and biological materials by Vanadium(III) reduction with chemiluminescence detection. *Analytical Chemistry*, **61**, 2715–2718.

Broecker, W.S. 1982. Ocean chemistry during glacial time. *Geochimica et Cosmochimica Acta*, **46**, 1689–1706.

Callahan, J.E. 1972. The structure and circulation of deep water in the Antarctic. *Deep Sea Research and Oceanographic Abstracts*, **19**(8), 563–575.

Carpenter, E.J., & Capone, D.G. 1992. *Marine Pelagic Cyanobacteria: Trichodesmium and other Diazotrophs*. Springer Netherlands. Chap. Nitrogen Fixation in Trichodesmium Blooms, pages 211–217.

Carpenter, E.J., Harvey, H.R., Fry, B., & Capone, D.G. 1997. Biogeochemical tracers of the marine cyanobacterium Trichodesmium. *Deep Sea Research I*, **44**(1), 27–38.

Casciotti, K. L., Sigman, D.M., Galanter Hastings, M., Böhlke, J.K., & Hilkert, A. 2002. Measurement of the Oxygen Isotopic Composition of Nitrate in Seawater and Freshwater Using the Denitrifier Method. *Analytical Chemistry*, **74**, 4905–4912.

Casciotti, K.L. 2009. Inverse kinetic isotope fractionation during bacterial nitrite oxidation. *Geochimica et Cosmochimica Acta*, **73**, 2061–2076.

Casciotti, K.L., Sigman, D.M., & Ward, B.B. 2003. Linking Diversity and Stable Isotope Fractionation in Ammonia-Oxidizing Bacteria. *Geomicrobiology Journal*, **20**, 335–353.

Casciotti, K.L., Böhlke, J.K., McIlvin, M.R., Mroczkowski, S.J., & Hannon, J.E. 2007. Oxygen Isotopes in Nitrite: Analysis, Calibration, and Equilibration. *Analytical Chemistry*, **79**, 2427–2436.

Chisholm, S.W., & Morel, F.M.M. 1991. What controls phytoplankton production in nutrient-rich areas of the open sea? *Limnology and Oceanography*, **36**(8), 1507–1970. Special volume.

Clark, D.R., Rees, A.P., & Joint, I. 2008. Ammonium regeneration and nitrification rates in the oligotrophic Atlantic Ocean: Implications for new production estimates. *Limnology and Oceanography*, **53**(1), 52–62.

Cline, J.D., & Kaplan, I.R. 1975. Isotopic fractionation of dissolved nitrate during denitrification in the eastern tropical North Pacific Ocean. *Marine Chemistry*, **3**, 271–299.

Cunningham, S.A. 2005. Southern Ocean circulation. *Archives of natural history*, **32**(2), 265–280.

de Boyer Montégut, C., Madec, G., Fischer, A.S., Lazar, A., & Iudicone, D. 2004. Mixed layer depth over the global ocean: An examination of profile data and a profile-based climatology. *Journal of Geophysical Research*, **109**(C12003).

Deacon, G.E.R. 1933. A general account of the hydrology of the South Atlantic Ocean. *Discovery Reports*, **7**, 171–238.

Deacon, G.E.R. 1937. The hydrology of the Southern Ocean. *Discovery Reports*, **15**, 1–24.

Deacon, G.E.R. 1982. Physical and biological zonation in the Southern Ocean. *Deep-Sea Research*, **29**(1), 1–16.

Diaz, F., & Raimbault, P. 2000. Nitrogen regeneration and dissolved organic nitrogen release during spring in a NW Mediterranean coastal zone (Gulf of Lions): Implication for the estimation of new production. *Marine Ecology Progress Series*, **197**, 51–65.

DiFiore, P. J., Sigman, D. M., Trull, T. W., Lourey, M. J., Karsh, K., Cane, G., & Ho, R. 2006. Nitrogen isotope constraints on subantarctic biogeochemistry. *Journal of Geophysical Research*, **111**(C08016).

DiFiore, P. J., Sigman, D. M., Karsh, K. L., Trull, T. W., Dunbar, R. B., & Robinson, R. S. 2010. Poleward decrease in the isotope effect of nitrate assimilation across the Southern Ocean. *Geophysical Research Letters*, **37**(L17601).

DiFiore, P.J., Sigman, D.M., & Dunbar, R.B. 2009. Upper ocean nitrogen fluxes in the Polar Antarctic Zone: Constraints from the nitrogen and oxygen isotopes of nitrate. *Geochmistry Geophysics Geosystems*, **10**(Q11016).

Dong, S., Sprintall, J., Gille, S.T., & Talley, L. 2008. Southern Ocean mixed-layer depth from Argo float profiles. *Journal of Geophysical Research*, **113**(C06013), 1–12.

Donners, J., Drijfhout, S.S., & Coward, A.C. 2004. Impact of cooling on the water mass exchange of Agulhas rings in a high resolution ocean model. *Geophysical Research Letters*, **31**(L16312).

Dore, J.E., & Karl, D.M. 1996. Nitrification in the euphotic zone as a source for nitrite, nitrate and nitrous oxide at Station ALOHA. *Limnology and Oceanography*, **41**(8), 1619–1628.

Dugdale, R.C., & Goering, J.J. 1967. Uptake of new and regenerated forms of nitrogen in primary productivity. *Limnology and Oceanography*, **12**(2), 196–206.

Dugdale, R.C., Menzel, D.W., & J.H., Ryther. 1961. Nitrogen fixation in the Sargasso Sea. *Deep Sea Research*, **7**, 298–300.

Eppley, R.W., & Peterson, B.J. 1979. Particulate organic matter flux and planktonic new production in the deep ocean. *Nature*, **282**, 677–680.

Eriksen, R. 1997. *A practical manual for the determination of salinity, dissolved oxygen, and nutrients in seawater*. Research Report, no. 11. Antarctic CRC, Hobart, Tasmania, Australia.

Fawcett, S.E., Lomas, M.W., Casey, J.R., Ward, B.B., & Sigman, D.M. 2011. Assimilation of upwelled nitrate by small eukaryotes in the Sargasso Sea. *Nature Geoscience*, **4**, 717–722.

Fawcett, S.E., Lomas, M.L., Ward, B.B., & Sigman, D.M. In review. The counterintuitive effect of summer-to-fall mixed layer deepening on eukaryotic new production in the Sargasso Sea. *Global Biogeochemical Cycles*.

Foriel, J., Weigand, M.A., Oleynik, S., Barnett, B., Smart, S.M., & Sigman, D.M. In preparation. Updated instrumentation and protocols for nitrogen and oxygen isotopic analysis of nitrate by the denitrifier method. *Rapid Communications in Mass Spectrometry*.

Francois, R., Altabet, M.A., & Burckle, L.H. 1992. Glacial to interglacial changes in surface nitrate utilization in the Indian sector of the Southern Ocean as recorded by sediment $\delta^{15}N$. *Paleoceanography*, **7**(5), 589–606.

Francois, R., Altabet, M.A., Yu, E.F., Sigman, D.M., Bacon, M.P., Frank, M., Bohrmann, G., Bareille, G., & Labeyrie, L.D. 1997. Contribution of Southern Ocean surface-water stratification to low atmospheric CO_2 concentrations during the last glacial period. *Nature*, **389**, 929–935.

Franks, P.J.S. 1992. Sink or swim: accumulation of biomass at fronts. *Marine Ecology Progress Series*, **82**, 1–12.

Fripiat, F., Sigman, D.M., Fawcett, S.E., Rafter, P.A., Weigand, M.A., & Tison, J.-L. Accepted. New insights into sea ice nitrogen biogeochemical dynamics from nitrogen isotopes. *Global Biogeochemical Cycles*.

Gandhi, N., Ramesh, R., Laskar, A.H., Sheshshayee, M.S., Shetye, S., Anilkumar, N., Patil, S.M., & Mohan, R. 2012. Zonal variability in primary production and nitrogen uptake rates in the southwestern Indian Ocean and the Southern Ocean. *Deep Sea Research I*, **67**, 32–43.

Garside, C. 1982. A chemiluminescent technique for the determination of nanomolar concentrations of nitrate and nitrite in seawater. *Marine Chemistry*, **11**, 159–167.

Gonfiantini, R., Stichler, W., & Rosanski, K. 1995. *Standards and intercomparison materials distributed by the IAEA for stable isotope measurements, in Reference and Intercomparison Material of Stable Isotopes of Light Elements*. Tech. rept. IAEATECDOC-825, pp. 13–29. International Atomic Energy Agency, Vienna.

Gordon, A.L. 1986. Interocean Exchange of Thermocline Water. *Jourrnal of Geophysical Research*, **91**(C4), 5037–5046.

Granger, J., & Sigman, D.M. 2009. Removal of nitrite with sulfamic acid for nitrate N and O isotope analysis with the denitrifier method. *Rapid Communications in Mass Spectrometry*, **23**, 3753–3762.

Granger, J., Sigman, D.M., Needoba, J.A., & Harrison, P.J. 2004. Coupled Nitrogen and Oxygen Isotope Fractionation of Nitrate during Assimilation by Cultures of Marine Phytoplankton. *Limnology and Oceanography*, **49**(5), 1763–1773.

Granger, J., Sigman, D.M., Prokopenko, M.G., Lehmann, M.F., & Tortell, P.D. 2006. A method for nitrite removal in nitrate N and O isotope analyses. *Limnology and Oceanography: Methods*, **4**, 205–212.

Granger, J., Sigman, D.M., Lehmann, M.F., & Tortell, P.D. 2008. Nitrogen and oxygen isotope fractionation during dissimilatory nitrate reduction by denitrifying bacteria. *Limnology and Oceanography*, **53**(6), 2533–2545.

Granger, J., Sigman, D.M., Rohde, M.M., Maldonado, M.T., & Tortell, P.D. 2010. N and O isotope effects during nitrate assimilation by unicellular prokaryotic and eukaryotic plankton cultures. *Geochimica et Cosmochimica Acta*, **74**, 1030–1040.

Hayes, J.M. 2002. Practice and Principles of Isotopic Measurements in Organic Geochemistry (Revision 2). Woods Hole Oceanographic Institution, Woods Hole, MA 02543. http://www.whoi.edu/fileserver.do?id=73290&pt=2&p=74886.

Higgins, M.B., Robinson, R.S., Casciotti, K.L., McIlvin, M.R., & Pearson, A. 2009. A Method for Determining the Nitrogen Isotopic Composition of Porphyrins. *Analytical Chemistry*, **81**, 184–192.

Hoch, M.P., Fogel, M.L., & Kirchman, D.L. 1992. Isotope fractionation associated with ammonium uptake by a marine bacterium. *Limnology and Oceanography*, **37**(7), 1447–1459.

Hoering, T.C., & Ford, H.T. 1960. The isotope effect in the fixation of nitrogen by Azotobacter. *Journal of the American Chemical Society*, **82**, 376–378.

Holliday, N.P., & Read, J.F. 1998. Surface oceanic fronts between Africa and Antarctica. *Deep Sea Research I*, **45**, 217–238.

Joubert, W.R., Thomalla, S.J., Waldron, H.N., Lucas, M.I., Boye, M., Le Moigne, F.A.C., Planchon, F., & Speich, S. 2011. Nitrogen uptake by phytoplankton in the Atlantic sector of the Southern Ocean during late austral summer. *Biogeosciences*, **8**, 2947–2959.

Karl, D., Michaels, A., Bergman, B., Capone, D., Carpenter, E., Letelier, R., Lipschultz, F., Paerl, H., Sigman, D., & Stal, L. 2002. Dinitrogen fixation in the world's oceans. *Biogeochemistry*, **57/58**, 47–98.

Karsh, K. L., Trull, T. W., Lourey, M. J., & Sigman, D. M. 2003. Relationship of nitrogen isotope fractionation to phytoplankton size and iron availability during the Southern Ocean Iron RElease Experiment (SOIREE). *Limnology and Oceanography*, **48**(3), 1058–1068.

Karsh, K.L. 2013. *Physiological and Environmental Controls on the Nitrogen and Oxygen Isotope Fractionation of Nitrate During Its Assimilation by Marine Phytoplankton*. Ph.D. thesis, Princeton University (USA) and CSIRO (Australia).

Kier, R.S. 1988. On the late Pleistocene ocean geochemistry and circulation. *Paleoceanography*, **3**, 413–445.

Knapp, A.N., Sigman, D.M., & Lipschultz, F. 2005. N isotopic composition of dissolved organic nitrogen and nitrate at the Bermuda Atlantic Time-series Study site. *Global Biogeochemical Cycles*, **19**, 1–15.

Knapp, A.N., DiFiore, P.J., Deutsch, C., Sigman, D.M., & Lipschultz, F. 2008. Nitrate isotopic composition between Bermuda and Puerto Rico: Implications for N_2 fixation in the Atlantic Ocean. *Global Biogeochemical Cycles*, **22**, 1–14.

Knox, F., & McElroy, M.B. 1984. Changes in atmospheric CO_2: influence of the marine biota at high latitude. *Journal of Geophysical Research*, **89**, 4629–4637.

Koroleff, F. 1983. *Methods of Seawater Analysis*. Verlag Chemie. Pages 150–157.

Lehmann, M.F., Bernasconi, S.M., Barbieri, A., & McKenzie, J.A. 2002. Preservation of organic matter and alteration of its carbon and nitrogen isotope composition during simulated and in situ early sedimentary diagenesis. *Geochimica et Cosmochimica Acta*, **66**(20), 3573–3584.

Liu, K.-K., Su, M.J., Hsueh, C.R., & Gong, G.C. 1996. The nitrogen isotopic composition of nitrate in the Kuroshio Water northeast of Taiwan: Evidence for nitrogen fixation as a source of isotopically light nitrate. *Marine Chemistry*, **54**, 273–292.

Lourey, M.J., Trull, T.W., & Sigman, D.M. 2003. Sensitivity of $\delta^{15}N$ of nitrate, surface suspended and deep sinking particulate nitrogen to seasonal nitrate depletion in the Southern Ocean. *Global Biogeochemical Cycles*, **17**(3), 1–18.

Lutjeharms, J.R.E., & van Ballegooyen, R.C. 1988. The Retroflection of the Agulhas Current. *Journal of Physical Oceanography*, **18**, 1570–1583.

Mantyla, A.W., & Reid, J.L. 1983. Abyssal characteristics of the World Ocean waters. *Deep Sea Research, Part A*, **30**(8), 805–833.

Marconi, D. In preparation. Nitrate isotope distributions on the US GEOTRACES North Atlantic cross-basin section: Signals of polar nitrate sources and low latitude nitrogen cycling.

Mariotti, A., Germon, J.C., Hubert, P., Kaiser, P., Letolle, R., Tardieux, A., & Tardieux, P. 1981. Experimental determination of nitrogen kinetic isotope fractionation: Some principles; illustration for the denitrification and nitrification processes. *Plant and Soil*, **62**, 413–430.

Martin, J.H. 1990. Glacial-interglacial CO_2 Change: The Iron Hypothesis. *Paleoceanography*, **5**(1), 1–13.

McCartney, M.S. 1977. *A Voyage of Discovery: George Deacon 70th Anniversary Volume*. Supplement to Deep-Sea Research. Pergamon Press, Oxford. Chap. Subantarctic Mode Water, pages 103–119.

McIlvin, M.R., & Casciotti, K.L. 2011. Technical Updates to the Bacterial Method for Nitrate Isotopic Analyses. *Analytical Chemistry*, **83**, 1850–1856.

Montoya, J.P., & McCarthy, J.J. 1995. Isotopic fractionation during nitrate uptake by phytoplankton grown in continuous culture. *Journal of Plankton Research*, **17**(3), 439–464.

Moore, J.K., & Abbott, M.R. 2000. Phytoplankton chlorophyll distributions and primary production in the Southern Ocean. *Journal of Geophysical Research*, **105**(C12), 28,709–28,722.

Mulholland, M.R., & Capone, D.G. 1999. Nitrogen fixation, uptake and metabolism in natural and cultured populations of Trichodesmium spp. *Marine Ecology Progress Series*, **188**, 33–49.

Needoba, J.A., & Harrison, P.J. 2004. Influence of low light and a light:dark cycle on NO3- uptake, intercellular NO3-, and nitrogen isotope fractionation by marine phytoplankton. *Journal of Phycology*, **40**, 505–516.

Needoba, J.A., Waser, N.A., Harrison, P.J., & Calvert, S.E. 2003. Nitrogen isotope fractionation in 12 species of marine phytoplankton during growth on nitrate. *Marine Ecology Progress Series*, **225**, 81–91.

Needoba, J.A., Sigman, D.M., & Harrison, P.J. 2004. The mechanism of isotope fractionation during algal nitrate assimilation as illuminated by the $^{15}N/^{14}N$ of intracellular nitrate. *Journal of Phycology*, **40**, 517–522.

Nowlin, W.D., & Klinck, J.M. 1986. The Physics of the Antarctic Circumpolar Current. *Reviews of Geophysics*, **24**(3), 469–491.

Olbers, D., Borowski, D., Völker, C., & Wölff, J.-O. 2004. The dynamical balance, transport and circulation of the Antarctic Circumpolar Current. *Antarctic Science*, **16**(4), 439–470.

Olson, R.J. 1981. Differential photoinhibition of marine nitrifying bacteria: A possible mechanism for the formation of the primary nitrite maximum. *Journal of Marine Research*, **39**, 227–238.

Orsi, A. H., Whitworth, T., & Nowlin, W.D. 1995. On the meridional extent and fronts of the Antarctic Circumpolar Current. *Deep-Sea Research*, **42**(5), 641–673.

Park, Y.H., Gamberoni, L., & Charriaud, E. 1993. Frontal structure, water masses, and circulation in the Crozet Basin. *Journal of Geophysical Research*, **98**(C7), 12361–12385.

Pennock, J.R., Velinsky, D.J., Ludlam, J.M., Sharp, J.H., & Fogel, M.L. 1996. Isotope fractionation of ammonium and nitrate during their uptake by Skeletonema Costatum: Implications for the $\delta^{15}N$ dynamics under bloom conditions. *Limnology and Oceanography*, **41**(3), 451–459.

Philibert, R., Clark, D.R., & Waldron, H.N. In preparation. A regional and seasonal comparison of nitrogen uptake by phytoplankton in the Southern Ocean.

Piola, A.R., & Georgi, D. 1982. Circumpolar properties of Antarctic Intermediate Waters and Subantarctic Mode Water. *Deep Sea Research, Part I*, **29**, 687–711.

Pollard, R.T., Lucas, M.I., & Read, J.F. 2002. Physical controls on biogeochemical zonation in the Southern Ocean. *Deep-Sea Research II*, **49**, 3289–3305.

Qi, H., Coplen, T.B., Geilmann, H., Brand, W.A., & Böhlke, J.K. 2003. Two new organic reference materials for $\delta^{13}C$ and $\delta^{15}N$ measurements and a new value for the $\delta^{13}C$ of NBS 22 oil. *Rapid Communications in Mass Spectrometry*, **17**, 2483–2487.

Rafter, P.A., DiFiore, P.J., & Sigman, D.M. 2013. Coupled nitrate nitrogen and oxygen isotopes and organic matter remineralization in the Southern and Pacific Oceans. *Journal of Geophysical Research*, **118**, 4781–4794.

Rau, G.H., Sullivan, C.W., & Gordon, L.I. 1991. $\delta^{13}C$ and $\delta^{15}N$ variations in Weddell Sea particulate organic matter. *Marine Chemistry*, **35**, 355–369.

Sallée, J.-B., Wienders, N., Speer, K., & Morrow, R. 2006. Formation of subantarctic mode water in the southeastern Indian Ocean. *Ocean Dynamics*, **56**(5-6), 525–542.

Sanders, R., Morris, P.J., Stinchcombe, M., Seeyave, S., Venables, H., & Lucas, M. 2007. New production and the f ratio around the Crozet Plateau in austral summer 2004–2005 diagnosed from seasonal changes in inorganic nutrient levels. *Deep Sea Research II*, **54**, 2191–2207.

Sarmiento, J.L., & Toggweiler, J.R. 1984. A new model for the role of the oceans in determining atmospheric pCO_2. *Nature*, **308**, 621–624.

Schmid, C., Boebel, O., Lutjeharms, J.R.E., Garzoli, S.L., Richardson, P.L., & Barron, C. 2003. Early evolution of an Agulhas Ring. *Deep Sea Research II*, **50**, 141–166.

Sigman, D. M., Altabet, M. A., McCorkle, D. C., Francois, R., & Fischer, G. 1999a. The $\delta^{15}N$ of nitrate in the Southern Ocean: Consumption of nitrate in surface waters. *Global Biogeochemical Cycles*, **13**(4), 1149–1166.

Sigman, D. M., Altabet, M. A., McCorkle, D. C., Francois, R., & Fischer, G. 2000. The $\delta^{15}N$ of nitrate in the Southern Ocean: Nitrogen cycling and circulation in the ocean interior. *Journal of Geophysical Research*, **105**(C8), 19599–19614.

Sigman, D. M., DiFiore, P. J., Hain, M. P., Deutsch, C., Wang, Y., Karl, D. M., Knapp, A. N., Lehmann, M. F., & Pantoja, S. 2009a. The dual isotopes of deep nitrate as a constraint on the cycle and budget of oceanic fixed nitrogen. *Deep-Sea Research I*, **56**, 1419–1439.

Sigman, D.M., & Boyle, E.A. 2000. Glacial/interglacial variations in atmospheric carbon dioxide. *Nature*, **407**, 859–869.

Sigman, D.M., McCorkle, D.C., & Martin, W.R. 1998. The calcite lysocline as a constraint on glacial/interglacial low latitude production changes. *Global Biogeochemical Cycles*, **12**, 409–428.

Sigman, D.M., Altabet, M.A., Francois, R., McCorkle, D.C., & Gaillard, J.F. 1999b. The isotopic composition of diatom-bound nitrogen in Southern Ocean sediments. *Paleoceanography*, **14**(2), 118–134.

Sigman, D.M., Casciotti, K.L., Andreani, M., Barford, C., Galanter, M., & Böhlke, J.K. 2001. A Bacterial Method for the Nitrogen Isotopic Analysis of Nitrate in Seawater and Freshwater. *Analytical Chemistry*, **73**, 4145–4153.

Sigman, D.M., Robinson, R., Knapp, A.N., van Geen, A., McCorkle, D.C., Brandes, J.A., & Thunell, R.C. 2003. Distinguishing between water column and sedimentary denitrification in the Santa Barbara Basin using the stable isotopes of nitrate. *Geochemistry Geophysics Geosystems*, **4**(5), 1–20.

Sigman, D.M., Granger, J., DiFiore, P.J., Lehmann, M.M., Ho, R., Cane, G., & van Geen, A. 2005. Coupled nitrogen and oxygen isotope measurements of nitrate along the eastern North Pacific margin. *Global Biogeochemical Cycles*, **19**(GB4022).

Sigman, D.M., Karsh, K.L., & Casciotti, K.L. 2009b. *Encyclopedia of ocean science*. 2nd edn. Elsevier, Amsterdam. Chap. Ocean process tracers: nitrogen isotopes in the ocean, pages 4138–4152.

Sigman, D.M., DiFiore, P.J., Hain, M.P., Deutsch, C., & Karl, D.M. 2009c. Sinking organic matter spreads the nitrogen isotope signal of pelagic denitrification in the North Pacific. *Geophysical Research Letters*, **36**(L08605), 1–5.

Speich, S., Arhan, M., Rusciano, E., Faure, V., Ollitrault, M., Prigent, A., & Swart, S. 2012. Use of ARGO floats to study the ocean dynamics south of Africa: What we have learned

from the GoodHope Project and what we plan within the SAMOC International Programme. *Mercator Ocean-Coriolis Quarterly*, **45**, 21–27.

Strickland, J.D.H., & Parsons, T.R. 1972. *A Practical Handbook of Seawater Analysis*. 2nd edn. Vol. 167. Bulletin of the Fisheries Research Board of Canada.

Swart, S., Thomalla, S., Monteiro, P.M.S., & Ansorge, I.J. 2012. Mesoscale features and phytoplankton biomass at the GoodHope line in the Southern Ocean during austral summer. *African Journal of Marine Science*, **34**(4), 511–524.

Talley, L. D. 1996. *The South Atlantic: Present and Past Circulation*. Springer Berlin Heidelberg. Chap. Antarctic Intermediate Water in the South Atlantic, pages 219–238.

Trull, T.W., Davies, D., & Casciotti, K. 2008. Insights into nutrient assimilation and export in naturally iron-fertilized waters of the Southern Ocean from nitrogen, carbon and oxygen isotopes. *Deep-Sea Research II*, **55**, 820–840.

Verheye, H.M. 2013. Personal Communication. Specialist Scientist and Head of Biological Oceanography in the Department of Environmental Affairs (Oceans and Coasts Research), Cape Town, South Africa. Fellow scientist aboard the S.A. Agulhas II July 2012 research voyage.

Vo, J., Inwood, W., Hayes, J.M., & Kustu, S. 2013. Mechanism for nitrogen isotope fractionation during ammonium assimilation by Escherichia coli K12. *Proceedings of the National Academy of Sciences*, **110**(21), 8696–8701.

Wada, E., & Hattori, A. 1976. Natural abundance of ^{15}N in particulate organic matter in the North Pacific Ocean. *Geochimica et Cosmochimica Acta*, **40**, 249–251.

Wada, E., & Hattori, A. 1978. Nitrogen isotope effects in the assimilation of inorganic nitrogenous compounds by marine diatoms. *Geomicrobiology Journal*, **1**(1), 85–101.

Ward, B.B. 1987. Nitrogen transformations in the Southern California Bight. *Deep Sea Research*, **34**(5/6), 785–805.

Ward, B.B. 2005. Temporal variability in nitrification rates and related biogeochemical factors in Monterey Bay, California, USA. *Marine Ecology Progress Series*, **292**, 97–109.

Waser, N.A.D., Harrison, P.J., Nielsen, B., Calvert, S.E., & Turpin, D.H. 1998. Nitrogen Isotope Fractionation During the Uptake and Assimilation of Nitrate, Nitrite, Ammonium, and Urea by a Marine Diatom. *Limnology and Oceanography*, **43**(2), 215–224.

Wefer, G., & Fischer, G. 1991. Annual primary production and export flux in the Southern Ocean from sediment trap data. *Marine Chemistry*, **35**, 597–613.

Whitworth, T. 1980. Zonation and geostrophic flow of the Antarctic circumpolar current at Drake Passage. *Deep Sea Research*, **27**(7), 497–507.

Whitworth, T., & Nowlin, W.D. 1987. Water Masses and Currents of the Southern Ocean at the Greenwich Meridian. *Journal of Geophysical Research*, **92**(C6), 6462–6476.

Wu, J., Calvert, S.E., & Wong, C.S. 1997. Nitrogen isotope variations in the subarctic northeast Pacific: relationships to nitrate utilization and trophic structure. *Deep Sea Research*, **44**(2), 287–314.

Yool, A., Martin, A.P., Fernández, C., & Clark, D.R. 2007. The significance of nitrification for oceanic new production. *Nature*, **447**, 999–1002.

Auxiliary data and software

Garcia, H.E., Locarnini, R.A., Boyer, T.P., Antonov, J.I., Zweng, M.M., Baranova, O.K., & Johnson, D.R. 2010. *World Ocean Atlas 2009, Volume 4: Nutrients (phosphate, nitrate, silicate)*. Levitus, S., Ed. NOAA Atlas NESDIS 71, U.S. Government Printing Office, Washington, D.C., 398 pp. Data available at: http://www.nodc.noaa.gov/OC5/WOA09/pr_woa09.html. [Accessed 20 January 2014].

Locarnini, R.A., Mishonov, A.V., Antonov, J.I., Boyer, T.P., Garcia, H.E., Baranova, O.K., Zweng, M.M., & Johnson, D.R. 2010. *World Ocean Atlas 2009, Volume 1: Temperature.* Levitus, S., Ed., NOAA Atlas NESDIS 68, U.S. Government Printing Office, Washington, D.C., 184 pp. Data available at: http://www.nodc.noaa.gov/OC5/WOA09/pr_woa09.html. [Accessed 10 August 2013].

Schlitzer, R., Ocean Data View, http://odv.awi.de, 2012.